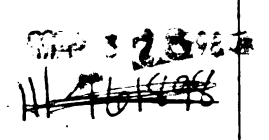


RETURNING MATERIALS:
Place in book drop to remove this checkout from your record. FINES will be charged if book is returned after the date stamped below.



ACTIVE PARAMETRIC CONTROL OF BEAM TRANSVERSE VIBRATION

Ву

Mostafa S.A. Habib

A DISSERTATION

Submitted to
Michigan State University
in partial fulfillment of the requirements
for the degree of

DOCTOR OF PHILOSOPHY

Department of Mechanical Engineering Michigan State University East Lansing, Michigan 48824

ABSTRACT

ACTIVE PARAMETRIC CONTROL OF REAM TRANSVERSE VIBRATION

By

Mostafa S. A. Habib

An active parametric vibration control theory was developed which uses parametric fluctuation to control the beam transverse vibration. The beam was modelled as non-linear, dynamic, simply-supported Bernoulli-Euler beam using the extended Hamilton's principle. The closed-loop system was deduced using the direct method of Liapunov from which the control algorithm for asymptotic stability was derived.

The closed-loop system model was reduced to a nonhomogeneous wave equation for the longitudinal vibration u(x,t) subject to the nonhomogeneous boundary conditions which could be solved analytically using the finite Fourier transform, and a nonlinear fourth order parabolic equation in the transverse vibration y(x,t) which was approximated using finite difference method.

A prototype control system was designed and constructed to demonstrate and verify the approach and to evaluate its performance. The basic measured quantities were the transverse vibration y(x,t), the acceleration (or the displacement) of the end point of the beam

and the exciting force. Analog integrator and differentiator circuits were designed and built to implement the control algorithm.

Both the simulation and the prototype control system were tested and compared to evaluate stability of the transient vibration and dynamic motions due to external disturbances. The comparison of the simulation with experiment results showed good agreement. The significant increases in stability of the test beam were measured and feasibility of employing active parametric vibration control demonestrated.

This is to certify that the

dissertation entitled

ACTIVE PARAMETRIC CONTROL OF BEAM TRANSVERSE VIBRATION

presented by

Mostafa S.A. Habib

has been accepted towards fulfillment of the requirements for

Ph.D. degree in Mechanical Engineering

MSU is an Affirmative Action/ Equal Opportunity Institution

0-12771

ACKNOWLEDGMENTS

The author wishes to express his sincere appreciation and gratitude to his major advisor Professor Clark J. Radcliffe for his continued suport in the form of knowledge, enthusiasm, and guidance during the course of this research. Professor Radcliffe deserves much credit for his contributions during my graduate study and also for his friendship and painstaking review of my dissertation.

The efforts of the other members of my doctoral Guidance Committee, Drs. David Yen, Hassan Khalil, and Allan Haddow are greatly appreciated. Their comments concerning this dissertation were very valuable. They provided guidance and are examples for me to follow. Thanks are also due to my fellow students in the laboratory for their good advice and encouragement.

Finally the author is indebted to the government of Egypt, which provided the fellowship support necessary for completion of this dissertation.

TABLE OF CONTENTS

			PAGE
LIST OF	TABLES	s	iix
LIST OF	FIGUR	ES	x
NOMENCL	ATURE	•••••	xvi
CHAPTER	1 -	INTRODUCTION	1
	1.1	Active vibration control	1
	1.2	A new approach	4
	1.3	Scope of dissertation	5
CHAPTER	2-	PROBLEM FORMULATION AND ACTIVE	
		PARAMETRIC VIBRATION CONTROL THEORY	6
	2.1	Problem formulation	6
	2.2	Stability analysis	16
	2.2.1	Liapunov functional for asymptotic stability	17
CHAPTER	3 -	ANALYTICAL-NUMERICAL SOLUTION	30
	3.1	Analytical solution for beam axial motion	30
	3.2	Numerical solution of the parapolic equation	35
	3.3	Steps of solution	40
	3.4	Simulation results and discussion	41
	3.4.1	Control force	42
	3.4.2	Internal energy and work done	43
CHAPTER	4 -	EXPERIMENTAL FACILITIES, PROCEDURES AND RESULTS	79
	4.1	Simply-supported beam test stand	79
	4.2	Active control prototype	84
	4.2.1	Main instrumentation circuits	84
	422	End heam motion measurement	87

	4.2.2	a End beam acceleration measurement	87
	4.2.21	End beam displacement measurement	92
	4.2.3	Transverse displacement measurement	95
	4.2.4	Beam excitation	95
	4.2.5	Control force measurement	96
	4.3	Experimental test results and discussions	96
•	4.4	Comparison of the uncontrolled ideal beam with	
		the modelled beam with respect to natural	
		frequencies and modulus of elasticity	115
CHAPTER	5 -	COMPARISON OF EXPERIMENTAL WITH SIMULATION RESULTS	118
	5.1	Comparison considerations	118
	5.1.1	Damping model for the uncontrolled beam	119
	5.1.2	Open-loop modal frequencies	120
	5.2	Comparison cases	122
CHAPTER	6	SUMMARY AND CONCLOSIONS	128
APPENDIC	CES		130
APPENDIX	K A	Displacement and Forces Measurements and Calibrations	131
	A1	Displacement Sensor Calibration	131
	A2	Forces Measurements and Calibration	133
APPENDIX	СВ	Real Time Record For the Steady-State	
		Second-Mode Test Results For $\alpha = 35.46 \text{ N}$	143
APPENDIX	C C	Time Domain Test Results For Two-Mode Excitation	148
LIST OF	BEEFF	FNCES	152

LIST OF TABLES

	PAGE
Table 3.1	A subset of the simulation results for the initial displacement for $\alpha = 40 \text{ N}$ for test case 1
Table 3.2	Effect of the control gain α on the amplitude ratio a_n ,
	the energy ratio e_n and the efficiency factor η for
	the initial displacement test results for test case 1,51
Table 3.3	Effect of the control gain α on the amplitude ratio a_j ,
	the energy ratio e_j and the efficiency factor η
	for initial velocity test results for test case 2 55
Table 3.4	Effect of the control gain α on the amplitude ratio a_n ,
	the energy ratio e_n and the efficiency factor η
	for initial displacement of an infinite number of modes test results for test case 5
Table 3.5	Effect of the control gain α on the amplitude ratio a_j ,
	the energy ratio e_j and the efficiency factor η for
	initial impulse of an infinite number of modes for
	test case 670
Table 3.6	Effect of the control gain α on the amplitude ratio a_j ,
	the energy ratio e_j and the efficiency factor η for
	internally unstable system test results for test case 776
Table 4.1	Effect of the control gain on the transient
	motion amplitudes test results103
Table 4.2	Effect of the control gain on the steady state
	first mode response for test case 2

Table 4.3	Effect of the control gain on the steady state second mode response for test case 2
Table 4.4	Effect of the control gain on the steady state
	tow-mode excitation110
Table 4.5	Effect of the control gain on the transfer
	function at the first four modal frequencies
	for the random noise excitation test results
Table 4.6	Comparison of the uncontrolled natural
	frequencies and Young's modulus of the ideal
	beam with those of the modelled beam116
Table 5.1	Open-loop natural frequencies of the experimental
	and simulation results of the beam
Table 5.2	Experimental and simulation results for
	transient motions of the beam
Table 5.3	Experimental and numerical amplitude test
	results for the steady-state motion of the
	beam126
Table B.1	A subset of the measured displacement, exciting
	force and control force histories for the
	steady state second mode test result for α -
	35.46 N

LIST OF FIGURES

			PAGE
Figure	1.1	Flexible beam model	3
Figure	2.1a	Beam configuration	8
Figure	2.1b	Displacements and forces acting on an infinitesimal element of length Δx	8
Figure	2.2	Modified bang-bang control force	. 26
Figure	2.3	Active vibration control	26
Figure	3.1	Computational molecules for the finite	
		difference approximation	39
Figure	3.2a	Response of the transverse vibration at x-2/2 for initial displacement test results for various	
		control gains for test case 1	.44
Figure	3.2b	The required control forces, P(t) for test	
		case 1	.44
Figure	3.2c	The internal energy of the system, E(t) for	
		various control gains for test case 1	46
Figure	3.2d	The work done by the control force, P(t)for	
		various control gains for test case 1	.46
Figure	3.3a	Response of the transverse vibration at $x=l/2$	
		for initial velocity test results for various	
		control gains for test case 2	53
Figure	3.3ъ	The required control forces, P(t) for test	
		case 2	53

Figure 3.3c	The internal energy of the system, E(t) for
	various control gains for test case 254
Figure 3.3d	The work done by the control force, P(t)for
	various control gains for test case 254
Figure 3.4a	Response of the transverse vibration at $x=\ell/2$
	for resonance excitation test results for
·	various control gains for test case 3
Figure 3.4b	The required control forces, P(t) for test
	case 3
Figure 3.4c	The internal energy of the system, E(t) for
	various control gains for test case 3
Figure 3.4d	The work done by the control force, P(t)for
	various control gains for test case 3
Figure 3.5a	Response of the transverse vibration at x-1/2
	for steady-state excitation test results for
	various control gains for test case 461
Figure 3.5b	The required control forces, P(t) for test
	case 462
Figure 3.5c	Effect of the control action on the internal
	energy of the system for test case 462
Figure 3.6a	Response of the transverse vibration at $x=\ell/2$ for
	initial displacement of an infinite number of modes
	for various control gains for test case 564
Figure 3.6b	The required control forces, P(t) for test
	case 5

Figure 3.6c	Internal energy and work done for test case 565
Figure 3.7a	Response of the transverse vibration at x=1/2 for initial impulse of an infinite number of modes for various control gains for test case 6
Figure 3.7b	The required control forces, P(t) for test case 669
Figure 3.7c	Internal energy and work done for test case 669
Figure 3.8a	Response of the transverse vibration at x=1/2 for internally unstable system test results for various control gains for test case 7
Figure 3.8b	Curves of response and control force for α =40 N for test case 7
Figure 3.8c	The required control forces, P(t) for test case 7
Figure 3.8d	Internal energy for test case 7
Figure 3.8e	The work done for test case 7
Figure 4.1	Prototype active vibration controller showing the simply-supported beam test stand and the main instrumentation devices
Figure 4.2	Prototype active vibration controller showing the end motion sensors and the structure of the moving beam end and the control actuator
Figure 4.3	Measurement and control flow diagram 86
Figure 4.4	Integrator and analog switch circuit

Figure 4.5a	Integrator transfer function test results90
Figure 4.5b	Integrator test signal results at 20 HZ91
Figure 4.5c	Integrator test signal results at 200 HZ91
Figure 4.6	Differentiator and analog switch circuit93
Figure 4.7a	Differentiator transfer function test results94
Figure 4.7b	Differentiator test signal results at 20 HZ94
Figure 4.8	Sensors and electromagnets locations97
Figure 4.9	Transient response first-mode test results at x = 367.2 mm for the uncontrolled beam99
Figure 4.10	Transient vibration, first-mode test results for control gain $\alpha = 10.63$ N. a) the response at $x = 367.2$ mm b) the control force $P(t)$
Figure 4.11	Transient vibration, first-mode test results for control gain $\alpha = 13.98$ N. a) the response at $x = 367.2$ mm b) the control force $P(t)$
Figure 4.12	Transient vibration, first-mode test results for control gain at $\alpha = 58.67$ N. a) the response at $x = 367.2$ mm b) the control force $P(t)$
Figure 4.13	Steady state second-mode test results for $\alpha = 35.46 \text{ N}$. a) the exciting force. b) the response at $x = 367.2 \text{ mm}$. c) the control force

Figure 4.14	FFT of the steady state response of the two-
	mode test results109
Figure 4.15	Typical test results of the transfer function
	of the beam. The displacement sensor located
	at $x = 367.2$ mm and the exciting force applied
	at $x = 82.55$ mm.
	a) the transfer function for $\alpha = 0$
	b) the transfer function for $\alpha = 13 \text{ N} \dots 112$
Figure 4.16	Random noise excitation test results for the
	controlled beam for various control gains113
Figure 5.1	Results of experiment and simulation for
	steady-state first mode response for
	comparison case 2125
Figure Al	Displacement sensor calibration results
Figure A2	Four-arm strain gauge bridge for measuring the
	control force.
	a) bridge circuit.
	b) strain gauge orientation134
Figure A3	Four-arm strain gauge bridge for measuring the
	exciting force.
	a) bridge circuit.
	b) strain gauge orientation
Figure A4	Strain gauge calibration for the axial control
	force137
Figure A5	Magnet drive signal calibration results for
	the axial control force138
Figure A6	Strain gauge calibration results for the

	exciting force140
Figure A7	Magnet drive signal calibration results.for
	the exciting force141
Figure Cl	Steady state two-mode test results for the
	uncontrolled beam.
	a) the exciting force.
	b) the response at x = 367.2 mm149
Figure C2	Steady state two-mode test results for control
	gain $\propto -41.7 \text{ N}.$
	a) the exciting force.
	b) the response at $x = 367.2 \text{ mm}$
	c) the control force150
Figure C3	Steady state two-mode test results for control
	gain ∝ = 50 N.
	a) the exciting force.
	b) the response at x - 367.2 mm
	a) the central force

NOMENCLATURE

A	cross-sectional area of beam, m
a	speed of sound in beam material $(-\sqrt{E/\rho})$ m/sec
a _n ,a _j	transverse vibration amplitude ratio.
В	differential operator
С	damping cofficient Kg m/sec
E	
Ě	Young's modulus for the ideal beam material, N/m
E-E(t)	internal energy of the system N mm
e _i ,e _j	energy ratio
f=f(x,t)	transverse load N/m
f _i	modal natural frequency of the modelled beam, Hz
ŧ _i	modal natural frequency of the ideal beam, Hz
I	principal moment of inertia of beam cross section
	with respect to direction of bending m
i,j	finite difference node at x_i = $i\Delta x$ and t_j = $j\Delta t$
i	mode number
n	longitudinal vibration mode number
l	beam length
n	transverse vibration cycle number
p=p(x,t)	axial parametric force
P=P (t)	control force
q	state vector

T - T(t)	kinetic energy
u=u(x,t)	axial displacement of beam (positive
	u corresponds to extension of beam)
U(λ,t),U(n,t)finite Fourier transform for u(x,t)
V - V(q)	Liapunov functional
W - W(t)	work done N mm
×	axial co-ordinate m
y - y(x,t)	lateral deflection of beam mm
α	control gain N
γ	scalar positive number
δ	difference operator
Δ	total axial deflection mm
E	Bang-Bang control force modification factor m/Sec
ς	vector ϵ R
7	energy loss factor
λ	eigenvalue of the wave equation problem
ξ	vector ϵ R
ρ	
ρ_0, ρ_1	metrics
τ	time variable
ω	natural frequency of the transverse vibration
	of the heam rad/Sec

CHAPTER 1

INTRODUCTION

1.1 Active Vibration Control

Active vibration control of destributed parameter systems is an active area. One application is active control of large space structures [1-3]. Large space structures are generally lightly damped due to low structural damping in the material. Performance requirements for shape, orientation, alignment and pointing accuracy require the use of active vibration control because these systems have low frequency flexural modes.

The vibration of a distributed parameter system (DPS) is governed by one or more coupled partial differential equations (PDE's) [4] whose coefficients or parameters are, in general, functions of spatial variables and time. Three current approaches to control the vibrations of DPS include: Modal Active Control [5-7] Spectral Active Control [8] and Distributed Parameter Feedback [9,10]. Modal Active Control uses a finite number of modes to describe the motion of the vibrating DPS. A spatial description of each mode, e.g., its eigenfunction in this finite set is used to separate the total motion of the system into the motion of each of these modes. Because motion of the system in modes not included in the controlled modes always occurs, this motion results in truncation errors in the observation algorithm referred as observation spillover [5]. Spectral Active Control separates the motions of the modes using their different eigenvalues instead of the eigenfunctions used in the Modal

Active Control. This method also suffers from spillover problems associated with modes at identical eigenvalues or at eigenvalues above the operating eigenvalues of the controllers. Spatial filtering has been employed with this method to control frequency domain spillover and improve controller performance. The third approach is Distributed Parameter Feedback control, in which the system is treated as if it has infinity number of modes. To this date there are much theoretical work but few applications in the literature [11].

Active parametric control discussed here uses controlled parameter fluctuation to control transverse vibration. It is well known that transverse and longitudinal vibrations of a beam are coupled [12]. If a transversally vibrating rod is subjected to time dependent axial force; P(t), Figure 1.1 at its moving boundary, a parametric time varying force p(x,t) will be produced. If the force P(t) is applied with an appropriate control algorithm, the induced parametric time varying force will work as an active vibration control. Ball and Slemrod [20] and Ball, Marsden and Slemrod [21] studied the abstract problem of controlling a semilinear evolution equation and applied the formalism to the case of a Bernoulli-Euler beam with parametric force p(x,t)-p(t). They proved the controllability for finite-dimensional observations $(y,\partial y/\partial t)$ provided the initial data are active in all modes.

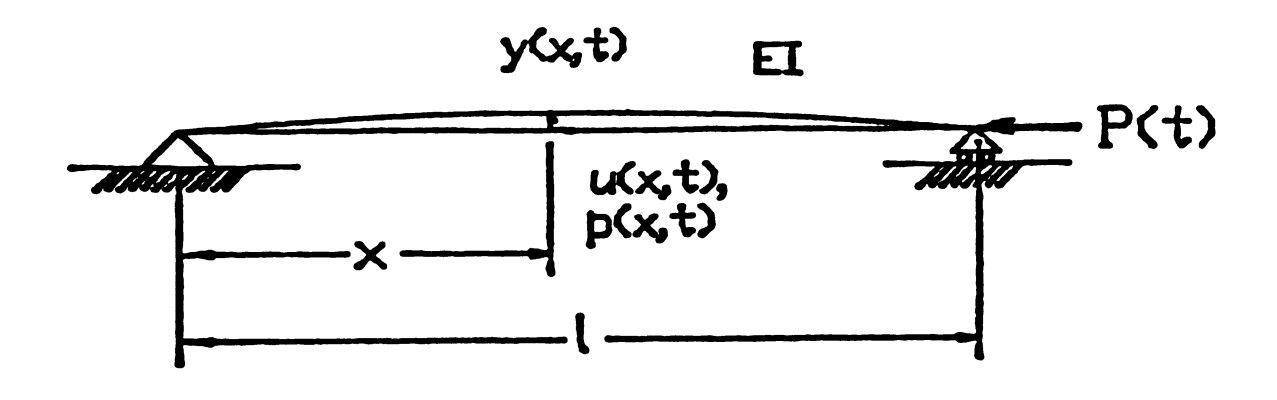


Figure 1.1 Flexible beam model

1.2 A New Approach

This dissertation presents a theoretical and experimental study for the application of the active parametric vibration control on a beam. The beam is modelled as a nonlinear, dynamic, simply-supported Bernoulli-Euler beam using the extended Hamilton principle. The direct method of Liapunov is applied to develop a control algorithm for asymptotic stability of the system. The control algorithm enables one to map from observing and controlling a theoretically infinite number of points of the domain into observing and controlling just one point to stabilize the system. Since no truncation associated with the control algorithm, the control does not suffer from the spillover problems. To demonstrate the effectiveness of the approach, a numerical finite difference approximation and an analytical solution are used to solve the closed-loop control system PDE's

Based on success with control simulations, a prototype control system was constructed to evaluate the performance of the active parametric vibration control system on a simply supported beam. The comparison of experimental system response with the simulation showed good agreement between the analytical and experimental results. Significant increases in stability of the test beam were measured and the feasibility of employing active parametric vibration control demonstrated.

1.3 Scope of Dissertation

This thesis is divided into six chapters. Following this introductory chapter, chapter 2 will develop the mathematical model of the beam and derive the control law. The mathematical model will be derived using Hamilton's principle and the control law from the direct method of Liapunov which will lead to a closed-loop system model. Chapter 3 will develop the analytical-numerical solution of this closed-loop system model. Seven simulation test cases are given to demonstrate the effectiveness of active parametric control. Chapter 4 will present the experimental facilities, procedures and results. The simply supported beam test stand design is presented. The actuator mechanisms, sensor systems and associated electronic circuits are presented. Typical experimental procedures and results are then discussed. Chapter 5 compares simulation and experiment results.

CHAPTER 2

PROBLEM FORMULATION AND ACTIVE PARAMETRIC VIBRATION CONTROL THEORY

Active parametric control is a new method for controlling the transverse vibration of an elastic beam. This chapter discusses the theoretical basis of this active control method after developing a mathematical formulation of the problem. The beam is modelled as a modified nonlinear, dynamic, Euler-Bernoulli beam using Hamilton's principle. The direct method of Liapunov is used to prove asymptotic stability, and a closed-loop system of equations are deduced. Since the main difficulty in applying the direct method of Liapunov is to choose a Liapunov functional, the energy integral procedure is given and compared to the time derivative of the Hamiltonian. In chapter 3, the closed-loop system will be simulated and results from the simulation will be discussed.

2.1 Problem Formulation

To develop a mathematical model of a structure two approaches may be used. In the first approach, the problem is formulated in terms of differential equations, which describe the local behavior of a typical infinitesimal region, and include auxiliary conditions on the motion. In the second approach, which will be used here, a variational formulation called "the principal of least action" is postulated which is valid over the whole domain of the structures.

Hamilton's principle is an example of a variational formulation which reduces the problems of dynamics to the investigation of a scalar integral which does not depend on the coordinates used. The condition rendering the value of the integral stationary leads to all the equations of motion with their admissible boundary conditions. Once Hamilton's principle is formulated, the total energy of the system can be found which is very helpful in choosing a Liapunov functional. We will consider the vibration of the beam due to excitation and elasticity in the transverse and longitudinal directions. mathematical model includes three unknown space and time-dependent quantities which characterize the beam motion in a plane: the transverse vibration y(x,t), the axial vibration u(x,t) and the axial parametric force p(x,t) (Figure 2.1). The following derivation involves the usual strength of material assumptions as to linearly elastic material behavior, small displacements, and uniform geometrical and physical properties, but neglects rotary inertia, effects due to shear strains and passive dampings. The parameters of the beam are the mass density ρ , the moment of inertia I, the modulus of elasticity E, the cross sectional area A and the length of the beam l.

The mathematical statement [22-25] of the extended Hamilton's principle is:

$$\int_{t_1}^{t_2} (\delta T + \delta W) dt = 0$$
 (2.1)

Where T is the kinetic energy and W is the the work function. The

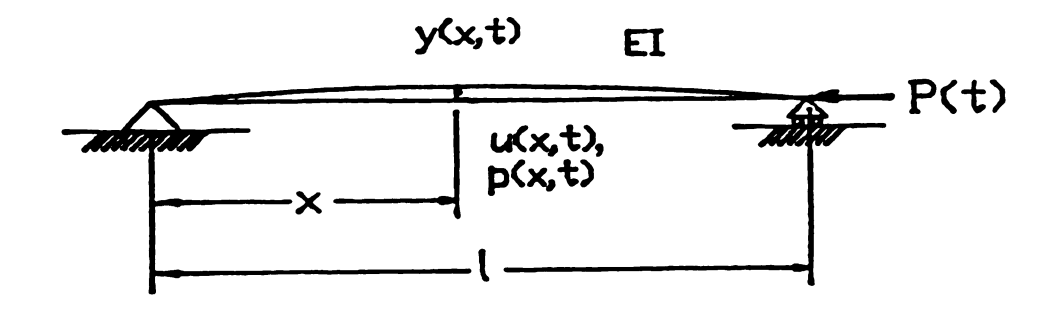


Figure 2.1a Beam configuration

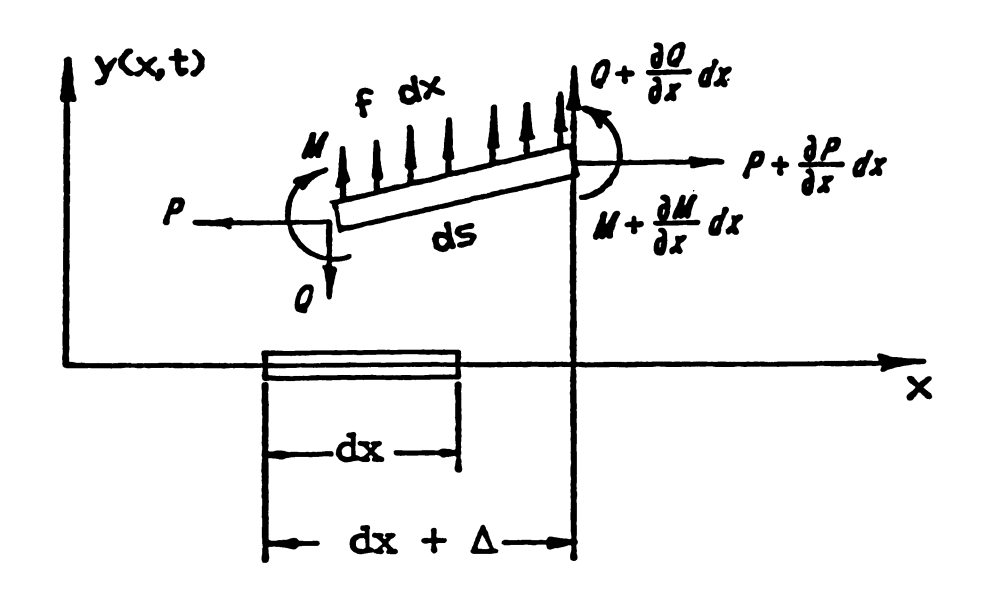


Figure 2.1b Displacements and forces acting on an infinitesimal element of length Δx

kinetic energy of the entire beam is:

$$T(t) = \frac{1}{2} \int_{0}^{\ell} \rho A \left[\frac{\partial y(x,t)}{\partial t} \right]^{2} dx + \frac{1}{2} \int_{0}^{\ell} \rho A \left[\frac{\partial u(x,t)}{\partial t} \right]^{2} dx \qquad (2.2)$$

To evaluate the work done by the axial force p(x,t) the total axial displacement Δ of the right hand end of element dx should be estimated. This total axial motion is due to the axial elastic elongation $[\partial u(x,t)/\partial x]dx$ and the change in the horizontal projection of the element ds due to bending which was initially dx, (ds - dx) (Figure 2.1), i.e.;

$$\Delta = \frac{\partial u(x,t)}{\partial x} dx + (ds - dx)$$

$$-\frac{\partial u(x,t)}{\partial x} dx + \left[(dx)^2 + \left(\frac{\partial y(x,t)}{\partial x} \right)^2 (dx)^2 \right]^{1/2} - dx$$

$$\approx \frac{\partial u(x,t)}{\partial x} dx + \frac{1}{2} \left[\frac{\partial y(x,t)}{\partial x} \right]^2 dx \qquad (2.3a)$$

where the assumption has been made that the displacements are sufficiently small that in the binomial expansion only the first two terms can be retained. The axial strain-displacement relation is given by

$$\frac{\mathbf{p}(\mathbf{x}.\mathbf{t})}{\mathbf{E}\mathbf{A}} = \frac{\partial \mathbf{u}(\mathbf{x}.\mathbf{t})}{\partial \mathbf{x}} + \frac{1}{2} \left(\frac{\partial \mathbf{y}(\mathbf{x}.\mathbf{t})}{\partial \mathbf{x}} \right)^2$$
 (2.3b)

For the purpose of derivation we assume that p(x,t) is a tensile force. We note that the force p(x,t) acts against Δ , so that the work is negative. It follows that the work function is

$$W(t) = -\frac{1}{2} \int_{0}^{\ell} EI \left[\frac{\partial^{2} y(x,t)}{\partial x^{2}} \right]^{2} dx$$

$$-\frac{1}{2} \int_{0}^{\ell} \frac{p^{2}(x,t)}{EA} dx + \int_{0}^{\ell} f(x,t) y(x,t) dx \qquad (2.4)$$

Where the first, second and third terms in the RHS of (2.4) represent the work done by the bending moment, the axial force and the transverse load respectively. The variation in kinetic energy is

$$\delta T = \int_{0}^{\ell} \rho A \frac{\partial y}{\partial t} \frac{\partial}{\partial t} (\delta y) dx + \int_{0}^{\ell} \rho A \frac{\partial u}{\partial t} \frac{\partial}{\partial t} (\delta u) dx$$

80

$$\int_{t_1}^{t_2} \delta T dt - \int_{t_1}^{t_2} \left[\int_{0}^{\ell} \rho A \frac{\partial y}{\partial t} \frac{\partial}{\partial t} (\delta y) dx + \int_{0}^{\ell} \rho A \frac{\partial u}{\partial t} \frac{\partial}{\partial t} (\delta u) dx \right] dt$$

$$-\int_{0}^{\ell} \left[\int_{t_{1}}^{t_{2}} \rho A \frac{\partial y}{\partial t} \frac{\partial}{\partial t} (\delta y) dt + \int_{t_{1}}^{t_{2}} \rho A \frac{\partial u}{\partial t} \frac{\partial}{\partial t} (\delta u) dt \right] dx$$

$$-\int_{0}^{2}\left[\rho A \frac{\partial y}{\partial t} \delta y \Big|_{t_{1}}^{t_{2}} - \int_{t_{1}}^{t_{2}} \rho A \left(\frac{\partial^{2} y}{\partial t^{2}}\right) \delta y dt + \rho A \frac{\partial u}{\partial t} \delta u \Big|_{t_{1}}^{t_{2}}\right]$$

$$-\int_{t_1}^{t_2} \rho A \frac{\partial^2 u}{\partial t^2} \delta u dt dt dx$$

$$- \int_{t_1}^{t_2} \left[\int_{0}^{\ell} \rho A \frac{\partial^2 v}{\partial t^2} \delta y \, dx + \int_{0}^{\ell} \rho A \frac{\partial^2 u}{\partial t^2} \delta u \, dx \right] dt \qquad (2.5)$$

The boundary terms vanish because, by definition, $\delta y(x,t)$ and, $\delta u(x,t)$ are zero at $t = t_1$ and t_2 . The virtual work can be written

$$\delta W = -\int_{0}^{\ell} EI \frac{\partial^{2} y}{\partial x} \frac{\partial^{2} z}{\partial x} (\delta y) dx - \int_{0}^{\ell} \frac{D}{EA} \delta p dx + \int_{0}^{\ell} f \delta y dx$$

using (2.3b) to find $\delta p(x,t)/EA$ yields

$$\delta W = -\int_{0}^{\ell} EI \frac{\partial^{2} y}{\partial x} \frac{\partial^{2}}{\partial x} (\delta y) dx - \int_{0}^{\ell} p \frac{\partial}{\partial x} (\delta u) dx$$

$$-\int_{0}^{\ell} p \frac{\partial y}{\partial x} \frac{\partial}{\partial x} (\delta y) dx + \int_{0}^{\ell} f \delta y dx$$

Integrating by parts yields

$$\delta W = - EI \frac{\partial^{2} y}{\partial x^{2}} \frac{\partial}{\partial x} (\delta y) \Big|_{0}^{\ell} + EI \frac{\partial^{3} y}{\partial x^{3}} \delta y \Big|_{0}^{\ell} - \int_{0}^{\ell} EI \frac{\partial^{4} y}{\partial x^{4}} \delta y \, dx - p \, \delta u \Big|_{0}^{\ell}$$
$$+ \int_{0}^{\ell} \frac{\partial p}{\partial x} \delta u \, dx - p \, \frac{\partial y}{\partial x} \delta y \Big|_{0}^{\ell} + \int_{0}^{\ell} \frac{\partial}{\partial x} \left(p \, \frac{\partial y}{\partial x} \right) \delta y \, dx$$

$$+\int_{0}^{\ell} f \, \delta y \, dx$$

$$- - \int_{0}^{\ell} \left[EI \frac{\partial_{-\mathbf{y}}^{4}}{\partial \mathbf{x}} - \frac{\partial_{-\mathbf{x}}}{\partial \mathbf{x}} \left(p \frac{\partial \mathbf{y}}{\partial \mathbf{x}} \right) - f \right] \delta \mathbf{y} \ d\mathbf{x} - EI \frac{\partial_{-\mathbf{y}}^{2}}{\partial \mathbf{x}} \frac{\partial_{-\mathbf{x}}}{\partial \mathbf{x}} (\delta \mathbf{y}) \Big|_{0}^{\ell}$$

+
$$\left[\text{ EI } \frac{\partial^{3} \mathbf{y}}{\partial \mathbf{x}} - \mathbf{p} \frac{\partial \mathbf{y}}{\partial \mathbf{x}} \right] \delta \mathbf{y} \Big|_{0}^{\ell} + \int_{0}^{\ell} \frac{\partial \mathbf{p}}{\partial \mathbf{x}} \delta \mathbf{u} \, d\mathbf{x} - \mathbf{p} \delta \mathbf{u} \Big|_{0}^{\ell}$$
 (2.6)

Introducing (2.5) and (2.6) in (2.1) we obtain

$$-\int_{t_1}^{t_2} \left[\int_{0}^{\ell} \left[EI \frac{\partial^4 y}{\partial x^4} - \frac{\partial}{\partial x} \left(p \frac{\partial y}{\partial x} \right) + \rho A \frac{\partial^2 y}{\partial t^2} - f \right] \delta y \ dx \right]$$

- EI
$$\frac{\partial^2 y}{\partial x^2} \delta \left(\frac{\partial y}{\partial x} \right) \Big|_0^{\ell}$$
 + $\left[EI \frac{\partial^3 y}{\partial x^3} - p \frac{\partial y}{\partial x} \right] \delta y \Big|_0^{\ell}$

$$+ \int_{0}^{\ell} \left[\frac{\partial \mathbf{p}}{\partial \mathbf{x}} - \rho \mathbf{A} \frac{\partial^{2} \mathbf{u}}{\partial \mathbf{t}^{2}} \right] \delta \mathbf{u} \, d\mathbf{x} + \mathbf{p} \, \delta \mathbf{u} \Big|_{0}^{\ell} \right] d\mathbf{t} = 0$$
 (2.7)

The integral must vanish for any arbitrary values of δy , $\delta(\partial y/\partial x)$, and δu , which obey the essential boundary conditions. Because each term

above is independent and the variations are arbitrary, each term in the equation must vanish. The first and fourth terms are integrals which yield the Euler equations

$$EI \frac{\partial^{4} y}{\partial x} - \frac{\partial}{\partial x} \left(p \frac{\partial y}{\partial x} \right) + \rho A \frac{\partial^{2} y}{\partial t^{2}} - f \qquad (2.8)$$

$$-\frac{\partial \mathbf{p}}{\partial \mathbf{x}} + \rho \mathbf{A} \frac{\partial^2 \mathbf{u}}{\partial \mathbf{t}^2} = 0 \tag{2.9}$$

which are the differential equations of motion for the beam. Furthermore, if we consider the boundary terms in (2.7), the nature of arbitrary variations yields

$$EI \frac{\partial^2 y}{\partial x^2} \delta \left(\frac{\partial y}{\partial x} \right) \Big|_0^{\ell} = 0$$
 (2.10a)

$$\left[EI \frac{\partial^{3} y}{\partial x} - p \frac{\partial y}{\partial x} \right] \delta y \Big|_{0}^{\ell} - 0$$
 (2.10b)

$$p \delta u \Big|_{0}^{\ell} = 0 \tag{2.11}$$

Equations (2.10) allow the possibilities that either

EI
$$\frac{\partial^2 y}{\partial x^2} = 0$$
 or $\delta \left[\frac{\partial y}{\partial x} \right] = 0$ at $x = 0$, ℓ (2.12a)

and that

EI
$$\frac{\partial^{3} y}{\partial x}$$
 - p $\frac{\partial y}{\partial x}$ - 0 or δy - 0 at x - 0, ℓ (2.12b)

Admissible variations are those for which $\delta(\partial y/\partial x)$ and δy vanish at the boundaries, e.g. admissible functions, y(x,t) always satisfy the low order boundary conditions. Equation (2.11) allows the possibility that either δu or p vanishes at either end; i.e.;

$$p = 0$$
 or $\delta u = 0$ at $x = 0$, ℓ (2.13)

If the beam is clamped at the end x = 0, the boundary condition is

$$u(0,t) = 0$$
 (2.14a)

and p(x,t) can be any force. If a force P(t) is applied at the end $x = \ell$, we will have

$$p(\ell,t) - P(t) \tag{2.14b}$$

and u(x,t) must satisfy the displacement condition at x = l exactly. Equations (2.10 to 2.13) represent the admissible boundary conditions. The equations (2.12a) require either the vanishing of the bending moment or requires exact satisfaction of the slope boundary conditions at each end. The equations (2.12b) require either the vertical force is zero or that admissible functions exactly satisfy the deflection boundary conditions at each end. Restricting ourselves to simply supported beam, the mathematical model is given by equations (2.8, 2.9 and 2.3b) with the boundary conditions given by first of (2.12a),

the second condition of (2.12b) and (2.14a, b). Now we can write the governing equations of motion of the open-loop system:

$$EI \frac{\partial^{4} y}{\partial x} - \frac{\partial}{\partial x} \left(p \frac{\partial y}{\partial x} \right) + \rho A \frac{\partial^{2} y}{\partial t} - f(x,t) \qquad (2.15a)$$

$$-\frac{\partial \mathbf{p}}{\partial \mathbf{x}} + \rho \mathbf{A} \frac{\partial^2 \mathbf{u}}{\partial \mathbf{t}^2} = 0 \tag{2.15b}$$

$$\frac{\mathbf{p}}{\mathbf{E}\mathbf{A}} = \frac{\partial \mathbf{u}}{\partial \mathbf{x}} + \frac{1}{2} \left(\frac{\partial \mathbf{y}}{\partial \mathbf{x}} \right)^2 \tag{2.15c}$$

with the appropriate boundary conditions

$$y(0,t) - y(\ell,t) = 0$$
 (2.16a)

$$\frac{\partial^2 y(0,t)}{\partial x^2} = \frac{\partial^2 y(\ell,t)}{\partial x} = 0$$
 (2.16b)

$$u(0,t) = 0$$
 (2.16c)

$$EA \left[\frac{\partial u(l,t)}{\partial x} + \frac{1}{2} \left(\frac{\partial y(l,t)}{\partial x} \right)^{2} \right] = P(t)$$
 (2.16d)

and the initial conditions

$$y(x,0) = f_1(x)$$
 $0 \le x \le l$ (2.17a)

$$\frac{\partial y(x,0)}{\partial r} = f_2(x) \qquad 0 \le x \le \ell \qquad (2.17b)$$

$$u(x,0) - g_1(x) \qquad 0 \le x \le \ell \qquad (2.17c)$$

$$\frac{\partial \mathbf{u}(\mathbf{x},0)}{\partial \mathbf{r}} = 0 \qquad 0 \le \mathbf{x} \le \ell \qquad (2.17d)$$

where $f_1(x)$ and $f_2(x)$ are the initial displacement and initial velocity distributions in the y-direction respectively. The function $g_1(x)$ is the initial displacement distribution in the x-direction. Equation (2.15a) expresses equilibrium of the beam in the transverse direction, equation (2.15b) expresses equilibrium of the beam in the axial direction and equation(2.15c) is the axial strain displacement relation. Equations (2.15) with their boundary and initial conditions, represent a complete system of equations for determining the three unknowns y(x,t), u(x,t) and p(x,t). Versions of this system of equations can be found in the literature [26-31 especially 29] concerned with the bending of columns under dynamically applied axial loads. The system of equations derived here from the energy functional indicates the accuracy of the functional which will be used to derive a parametric control law.

2.2 Stability Analysis

The active parametric vibration control theory is based upon using one of the time dependent distributed parameters to control transverse displacement under specific control law. It is clear that equation (2.15a) contains the parametric force p(x,t) as a

coefficient, our objective is to find a control law by which p(x,t) can be manipulated and transform the open-loop system into an asymptotically stable system. For the analysis of the stability of distributed parameter systems the direct method of Liapunov is used. We define a Liapunov functional which properly describes a kind of energy distribution of the system, and it is the purpose of the direct method to indicate whether the energy is always decreasing to zero. If this is the case then the system is asymptotically stable. The necessary theorem concerning stability of a partial differential equation system has been given by Zubov [32] and Wang [33,34]. The essence of such a theorem is to extend the Liapunov stability theory from a finite dimensional space to a space of infinite dimensions and the realm of partial differential equations. As with the simpler n-dimensional space method, the determination of the Liapunov functional V is the main difficulty [35].

2.2.1 Liapunov functional for asymptotic stability

Leipholz [36] showed the close connection between Liapunov's stability criterion and the classical energy (Hamiltonian, H) criterion, for autonomous, dynamic, continuous systems. He proved that for a conservative system, if V is chosen as the Hamiltonian, then

$$\frac{dV}{dt} - \frac{dH}{dt} - 0 \tag{2.18}$$

and for nonconservative system,

$$\frac{dV}{dt} - \frac{dH}{dt} - \int_{V_0} Q \dot{q} dV_0 \qquad (2.19)$$

where Q is the vector of generalized forces, \dot{q} is the derivative of the state vector q with respect to t and V_0 is the volume of the system. For a non-conservative system, the stability problem is more complicated. Leipholz's work showed that even then it might be advisable to use H as V [36,37]. Here, we choose V as the total internal energy of the system:

$$V(q) = T - W$$

$$-\frac{1}{2}\int_{0}^{\ell}\left[\rho A\left(\frac{\partial y}{\partial t}\right)^{2}+\rho A\left(\frac{\partial u}{\partial t}\right)^{2}+EI\left(\frac{\partial^{2} y}{\partial x^{2}}\right)^{2}\right]$$

$$+ \frac{p^2}{EA} \int dx \qquad (2.20)$$

where f(x,t) = 0. By using (2.15c) and if the velocities Y = Y(x,t) and U = U(x,t) are introduced where;

$$Y(x,t) = \frac{\partial y(x,t)}{\partial t}$$
, $U(x,t) = \frac{\partial u(x,t)}{\partial t}$

(2.20) becomes

$$V(q) = \frac{1}{2} \int_{0}^{\ell} \left[\rho A Y^{2} + \rho A U^{2} + EI \left(\frac{\partial^{2} Y}{\partial x^{2}} \right)^{2} + \frac{p^{2}}{EA} \right] dx$$
 (2.21)

It is also convenient to introduce the notation of vector q,

$$\mathbf{q}^{\mathbf{T}} - [Y U y p] \tag{2.22}$$

Then we can say that the vector q = 0 corresponds to the undeformed equilibrium position of the beam. The sign of V(q) and of its time derivative will be investigated [38]. Let us also introduce the auxiliary vectors ζ and ξ as

$$\xi^{T} = [\xi_{1}, \xi_{2}, \xi_{3}, \xi_{4}], \qquad \xi^{T} = [\xi_{1}, \xi_{2}, \xi_{3}, \xi_{4}] \qquad (2.23)$$

so that we can introduce also the metric $\rho_1(\zeta,\xi)$,

$$\rho_1(\zeta,\xi) = (1/2)^{\frac{1}{2}} \left[\rho A(\zeta_1 - \xi_1)^2 + \rho A(\zeta_1 - \xi_1)^2 \right]$$

+ EI
$$\left[\frac{\partial^2}{\partial x^2}(\zeta_3 - \xi_3)\right]^2 dx$$
 $\left[\frac{\partial^2}{\partial x^2}(\zeta_3 - \xi_3)\right]^2 dx$ (2.24)

It then follows that

$$\rho_{1}(q,0) = \left[\frac{1}{2}\int_{0}^{\ell} \left(\rho A Y^{2} + \rho A U^{2} + EI\left(\frac{\partial^{2} Y}{\partial x}\right)^{2}\right) dx\right]^{1/2}$$
 (2.25)

Thus $\rho_1(q,0)$ is a measure of the distance between the equilibrium state q=0 and the deformed state $q\neq 0$, further, if $\rho_1(q,0)$ is small, then each of the terms

$$\int_{0}^{\ell} \rho A Y^{2} dx, \qquad \int_{0}^{\ell} \rho a U^{2} dx \qquad \text{and} \qquad \int_{0}^{\ell} EI \left(\frac{\partial^{2} Y}{\partial x^{2}}\right)^{2}$$

must then be small, as the integrand of $\rho_1(q,0)$ is sum of these non-negative terms. It is clear that the metric $\rho_1(\zeta,\xi)$ satisfies the following properties [39]

- (i) $\rho_1(\zeta,\xi) \ge 0$, $\rho_1(\zeta,\xi) = 0$ if and only if $\zeta = \xi$
- (ii) $\rho_1(\zeta,\xi) = \rho_1(\xi,\zeta)$ (symmetry)
- (iii) $\rho_1(\zeta,\chi) \leq \rho_1(\zeta,\xi) + \rho_1(\xi,\chi)$ (the triangular inequality) where χ is a four dimensional vector. So the chosen metric $\rho_1(q,0)$ is a metric space in the Euclidean space R. To prove the stability of the equilibrium state q=0 we must prove that
- (a) V(q) is positive definite with respect to the metric $\rho_1(q,0)$;
- (b) V(q) admits an infinitely small upper bound in the neighborhood of q = 0; and
- (c) investigate the sign of dV(q)/dt.
- a) To prove that V(q) is positive definite; comparing (2.21) with (2.25) yields

$$V(q) \ge \alpha_1 \rho_1^2(q,0) \ge 0$$
 (2.26)

where α_1 is positive constant = 1 in this case. The equality holds only when q = 0. Therefore V(q) is positive definite since $\rho_1^2(q,0)$ is positive definite.

b) To prove that V(q) admits an infinitely small upper bound in the neighborhood of q=0; equivalently this requires that

$$V(q) \le \gamma \rho_0^2(q,0) \tag{2.27}$$

where γ is positive constant. The reason for this is to allow continuity of the solution of the PDEs (equations(2.15 and 2.16))with respect to the initial data (2.17). Thus by limiting the size of the initial disturbances $f_1(x)$ and $f_2(x)$, a bound can be placed on the response. If we choose

$$\gamma \ge 1 \text{ and } \rho_0^2 (q,0) - V(q,0)$$
 (2.28)

then (2.27) is true and requirement (b) is satisfied. The relation between the metrics ρ_1 and ρ_0 is given by

$$\rho_1^2 - \rho_0^2 - \frac{1}{2} \int_{0}^{\ell_{\frac{D}{2}}} dx \qquad (2.29a)$$

It is clear that ho_1 depends continuously on ho_0 and since

$$\frac{1}{2} \int_{0}^{2} \frac{\ell_{p}^{2}}{EA} dx > 0 \qquad \text{for } p > 0 \quad \text{and} \quad t \ge 0$$

therefore
$$\rho_0 > \rho_1$$
 for all $t \ge 0$ (2.29b)

then by (2.26 to 2.29) we get

$$\rho_1^2 (q,0) \le V(q) \le \gamma \rho_0^2 (q,0)$$
 (2.30)

c) Finally we need to examine the time derivative of V(q),

$$V(q) = V(y_{xx}, y_t, p, u_t)$$

$$\frac{dV(q)}{dt} = \frac{\partial V}{\partial y_{xx}} \frac{\partial y_{xx}}{\partial t} + \frac{\partial V}{\partial y_{t}} \frac{\partial y_{t}}{\partial t} + \frac{\partial V}{\partial p} \frac{\partial p}{\partial t} + \frac{\partial V}{\partial u} \frac{\partial u_{t}}{\partial t}$$
(2.31)

substituting (2.20) into (2.31) and making use of the boundary conditions (2.16) yields

$$\frac{dV(q)}{dt} = \int_{0}^{\ell} \left(EI y_{xx} y_{xxt} + \rho A y_{t} y_{tt} + \frac{pp_{t}}{EA} + \rho A u_{t} u_{tt} \right) dx$$

$$-\int_{0}^{\ell} \left(EI y_{xx} dy_{xt} + \int_{0}^{\ell} \rho A y_{t} y_{tt} dx + \int_{0}^{\ell} p \left(u_{xt} + y_{x} y_{xt} \right) dx \right)$$

$$+\int_{0}^{\ell} \rho A u_{t} u_{tt} dx$$

after integration by parts,

$$\frac{dV}{dt} - \int_{0}^{\ell} EI y_{xxxx} y_{t} dx + \int_{0}^{\ell} \rho A y_{t} y_{tt}^{+} \int_{0}^{\ell} p(u_{xt} + y_{x} y_{xt}) dx$$

$$+\int_{0}^{l} \rho A u_{t} u_{tt} dx$$

When the appropriate boundary conditions are applied,

$$\frac{dV}{dt} - \int_{0}^{\ell} \left(EI y_{xxxx} - \left[p y_{x} \right]_{x} + \rho A y_{tt} \right) y_{t} dx$$

$$+ \int_{0}^{\ell} \left(\rho A u_{tt} - p_{x} \right) u_{t} dx + p u_{t} \Big|_{0}^{\ell}$$

After making use of the equation of motion,

$$\frac{dV}{dt} - p(\ell, t) u_t (\ell, t) - P(t) u_t(\ell, t)$$
 (2.32)

which is of the form of (2.19).

The sign of $p(\ell,t)$ u $_{\ell}(\ell,t)$ is not known in general for all t>0, hence, the sign of dV(q)/dt undetermined. The stability of the system can not be judged unless the sign of dV/dt is guaranteed by some relationship between the applied force, P and velocity on the end of the beam.

Definition: Let d be a positive real number. The neighborhood S(o,d) of q=0 is defined as the set of q which belongs to the admissible

states for the system for which $0 \le \rho_0(q,0) < d$ where $\rho_0(q,0)$ is a metric measuring the distance between the equilibrium state q = 0 and the deformed state q = q. Now let us state the stability theorem by Zubov [32-34]:

In order for the solution q = 0 of the boundary value problem to be stable with respect to ρ_0 and ρ_1 , where ρ_1 depends continuously on ρ_0 , it is necessary and sufficient that in a sufficiently small neighborhood S(0,d) of q = 0 there exists a functional V having the following properties when $q \in S(0,d)$:

- 1) V is positive definite with respect to ρ_1 ;
- 2) V admits an infinitely small upper bound with respect to ρ_0 ;
- 3) $V(q(t,q^0))$ is non-increasing for $t \ge 0$, whenever $q^0 \in S(0,d)$. If, in addition, there exists a d', $0 < d' \le d$, such that.
- 4) $V(q(t,q^0)) \rightarrow 0$ as $t \rightarrow \infty$ whenever $q^0 \in S(0,d')$, then q = 0 is asymptotically stable with respect to ρ_0 and ρ_1

Properties 1 and 2 require

$$\rho_1^2$$
 (q,0) $\leq V(q) \leq \gamma \rho_0^2(q,0)$

which is inequality (2.30) given as a result of the discussion in subsection 2.2.1 items a and b. And if we force

$$P(t) u_t(\ell,t) < 0$$
 for all $t > 0$ (2.33)

Then dV/dt < 0 i.e. negative definite, therefore properties 3 and 4 are proven, and the system given by (2.15,2.16 and 2.17) is asymptotically stable subject to (2.33). Now any active control algorithm given by:

$$P(t) = g (u_{t}(l,t))$$
 (2.34)

where g (u_t (ℓ ,t)) is some function that depends on $\partial u(\ell,t)/\partial t$, and satisfies (2.33) will yield asymptotic stability. In the $\partial u(\ell,t)/\partial t$ - P(t) plane, any force in the second or fourth quadrant results in closed-loop asymptotic stability of the beam system. The control force shown in Figure 2.2 satisfies this condition. Figure 2.3 shows the structure of the active vibration control using this force.

It is worthwhile to mention that if we already have the mathematical model (2.15 to 2.17) and we wish to construct the energy integral of the given system by which a Liapunov functional and its total time derivative can be deduced easily, the following procedure may be suggested:

Multiply (2.15a) across by $\partial y/\partial t$, integrate over ℓ and use the boundary conditions to get;

$$\frac{1}{2} \frac{\partial}{\partial t} \int_{0}^{\ell} \left[EI \left(\frac{\partial^{2} y}{\partial x^{2}} \right)^{2} + \rho A \left(\frac{\partial y}{\partial t} \right)^{2} \right] dx$$

$$- - \int_{0}^{\ell} p \frac{\partial y}{\partial x} \frac{\partial^{2} y}{\partial x \partial t} dx = - \frac{1}{2} \int_{0}^{\ell} p \frac{\partial}{\partial t} \left(\frac{\partial y}{\partial x} \right)^{2} dx$$
 (2.36a)

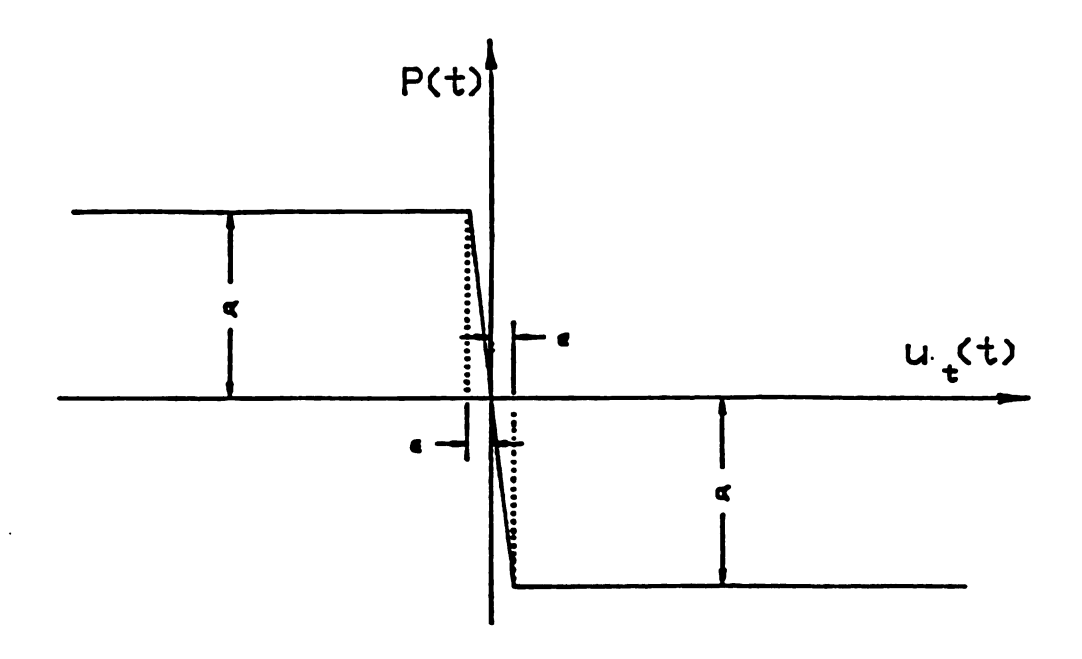


Figure 2.2 Modified bang-bang control force

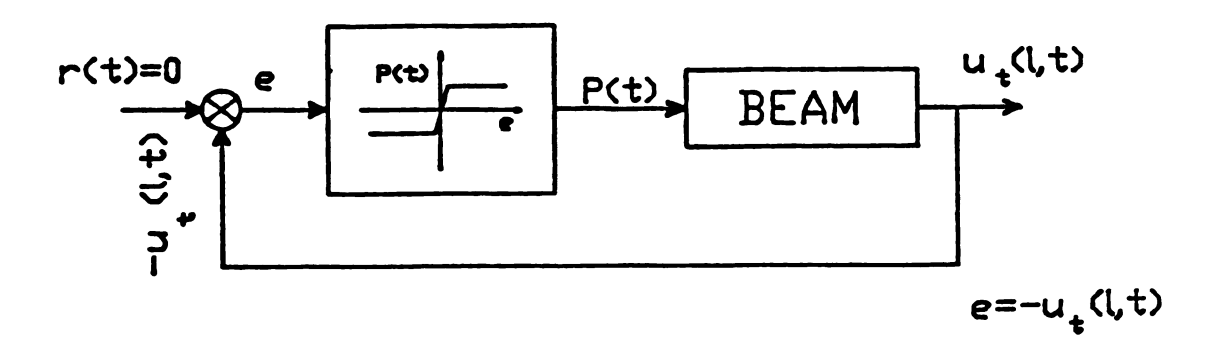


Figure 2.3 Active vibration control

By making use of (2.15c), equation (2.36a) becomes

$$\frac{1}{2} \frac{\partial}{\partial t} \int_{0}^{\ell} \left[EI \left(\frac{\partial^{2} y}{\partial x^{2}} \right)^{2} + \rho A \left(\frac{\partial y}{\partial t} \right)^{2} \right] dx$$

$$= -\frac{1}{2} \int_{0}^{\ell} p \frac{\partial}{\partial t} \left(\frac{2p}{EA} - 2 \frac{\partial u}{\partial x} \right) dx$$

$$= -\int_{0}^{\ell} \frac{\partial p}{EA} \frac{\partial p}{\partial t} dx + \int_{0}^{\ell} p \frac{\partial^{2} u}{\partial x \partial t} dx$$

$$= -\frac{1}{2} \frac{\partial}{\partial t} \int_{0}^{\ell} \frac{p^{2}}{EA} dx + \int_{0}^{\ell} p \frac{\partial^{2} u}{\partial x \partial t} dx \qquad (2.36b)$$

Now multiply (2.15b) across by $\partial u/\partial t$, integrate over ℓ and use the boundary conditions; yielding

$$\frac{1}{2} \frac{\partial}{\partial t} \int_{0}^{\ell} \rho A \left(\frac{\partial u}{\partial t} \right)^{2} dx - \int_{0}^{\ell} \frac{\partial p}{\partial x} \frac{\partial u}{\partial t} dx$$

-
$$P(t) \frac{\partial u(\ell, t)}{\partial t} - \int_{0}^{\ell} p \frac{\partial^{2} u}{\partial x \partial t} dx$$
 (2.37a)

(2.36b)

From which

$$\int_{0}^{\ell} p \frac{\partial^{2} u}{\partial x \partial t} dx - P(t) \frac{\partial u(\ell, t)}{\partial t} - \frac{1}{2} \frac{\partial}{\partial t} \int_{0}^{\ell} \rho A \left(\frac{\partial u}{\partial t} \right)^{2} dx \qquad (2.37b)$$

$$\frac{1}{2} \frac{\partial}{\partial t} \int_{0}^{A} \left[EI \left(\frac{\partial^{2} y}{\partial x^{2}} \right)^{2} + \rho A \left(\frac{\partial y}{\partial t} \right)^{2} + \frac{p}{EA} + \rho A \left(\frac{\partial u}{\partial t} \right)^{2} \right] dx$$

$$- P(t) \frac{\partial u(l,t)}{\partial t}$$
 (2.38a)

If we take V(q) as

$$V(q) = \frac{1}{2} \int_{0}^{\ell} \left[EI \left(\frac{\partial^{2} y}{\partial x^{2}} \right)^{2} + \rho A \left(\frac{\partial y}{\partial t} \right)^{2} + \frac{p^{2}}{EA} + \rho A \left(\frac{\partial u}{\partial t} \right)^{2} \right] dx$$
(2.38b)

Then (2.38a) can be written as:

$$\frac{dV(q)}{dt} = P(t) \frac{\partial u(l,t)}{\partial t}$$
 (2.38c)

By comparing (2.38c) with (2.32) we find that both the the infinitesimal and the variational approaches yield the same result. In fact this procedure yields a relationship between the rate of change of the total internal energy of the system with respect to time and the external power applied on the system which agrees with (2.19).

In this chapter the theoretical basis of the active parametric control theory for controlling an elastic beam was presented. The mathematical model was derived using Hamilton's principle which led to a modified nonlinear, dynamic, Bernoulli-Euler beam. Also asymptotic stability using the direct method of the Liapunov was proven from which the closed-loop control system was deduced. The energy integral

as an alternative procedure and the time derivative of the internal energy led to the same result.

CHAPTER 3

ANALYTICAL-NUMERICAL SOLUTION

To see the effectiveness of the approach, the closed-loop control system is simulated. An analytical-numerical solution of the closed-loop control system is presented in section 3.1 and 3.2 followed by section 3.3 which discusses the steps of solution. The numerical-analytical results of the closed-loop system simulation are given and discussed in section 3.4. The simulation results show the effectiveness of the closed-loop control law derived in chapter 2 from the Liapunov function for the beam.

3.1 Analytical Solution For Beam Axial Motion

This subsection presents the analytical solution of the wave equation which gives beam axial motion. The two governing equations of motion of the closed-loop system are coupled and nonlinear ingeneral, and it has not been possible to find an analytical solution to the beam equations. However, an analytical solution for the wave equation can be obtained from which the parametric force p(x,t) coupling the two equations can be evaluated and used in the approximate solution of the parabolic equation modelling beam transverse motion.

The axial force p(x,t) may be eliminated when combining (2.15b) and (2.15c) to yield

$$\frac{\partial^2 \mathbf{u}}{\partial \mathbf{t}} - \mathbf{a}^2 \frac{\partial^2 \mathbf{u}}{\partial \mathbf{x}} = \frac{\partial \phi(\mathbf{x}, \mathbf{t})}{\partial \mathbf{x}}$$
(3.1a)

where

$$a^2 - \frac{E}{\rho} ,$$

$$\phi(x,t) = \frac{a^2}{2} \left(\frac{\partial y}{\partial x} \right)^2$$
 (3.1b)

This is recognized as a nonhomogeneous wave equation for u, subject to the nonhomogeneous boundary conditions of (2.16d). A formal solution of (3.1a) can be obtained using Finite Fourier Transform [14]. Let the Finite sine transform of u(x,t) be defined by

$$U(\lambda,t) = \int_0^L u(x,t) \sin \lambda x \, dx \qquad (3.2a)$$

where λ^2 is the eigenvalue to be determined. In addition, the Fourier sine transform of $\frac{\partial^2 u(x,t)}{\partial x}$ is given by

$$U^{(2)}(\lambda,t) - \int_{0}^{\ell} \frac{\partial^{2} u(x,t)}{\partial x^{2}} \sin \lambda x \, dx$$

$$-\frac{\partial \mathbf{u}}{\partial \mathbf{x}} \sin \lambda \mathbf{x} \Big|_{0}^{\ell} - \lambda \int_{0}^{\ell} \frac{\partial \mathbf{u}}{\partial \mathbf{x}} \cos \lambda \mathbf{x} \, d\mathbf{x}$$

$$U^{(2)}(\lambda,t) = \frac{\partial u(\ell,t)}{\partial x} \sin \lambda \ell - \lambda [u(x,t) \cos \lambda x] \Big|_{0}^{\ell}$$

$$-\lambda^2\int_0^\ell u(x,t) \sin \lambda x \, dx$$

$$= \frac{\partial u(\ell, t)}{\partial x} \sin \lambda \ell - \lambda u(\ell, t) \cos \lambda \ell - \lambda^2 U(\lambda, t)$$
 (3.2b)

where the boundary conditions have been used. Since $u(\ell,t)$ is not available we search for eigensolutions with $\cos \lambda \ell = 0$, which leads to

$$\lambda = (2n - 1) \frac{\pi}{2\ell}; \qquad n = 1, 2, 3, \dots$$
 (3.2c)

It follows that

$$\sin \lambda \ell - \sin (2n - 1) \frac{\pi}{2} - (-1)^{n-1}; n - 1, 2, ...$$
 (3.2d)

Transforming (3.1a) we obtain

$$\frac{d^2U(n,t)}{dt^2} + \left[(2n-1) \frac{\pi a}{2\ell} \right]^2 U(n,t)$$

$$-(-1)^{n-1} a^2 \frac{\partial u(\ell,t)}{\partial x} - (2n-1) \frac{\pi}{2\ell} \int_0^\ell \phi(x,t) \cos(2n-1) \frac{\pi ax}{2\ell} dx$$

$$+ \phi(\ell,t)(-1)^{n-1}$$
 (3.2e)

since

$$\int_{0}^{\ell} \frac{\partial \phi(\mathbf{x},t)}{\partial \mathbf{x}} \sin \lambda \mathbf{x} \, d\mathbf{x} = -\lambda \int_{0}^{\ell} \phi(\mathbf{x},t) \cos \lambda \, d\mathbf{x} + \phi(\ell,t)(-1)^{n-1}$$

therefore

$$U(n,t) = \frac{2\ell a(-1)^{n-1}}{\pi(2n-1)} \int_{0}^{t} \frac{\partial u(\ell,r)}{\partial x} \sin(2n-1) \frac{\pi a}{2\ell} (t-r) dr$$

$$-\frac{1}{a} \int_{0}^{t} \sin(2n-1) \frac{\pi a}{2\ell} (t-r) \int_{0}^{\ell} \phi(x,r) \cos(2n-1) \frac{\pi a}{2\ell} x \, dx dr$$

$$+\frac{2\ell (-1)^{n-1}}{a\pi(2n-1)} \int_{0}^{\ell} \phi(\ell,\tau) \sin(2n-1) \frac{\pi a}{2\ell} (t-\tau) d\tau$$

+
$$U(n,0) \cos(2n-1) \frac{\pi a}{2l} t$$
 (3.2f)

where
$$U(n,0) = \int_{0}^{\ell} u(x,0) \sin \lambda t$$

The corresponding inverse formula of (3.2a) is

$$u(x,t) = \frac{2}{\ell} \sum_{n=1}^{\infty} U(n,t) \sin(2n-1) \frac{\pi x}{2\ell}$$
 (3.3a)

which yields

$$u(x,t) - \frac{2}{l} \sum_{n=1}^{\infty} \left[\sin(2n - 1) \frac{\pi x}{2l} \left(\frac{2la(-1)^{n-1}}{\pi(2n-1)} \right) \right]$$

$$\int_{0}^{t} \frac{\partial u}{\partial x} (l, \tau) \sin(2n-1) \frac{\pi a}{2l} (t-\tau) d\tau$$

$$-\frac{1}{a}\int_{0}^{t}\sin(2n-1)\frac{\pi a}{2\ell}(t-r)\int_{0}^{\ell}\phi(x,r)\cos(2n-1)\frac{\pi a}{2\ell}xdxdr$$

+
$$\frac{2l(-1)^{n-1}}{a\pi(2n-1)} \int_{0}^{l} \phi(l,r) \sin(2n-1) \frac{\pi a}{2l} (t-r) dr$$

+
$$U(n,0) \cos(2n-1) \frac{\pi a}{2l} t$$
 (3.3b)

Therefore the distributed parameter force (2.3b) is given by

$$p(x,t) - EA \frac{\partial u}{\partial x} + \frac{EA}{2} \left(\frac{\partial y}{\partial x} \right)^2$$

$$- EA \frac{\partial u}{\partial x} + \frac{\phi EA}{a^2}$$
 (3.4a)

where $\partial u/\partial x$ is given by

$$\frac{\partial u(x,t)}{\partial x} = \sum_{n=1}^{\infty} \cos(2n-1) \frac{\pi x}{2\ell} \left[\frac{2 \cdot a(-1)^{n-1}}{\ell} \right]$$

$$\int_{0}^{t} \left(\frac{P(\tau)}{EA} - \frac{1}{2} \left[\frac{\partial y(\ell, \tau)}{\partial x} \right]^{2} \right) \sin(2n - 1) \frac{\pi a}{2\ell} d\tau$$

$$-\frac{2n-1}{n\ell^2}\int_0^t\int_0^{\ell}\sin(2n-1)\frac{\pi a}{2\ell}(t-r)\phi(x,r)\cos(2n-1)\frac{\pi a}{2\ell}x\,dx\,dr$$

$$+ \frac{2 (-1)^{n-1}}{\ell a} \int_{0}^{t} \phi(\ell, \tau) \sin(2n-1) \frac{\pi a}{2\ell} (t-\tau) d\tau + \frac{(2n-1)\pi}{\ell^{2}}$$

$$U(n,0) \cos(2n-1) \frac{\pi a}{2\ell} t$$
 (3.4b)

3.2 Numerical Solution of the Parabolic Equation.

Equation (2.15a) is a nonlinear parabolic equation. Since no analytic solution is known for this equation with its boundary conditions and initial values, an approximate solution is developed here. It is assumed that the x-t solution domain is covered by a uniform rectangular lattice with Δx and dt denoting space and time increments, respectively. Furthermore, it is assumed that the point considered is the point $x = i\Delta x$, $t = j\Delta t$ of the solution domain. Then if we agree to denote $y(i\Delta x, j\Delta t)$ by $y_{i,j}$ we have the following finite difference approximation.

$$\frac{\partial^{2} y}{\partial r^{2}} = \frac{1}{\Delta r^{2}} (y_{i,j+1} - 2y_{i,j} + y_{i,j-1}) + o(\Delta r^{2})$$

$$\frac{\partial^2 \mathbf{y}}{\partial \mathbf{t}} \stackrel{\Delta}{=} \frac{1}{\Delta \mathbf{t}} \delta_{\mathbf{t}}^2 + o(\Delta \mathbf{t}^2)$$
 (3.5a)

$$\frac{\partial^{2} y}{\partial x^{2}} = \frac{1}{\Delta x^{2}} (y_{i+1,j} - 2y_{i,j} + y_{i-1,j}) + o(\Delta x^{2})$$

$$\frac{\Delta}{\Delta x} \frac{1}{\delta x} + o(\Delta^2) \tag{3.5b}$$

$$\frac{\partial^{4} y}{\partial x^{4}} - \frac{1}{\Delta x^{4}} (y_{i+2,j} - 4y_{i+1,j} + 6y_{i,j} - 4y_{i-1,j} + y_{i-2,j}) + o(\Delta x^{2})$$

$$\stackrel{\Delta}{=} \frac{1}{\Delta x} \delta_{x}^{4} + o(\Delta x^{4}) \tag{3.5c}$$

$$\frac{\partial}{\partial \mathbf{x}} \left(\mathbf{p}(\mathbf{x}, \mathbf{t}) \frac{\partial \mathbf{y}}{\partial \mathbf{x}} \right) - \delta_{\mathbf{x}}^{1} \left[\mathbf{p}_{\mathbf{i}, \mathbf{j}} \delta_{\mathbf{x}}^{1} \right] \mathbf{y}_{\mathbf{i}, \mathbf{j}}$$

$$- \frac{1}{\Delta \mathbf{x}} \delta_{\mathbf{x}}^{1} \left[\mathbf{p}_{\mathbf{i}, \mathbf{j}} \left(\mathbf{y}_{\mathbf{i}+1/2, \mathbf{j}} - \mathbf{y}_{\mathbf{i}-1/2, \mathbf{j}} \right) + o(\Delta \mathbf{x}^{2}) \right]$$

$$- \frac{1}{\Delta \mathbf{x}^{2}} \left[\mathbf{p}_{\mathbf{i}+1/2, \mathbf{j}} \left(\mathbf{y}_{\mathbf{i}+1, \mathbf{j}} - \mathbf{y}_{\mathbf{i}, \mathbf{j}} \right) \right]$$

$$- \mathbf{p}_{\mathbf{i}-1/2, \mathbf{j}} \left(\mathbf{y}_{\mathbf{i}, \mathbf{j}} - \mathbf{y}_{\mathbf{i}-1, \mathbf{j}} \right) + o(\Delta \mathbf{x}^{2})$$

$$(3.5)$$

(3.5d)

where
$$\delta_{x}^{i} y_{i,j} = \frac{1}{\Delta x} \left(y_{i+1/2,j} - y_{i-1/2,j} \right)$$

Making use of (3.5), the finite difference approximation for (2.15a)takes the form

$$y_{i,j+1} = 2y_{i,j} - y_{i,j-1} - \frac{EI}{\rho A} \left(\frac{\Delta t}{\Delta x^2} \right)^2 \delta_x^4 y_{i,j}$$

$$-\frac{1}{\rho A} \frac{\Delta t}{\Delta x^2} - \Delta t \left[p_{i+1/2,j} \left(y_{i+1,j} - y_{i,j} \right) \right]$$

$$- p_{i-1/2,j} \left(y_{i,j} - y_{i-1,j} \right) - \frac{\Delta t}{\rho A}^2 f_{i,j}$$

$$+ o \left(\Delta x^2 \right) \Delta t^2$$

$$\approx - c_1 r^2 y_{i-2,j} + \left(4c_1 r^2 + c_2 r p_{i-1/2,j} \right) y_{i-1,j}$$

$$\left(- 6c_1 r^2 + c_2 r p_{i+1/2,j} + c_2 r p_{i-1/2,j} + 2 \right) y_{i,j}$$

$$\left(4c_1 r^2 + p_{i+1/2,j} c_2 r \right) y_{i+1,j} - c_1 r^2 y_{i+2,j}$$

$$- y_{i,j-1} \qquad (3.6a)$$

where
$$r = \frac{\Delta t}{\Delta x^2}$$
, $c_1 = \frac{EI}{\rho A}$ and $c_2 = \frac{\Delta t}{\rho A}$

The boundary and initial conditions of (2.16a,b) and (2.17a,b) require

$$y_{i,0} - f_1(i\Delta x), \quad y_{i,0} - y_{i,-1} + \Delta t f_2(i\Delta x)$$
 (3.6b)

$$y_{0,j} = 0$$
 , $y_{N,j} = 0$ (3.6c)

$$y_{N+1,j} = y_{N-1,j}, y_{-1,j} = y_{1,j}$$
 (3.6d)

$$i = 0,1,2,3,....N$$

where N is the number of mesh divisions in the x-direction; i.e. $N\Delta x = l$. If $p_{i\pm 1/2}$ are known equations (3.6) yield a value of y at a point in the j + 1 row in terms of already known values in the j-1 and j-rows. Thus the entire y-mesh can be computed, and the solution can be generated one row at a time. Figure 3.1 illustrates the computational molecules for the explicit difference approximation of (3.6).

To study the convergence of the finite difference approximation, it is sufficient to study the stability and consistency. To study the stability of (3.6), p(x,t) is assumed to be constant. Now since the stability bounds are not affected by the lower-order terms; i.e., in which $p_{i\pm1/2,j}$ are coefficients of them, the nature of the problem assumes that the vibration is governed mainly, by the beam stiffness EI, rather than the axial force $p_{i\pm1/2,j}$. Fourier stability method yield [16]

$$0 < \frac{4EI}{\rho A} \left(\frac{\Delta t}{\Delta x} \right)^2 \le 1$$

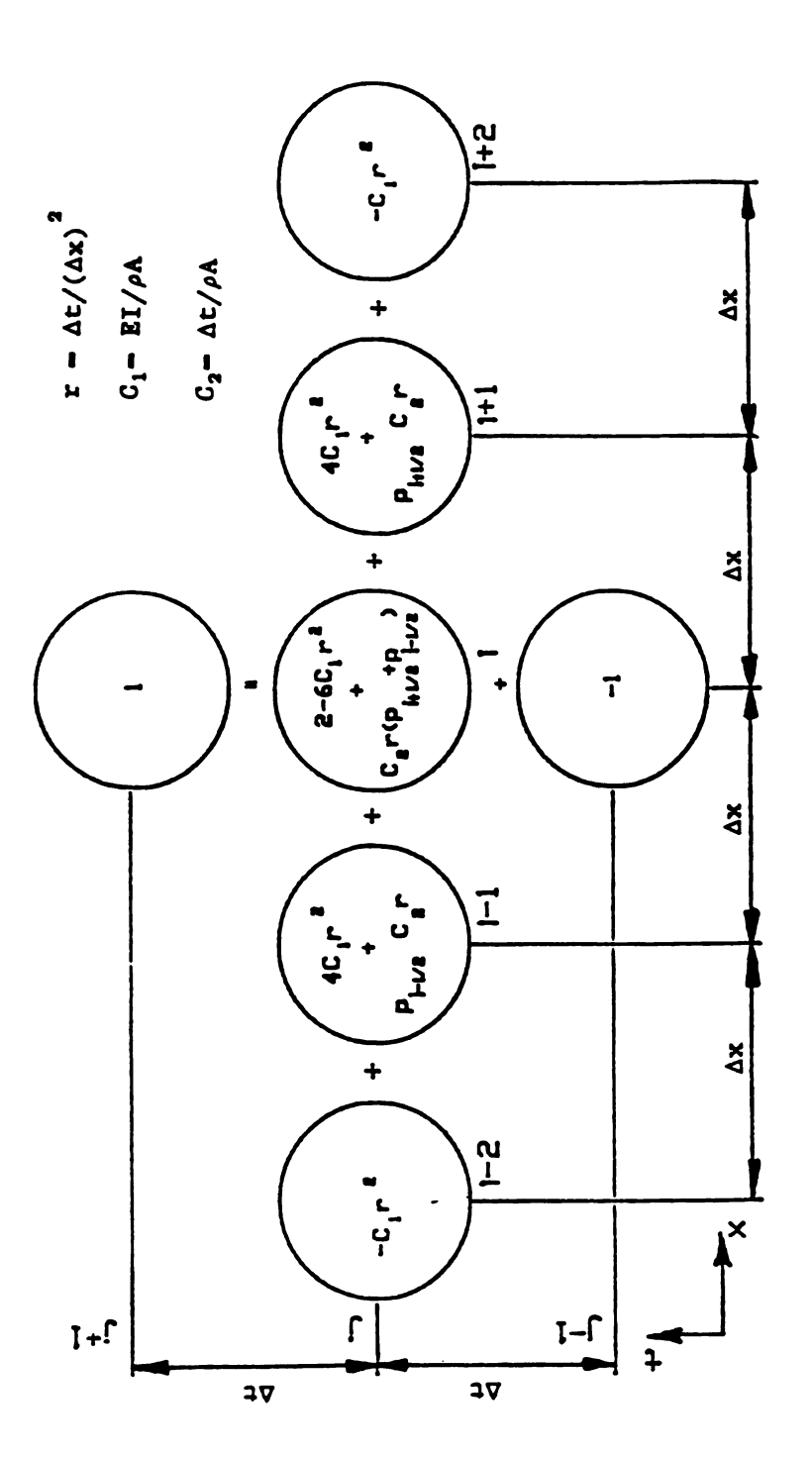


Figure 3.1 Computational molecules for the finite difference approximation

$$\frac{\Delta t}{\Delta x} \le \frac{1}{2} \left(\frac{\rho A}{EI} \right)^{1/2} \tag{3.7}$$

This stability bound was found to give good results.

The numerical approximation was derived from the PDE, i.e. (2.15a), and since that the truncation errors go to zero as Δt , $\Delta x \rightarrow 0$ no matter how this limit is taken, the explicit finite difference approximation (3.6) is consistent with the differential equation (2.15a), and as long as (3.7) holds, the system is stable. By Lax's theorem; [14,17,40] and [41] stability and consistency imply convergence, provided that the parabolic PDE is well posed.

3.3 Steps of Solution

The analytical-numerical solution presented in the previous sections are given in order to find the response of the beam at any point x under the action of a control force $P(t) = g(\partial u(\ell,t)/\partial t)$ and some initial and working data. This section presents the steps of solution to achieve this purpose below

- 1) Select initial values $f_1(x)$, $f_2(x)$ in (3.6b), working conditions f(x,t) in (3.6a) and a control gain α .
- 2) Calculate the corresponding response of the initial values using (3.6b), i.e., $y_{i,0}$, i = 1,2,3,....N.
- 3) Calculate the end velocity of the beam using the approximation:

$$\frac{\partial u(\ell,t)}{\partial t} \approx -\frac{1}{2} \frac{\partial}{\partial t} \int_{0}^{\ell} \left(\frac{\partial y(x,t)}{\partial x} \right)^{2} dx \qquad (3.8)$$

- 4) Calculate the control force P(t) using (2.34) subject to (2.33).
- 5) Find the distributed parameter force $p_{i\pm 1/2,j}$, i.e., $[p((i\pm 1)\Delta x,j\Delta t)] \text{ which requires that } P(t) \ [-g(\partial u(\ell,\,t)/\partial t)]$

and $\partial y(l, t)/\partial x$ to be known at $t = j\Delta t$ using (3.4) with truncation number of 20 modes.

- 6) Calculate the response $y_{i,j+1}$ using (3.6)
- 7) Increase j by 1 and repeat steps 3-6

3.4 Simulation Results and Discussion

This section contains the numerical-analytical results of the closed-loop control system simulation. The simulation is designed to illustrate of the following aspects of the controlled system's dynamics:

- 1- The stability.
- 2- The transient motions due to initial data.
- 3- The dynamic system response due to external disturbances.

The simulation were run on a Prime 750 computer at the Albert H. Case Center for Computer-Aided Design at Michigan State University. The calculations for the test case are carried out using a mesh of N =15 nodes in the x-direction and $\frac{\Delta t}{(\Delta x)^2}$ = .219 sec/m²[.0203 sec/ft].

The steel beam material properties and dimensions for laboratory tests, which will be presented in the following chapter are:

E =
$$2.10(10^4)$$
 kg/mm² [$3(10^7)$ 1b/in²]

 ρ = 8304 kg/m³ [$.3$ 1b/in³]

 ℓ = $.61$ m [2ft]

A = 50.8mm width x 1.588mm thickness [2in x .0625in]

For a particular control gain α , the results of the simulations are the response at a point $x_i = i\Delta x$, the required control force P(t), the internal energy and the work done by the external disturbance.

3.4.1 Control Force.

For our control system, the asymptotic stability is guaranteed when (2.34) and (2.33) are satisfied. The function g in (2.34) may be chosen such that the relationship between g and $u_t(\ell,t)$ lies in the second or fourth quadrant in the g- $u_t(\ell,t)$ plane. In the test cases the modified bang-bang control force as shown in Figure 2.2 is chosen. In all simulation test cases $\epsilon = 3(10^{-8})$ m/sec.

3.4.2 Internal Energy and Work Done.

The relationship between the internal energy E(t) and the work done by the control force P(t) can be deduced by integrating (2.38c) from 0 to t:

$$E(t) - E(0) = \int_{0}^{t} P(r) \frac{\partial u(\ell, r)}{\partial t} dr$$
 (3.9a)

$$E(t) = \frac{1}{2} \int_{0}^{2} \left[EI \left(\frac{\partial^{2} y}{\partial x^{2}} \right)^{2} + \rho A \left(\frac{\partial y}{\partial t} \right)^{2} + \frac{p^{2}}{EA} + \rho A \left(\frac{\partial u}{\partial t} \right)^{2} \right] dx$$
(3.9b)

The work done by an external force f(x,t) can be added to (3.9a) to yield

$$E(t) - E(0) = \int_{0}^{t} P(r) \frac{\partial u(\ell, r)}{\partial t} dr + \int_{0}^{t} \int_{0}^{t} f(x, r) \frac{\partial y(x, r)}{\partial t} dx dr$$
(3.9c)

Test Case 1: Initial Displacement.

In this case the initial displacement is, $y(x,0) = \sin(\pi x/\ell)mm$, which is the first eigenfunction of the beam. Figure 3.2a shows the response of the middle of the beam, $y(\ell/2,t)$ versus time and control gains $\alpha = 0.40.80$ and 108 N. In Figure 3.2a the curve for $\alpha = 0$ (control is off) is the response of the free stable vibration. The frequency of this response is 9.654 Hz. which is the first natural frequency of the beam. The curves for $\alpha = 40.80$ decay rapidly in the first two cycles of oscillation. For $\alpha = 108$ N the motion decreases

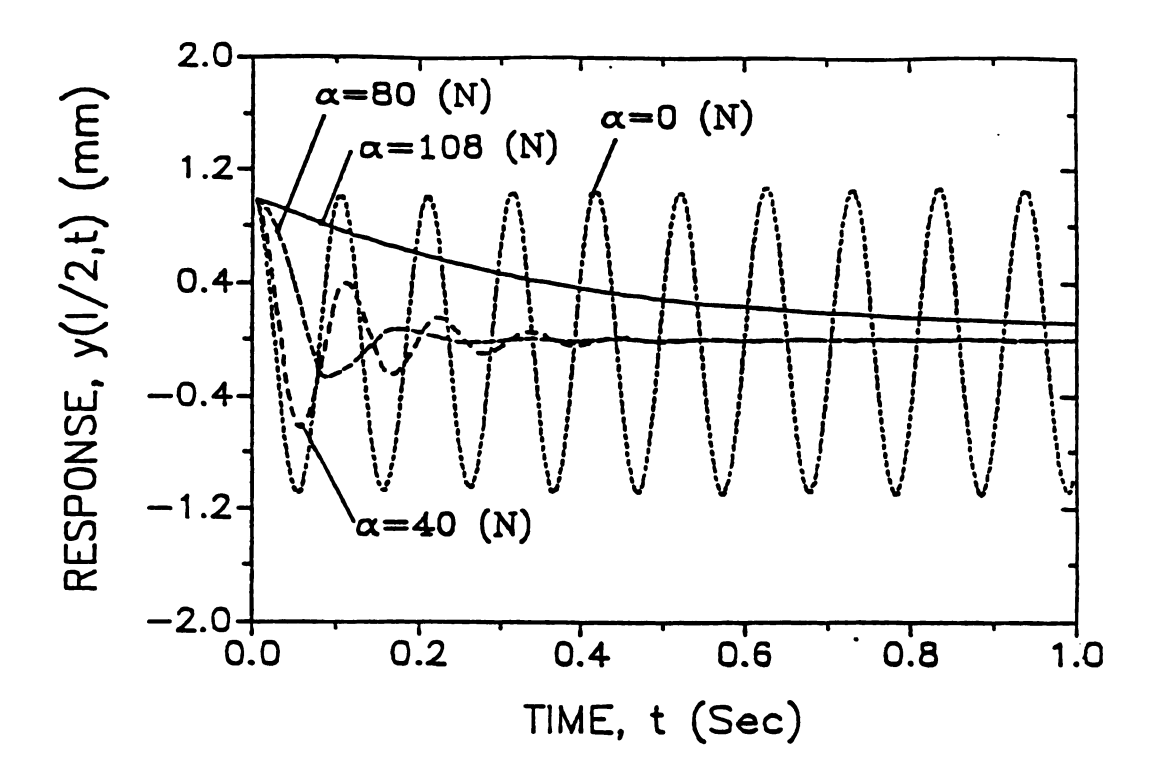


Figure 3.2a Response of the transverse vibration at x-1/2 for initial displacement test results for various control gains for test case 1

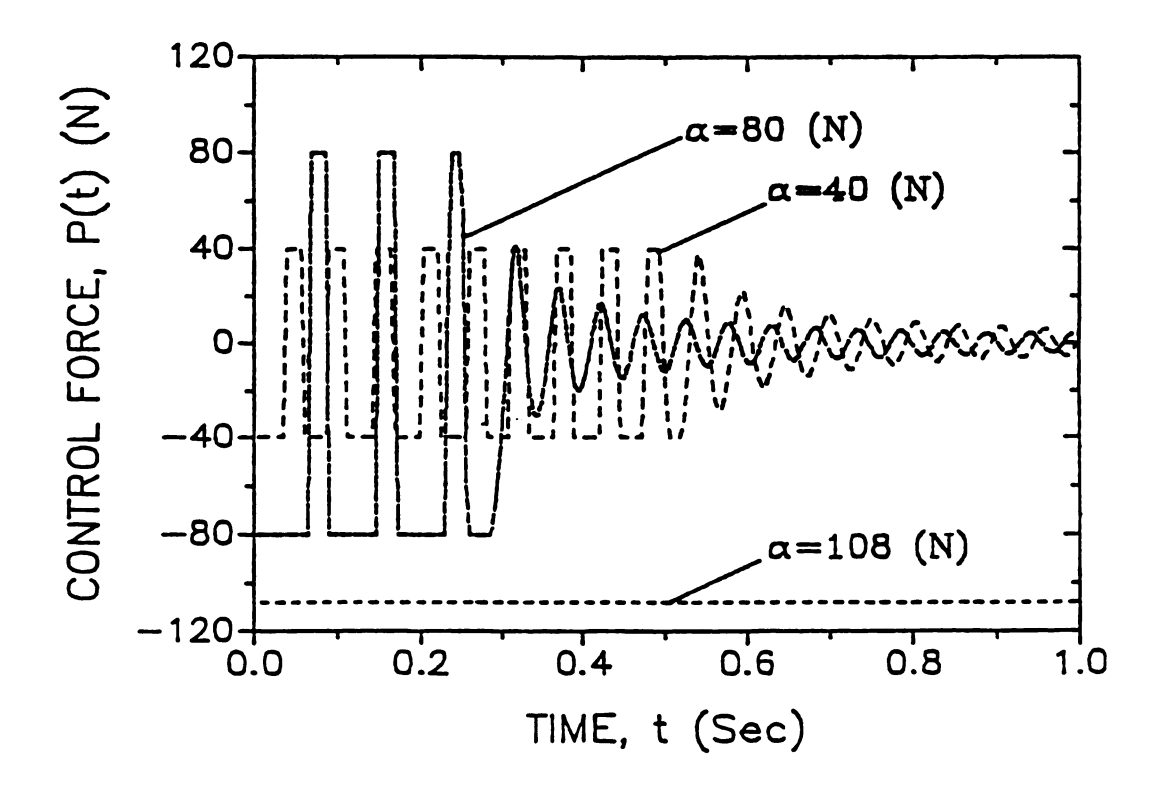


Figure 3.2b The required control forces, P(t) for test case 1

monotonically with increasing t; i.e., the active control overdamps the vibration in this case. For $\alpha=80$ N the vibration almost dies out in two cycles (the amplitude is .001mm), for $\alpha=40$ N it almost dies out in 4 cycles (the amplitude is =.059 mm). Figure 3.2b shows the required control force versus time for $\alpha=0,40,80$ and 108 N. It is clear from Figure 3.2b that the end velocity of the beam $\partial u(\ell,t)/\partial t$ reflects the internal energy content E(t) and $|u_t|$ falls in the interval $(+\epsilon,-\epsilon)$ faster for bigger α . This is not the case for $\alpha=108$ N it seems that the control action freezes the initial shape of the beam by slowing down the conversion of the initial energy, i.e. the potential energy, into kinetic energy and dissipate the energy dissipated.

The internal energy E(t) given by (3.9b) is plotted versus time for $\alpha = 0,40,80$ and 108 N. in Figure 3.2c. For $\alpha = 0$ the system is conservative, also it is clear in Figure 3.2c that at the early times i.e. 0 < t < .025 sec. the smaller the gain, the bigger the energy dissipation is and at later times the energy dissipation is proportional to the control gain. Except for $\alpha = 108$ N (the overdamped gain) which verifies the freezing phenomena mentioned above.

The work done by the control force p(t) is shown in Figure 3.2d. Comparing the corresponding curves in Figure 3.2c and 3.2d for the same α , one can see that (3.9a) is satisfied for each α which proves the energy balance of the system at any time t. Again, contrary to other α 's the work done by p(t) for $\alpha = 108$ N is less for 0 < t < 1 sec.

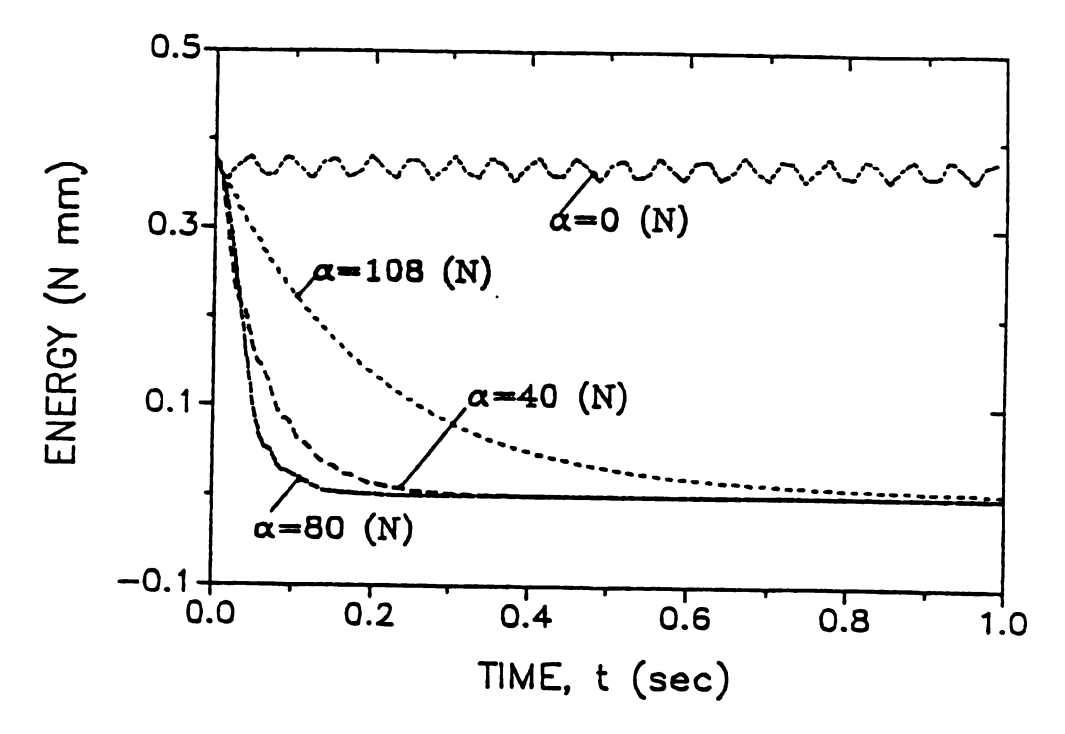


Figure 3.2c The internal energy of the system, E(t) for various control gains for test case 1

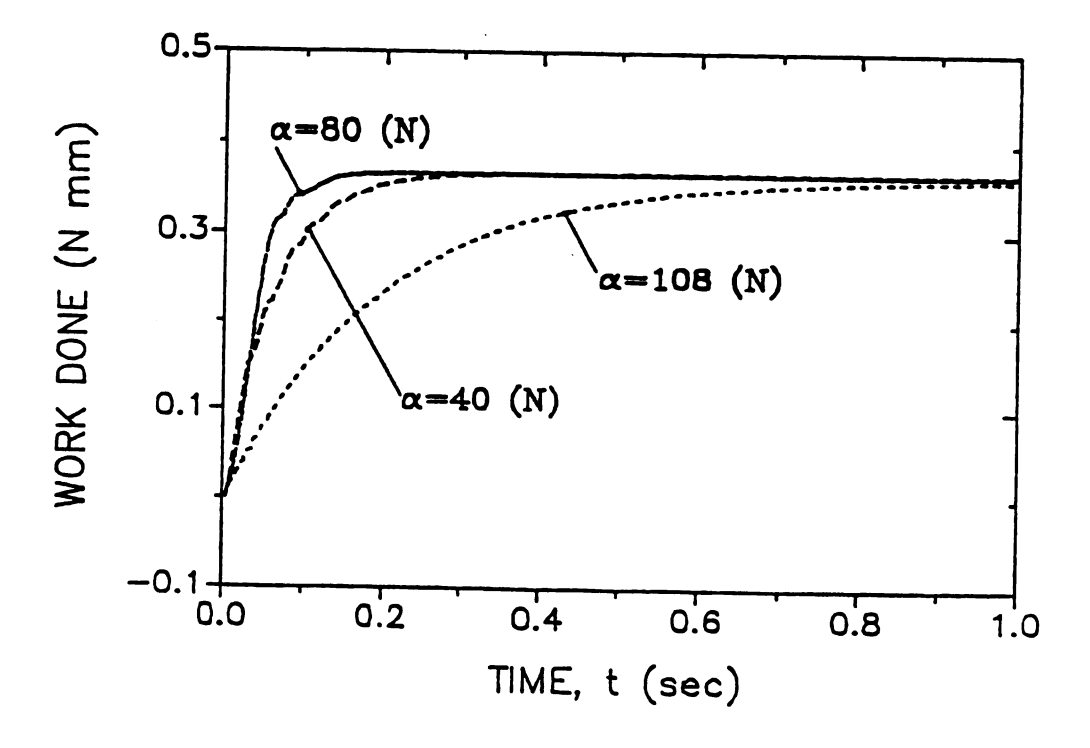


Figure 3.2d The work done by the control force, P(t)for various control gains for test case 1

A subset of the simulated test results for $\alpha=40$ N is shown in table 3.1. Table 3.2 shows the effect of the control gain α on the amplitude ratio $a_n=y_n/y_{n-1}$ the energy ratio $e_n=\sqrt{E_n/E_{n-1}}$ and the efficiency factor $\eta=(E(0)-E(t_n)/E(0))$, where n is the amplitude number. Notice the closed connection between the energy ratio e_n and the amplitude ratio a_n for low values of control gain α . For low α it is clear that the amplitude ratio a_n and the energy ratio e_n are almost constant and equal for the first three cycles. The observation on the amplitude ratio a_n agrees with Flouquet Liapunov theorem for this kind of system [26 and 42]

In this test case, i.e., case of controlling the transient motion due to an initial displacement of the first mode, the control algorithm could successfully transform the stable system into an asymptotically stable system, and for $\alpha = 108$ N the vibration monotonically decreases with time.

Table 3.1 A subset of the simulated test results for α = 40 N for test case 1.

time sec y(l/2,t) mm P(t) N WD N mm E(t) N mm 0.3681737185 0.3203043387 0.324042387 0.2728727269 0.2618064880 0.2356384993 0.2124738295 0.2085231808 0.192391803 0.1738128066 0.1567240337 0.1458364339 0.1458278329 0.1373088672 0.1373088672 0.138338712 0.1017337111 0.0919743776 0.0860384974 0.0847723011 0.0820000917 0.0733963527 0.00397700391.
0.0083007897.
0.0126317416.
0.0126317416.
0.0212738450.
0.0256247767.
0.0279357485.
0.0342867002.
0.386176336.
0.0472793971.
0.0316103071.
0.03574146236.
0.0472793971.
0.0516103071.
0.0562734105.
0.0687343214.
0.0732632674.
0.0773962174.
0.0817271634.
0.09028917634. 0. 0042643817
0. 0201522782
0. 0201522782
0. 0201522782
0. 0431223747
0. 0733202368
0. 1060856730
0. 1326690314
0. 1309673682
0. 1381367824
0. 1632063783
0. 1782484631
0. 2140207589
0. 2211214602
0. 2238681018
0. 2238681018
0. 2238681018
0. 2310747307
0. 2823004723
0. 2823004723
0. 3014779091
0. 3073600231
0. 3073600231
0. 3073600231
0. 3073600231
0. 3073600231
0. 3073600231
0. 3073600231
0. 3073600231
0. 3073600231
0. 3073600231
0. 3073600231
0. 3073600231
0. 3073600231
0. 3073600231
0. 3073600231
0. 3073600231
0. 3073600231
0. 3073600231
0. 3073600231
0. 3073600231
0. 3073600231
0. 3073600231
0. 3073600231
0. 3073600231
0. 3073600231
0. 3073600231
0. 3073600231
0. 3073600231
0. 3073600231
0. 3073600231
0. 3073600231
0. 3073600231
0. 3073600231
0. 3073600231
0. 3073600231
0. 3073600231
0. 3073600231
0. 3073600231 0. 7745104313
0. 9143219729
0. 8224261979
0. 8224261979
0. 4964836121
0. 3434001684
0. 3691416979
0. 1804972853
-0. 0131777063
-0. 2379338677
-0. 38039231330
-0. 3137093174
-0. 6069062691
-0. 367906868
-0. 2074452043
-0. 0367603910
0. 1363341623
0. 0367603910
0. 1363341623
0. 2610633737
0. 3858976630
0. 394201393
0. 394201393
0. 394201393
0. 394201393
0. 31788862
0. 2471666634
0. 18183147600
0. 262891777
-0. 2478133374
-0. 1197831030
-0. 12833147807
-0. 2478133374
-0. 1197831030
-0. 12833147807
-0. 2478133776
-0. 12833147807
-0. 2478133776
-0. 12833147807
-0. 2478133776
-0. 12833147807
-0. 2478133776
-0. 1283393276
-0. 1462930110
-0. 1283393276
-0. 1462930110
-0. 1283393276
-0. 1462930110
-0. 1283393276
-0. 1462930110
-0. 1283393276
-0. 1462930110
-0. 1283393276
-0. 1462930110
-0. 1283393276
-0. 1462930110
-0. 1283393276
-0. 1462930110
-0. 1283393276
-0. 1462930110
-0. 036494111
0. 1283393276
-0. 1304887398
-0. 0364847391
-0. 0364873984
-0. 037989466
-0. 07939178103
-0. 064482391
-0. 03232873103
-0. 07643613396
-0. 0794970866
-0. 0794970866
-0. 0794970866
-0. 0794970866
-0. 0794970866
-0. 0794970866
-0. 0794970866
-0. 0794970866
-0. 0794970866
-0. 0794970866
-0. 0794970866
-0. 0794970866
-0. 0794970866
-0. 0794970866
-0. 0794970866
-0. 0794970866
-0. 0794970866
-0. 0794970866
-0. 0794970866
-0. 0794970866
-0. 0794970866
-0. 0794970866
-0. 0794970866
-0. 0794970866
-0. 0794970866 -40. 0000
-40. 0000
-40. 0000
-40. 0000
-40. 0000
-40. 0000
-40. 0000
-40. 0000
-40. 0000
-40. 0000
-40. 0000
-40. 0000
-40. 0000
-40. 0000
-40. 0000
-40. 0000
-40. 0000
-40. 0000
-40. 0000
-40. 0000
-40. 0000
-40. 0000
-40. 0000
-40. 0000
-40. 0000
-40. 0000
-40. 0000
-40. 0000
-40. 0000
-40. 0000
-40. 0000
-40. 0000
-40. 0000
-40. 0000
-40. 0000
-40. 0000
-40. 0000
-40. 0000
-40. 0000
-40. 0000
-40. 0000
-40. 0000
-40. 0000
-40. 0000
-40. 0000 0.0903890763 0.0947200243 0.0972309723 0.1033819332 0.1079128632 0.1122438312 0.122438312 0.1207037420 0.123364900 0.123364900 0.138783860 0.138273489 0.1423604820 0.1423604820 0.1423604820 0.1423604820 0.1533333409 0. 09058907434 0.0520000717 0.073763527 0.0674976707 0.0613130406 0.03719899779 0.0372336880 0.0336331874 0.0489331733 0.0439123362 0.0339018130 0.0339018130 0. 0339837334
0. 0337837334
0. 0337837334
0. 0320667103
0. 0220667103
0. 02206711943
0. 02402234770
0. 0223114871
0. 0190162063
0. 0170197114
0. 0152648034
0. 0140223974
0. 0133374022
0. 0133374022
0. 0133374022
0. 0133374022
0. 0133374022
0. 0133374022
0. 0133374022
0. 003484298
0. 0133374022
0. 004736321
0. 0073853817
0. 0073853817
0. 0059403766
0. 0053687081
0. 0053687081
0. 0031687081
0. 0031687081
0. 0031687081
0. 0031687081
0. 0031687081
0. 0031687081
0. 0031687081
0. 0031687081
0. 0031687081
0. 0031687081
0. 0031687081
0. 0031687081
0. 0031687081
0. 0031687081
0. 0031676231
0. 0031676231
0. 0031676231
0. 0031676331
0. 00316737343
0. 00170065746
0. 0015461633
0. 0015461633
0. 0015461633
0. 0015461633
0. 0015461633
0. 0015461633
0. 00113168809
0. 00113168809
0. 00113168809
0. 00113168809 0. 1578843038. 0. 1642152667. 0. 1685461**778.** 0. 1728771627. 0.1728771627, 0.1772080738, 0.1813370387, 0.1835700216, 0.1902007347, 0.1743317176, 0.2031738136, 0.2031738136, 0.2118357076, 0.2118357076, 0.2161866724, 0.2205176333, 0.2248485684, 0. 3364883833 0. 3376113382 0. 3382240343 0. 3383728073 0. 3383728073 0. 3383729733 0. 3374076037 0. 3601701836 0. 3616153378 0. 3620748320 0. 3622364320 0. 362236487 0. 3623631868 0. 362364878 0. 363241893 0. 363914075 0. 3649786681 0. 3649786481 0. 3649786481 0. 3649786481 0. 3649786481 0. 3649786481 0. 3649786481 0. 2248485684. 0. 2248485684. 0. 2291795313. 0. 2335104942. 0. 2378414273. 0. 2421721902. 0. 2463033233. 0. 2308342862. 0. 2391632193. 0. 2394962120. 0. 2681380762. 0. 2724890709. 40. 0000
40. 0000
40. 0000
40. 0000
-40. 0000
-40. 0000
-40. 0000
-40. 0000
-40. 0000
40. 0000
40. 0000
40. 0000
-40. 0000
-40. 0000
-40. 0000
-40. 0000
-40. 0000
-40. 0000
-40. 0000
-40. 0000
-40. 0000
-40. 0000
-40. 0000 0.2724890707. 0.2768200040. 0.2811309371. 0.2834819298. 0. 2878128627 0.2878128627, 0.2741437760, 0.2784747271, 0.3028037218, 0.3071366549, 0.3114673879, 0.3157983806, 0.3201273137, 0.3244604468, 0. 3633884530 0. 3633884530 0. 3634341698 0. 3635118346 0. 363679793 0. 3660213351 Ō. 3287914395 0.3660647327 0.3661075234 0.3661075234 0.3661903143 0.36643026670 0.3664271832 0.3664271832 0. 3431223726, 0. 3374233057, 0. 3417842984, 0. 3461132313, 0. 3504461646, 0. 3547771573,

Table 3.1 (Continued)

time sec	y(1/2,t) mm	P(t) N	WD M mm	E(t) N mm
0. 3571080704. 0. 3634370233. 0. 36376370233. 0. 3764318824. 0. 3721007473. 0. 3807628153. 0. 3807628153. 0. 3807628153. 0. 3807628153. 0. 39737356744. 0. 3980866471. 0. 4067483332. 0. 4110773237. 0. 4134104390. 0. 4177413721. 0. 4284033177. 0. 4384033177. 0. 43870631841. 0. 44370631841. 0. 44370631841. 0. 4457271097. 0. 4500380430. 0. 4543890337. 0. 4587179688. 0. 4630307017. 0. 47673818946. 0. 4717128277. 0. 4760437608. 0. 4890364177. 0. 477678343. 0. 4870366177. 0. 476738187408. 0. 5100223970. 0. 513323703. 0. 3063604116. 0. 513323703. 0. 313323703. 0. 313323703. 0. 3236842632. 0. 328013223770. 0. 513332703. 0. 513332703. 0. 513332703. 0. 513332703. 0. 513332703. 0. 513332703. 0. 513332703. 0. 513332703. 0. 513332703. 0. 513332703. 0. 513332703. 0. 5133387883. 0. 57733387883. 0. 57733387883. 0. 57733387883. 0. 57733387883. 0. 57733387883. 0. 57733387883. 0. 57733387883. 0. 5773337704237. 0. 5133247061. 0. 57733387883. 0. 57733247061. 0. 5773	0. 0176762640 0. 0054620423 -0. 0069471363 -0. 0285730436 -0. 0356538396 -0. 03932137790 -0. 0374044327 -0. 03740247373 -0. 0273272888 -0. 0273272888 -0. 0273272888 -0. 0273272888 -0. 0013430048 0. 0013430048 0. 00134302163 0. 0134302163 0. 0134302163 0. 0134302163 0. 0233228318 0. 0233228318 0. 0233228318 0. 0233228318 0. 0233228318 0. 023127979 0. 02462303117 0. 0136123430 0. 0071860127 0. 004612647 -0. 013228718 -0. 0134720013 -0. 0134720364 -0. 0134720364 -0. 0134720364 -0. 0134720364 -0. 0134720364 -0. 0134720364 -0. 0134720364 -0. 0134720364 -0. 0134720364 -0. 0134720364 -0. 0134720364 -0. 0134720364 -0. 0134720364 -0. 0134720364 -0. 0134720364 -0. 0134720364 -0. 0134720364 -0. 0073473746 -0. 0073473746 -0. 0073473746 -0. 0073477364 0. 0073427726 0. 00736277274 -0. 0038157749 -0. 0038157749 -0. 0038157749 -0. 0038157774 -0. 0038157774 -0. 0038157774 -0. 0038157774 -0. 0038157774 -0. 0038157774 -0. 0038157774 -0. 0038157774 -0. 0038157774 -0. 0058037753 -0. 0062387809	-40. 0000 -40. 0000	0. 3646368127 0. 3666896224 0. 3666896224 0. 3666896224 0. 3667813628 0. 366781372246 0. 3669136272 0. 3669136712 0. 3669136712 0. 3669136737377 0. 367737377 0. 367737377 0. 367737377 0. 3671314768 0. 3671314768 0. 36726368202 0. 367268202 0. 367268202 0. 367268202 0. 367268202 0. 367268202 0. 367268202 0. 367268202 0. 367268202 0. 367268202 0. 367268202 0. 367268202 0. 367268202 0. 367268202 0. 367268202 0. 3673149943 0. 3673149943 0. 3673149943 0. 3673149943 0. 36747282323 0. 36747282323 0. 36747282323 0. 3674728393 0. 3674728393 0. 3674728393 0. 3674728393 0. 36747928393 0. 36747928393 0. 3674933930 0. 3674933930 0. 3674933930 0. 3674933930 0. 3674933930 0. 3674933930 0. 3674933930 0. 3674982786 0. 3675038218	0. 0009052675 0. 0008377919 0. 00083089769 0. 0008108866 0. 0007380930 0. 0006602516 0. 0003927070 0. 00036917936 0. 0003846739 0. 0003846739 0. 0003846739 0. 0003846739 0. 0003846739 0. 000387736 0. 0002377824 0. 0002377824 0. 0002378287 0. 0003868227 0. 0001368227 0. 0001368227 0. 0001368227 0. 000137114 0. 0001368227 0. 000137114 0. 0001368227 0. 000137114 0. 0001368227 0. 000137114 0. 0001368227 0. 000137114 0. 0001368227 0. 000137114 0. 0001368227 0. 000137114 0. 0001368227 0. 000137114 0. 0001368227 0. 000137114 0. 0001368227 0. 000137114 0. 0001368227 0. 0001368227 0. 000137114 0. 000136872 0. 000076873 0. 000076873 0. 0000827473 0. 0000387719
0. 6187631487, 0. 6232761416, 0. 6276271343, 0. 6317380078, 0. 6466197932, 0. 6447308667, 0. 64472818374, 0. 6336128321, 0. 6377437236,	-0.0062387809 -0.0046310575 -0.0028053755 -0.0007752723 0.0012654345 0.0032324884 0.0049490275 0.0062704897 0.0070949420 0.0073877890	-17. 0260 -17. 9861 -13. 1184 -3. 3584 3. 6779 11. 6719 16. 0569 13. 3768 10. 0439 2. 1636	0. 3675110340 0. 36751324949 0. 3675132596 0. 3675136366 0. 3675137366 0. 3675137346 0. 3675147273 0. 367516332 0. 3675163385 0. 3675163166	0.000243340 0.000236811 0.000234537 0.000235603 0.000236783 0.000226783 0.000216706 0.000209446 0.000206497
0. 6187631487, 0. 6232761416, 0. 6276271343, 0. 6317380078, 0. 646197932, 0. 6406197932, 0. 6447308667, 0. 6436128521, 0. 6536128521, 0. 65374437236, 0. 6624747183, 0. 66666057110,	-0.0062387809 -0.0046510575 -0.0028053755 -0.00126343145 0.00126343145 0.0032324884 0.0049490275 0.0062704877 0.0070847420 0.0073877890 0.0071666072 0.0064874794	-17. 0260 -17. 9861 -13. 1184 -3. 3384 3. 6772 11. 6719 16. 0369 13. 3768 10. 0437	0. 3675110340 0. 3675124049 0. 3675132990 0. 3675136566 0. 3675136566 0. 3675136566 0. 3675147295 0. 3675156338 0. 3675163388 0. 3675164580 0. 3675165176 0. 3675168176 0. 3675168176	0.000243340 0.000236811 0.000234537 0.000234033 0.000234083 0.000226783 0.000227466 0.000207446
0.6707363843, 0.67737673772, 0.6773784307, 0.6837274434, 0.6882604361, 0.6723713073, 0.6767223022, 0.7012332747, 0.7033841684, 0.7097131611,	0.004173747 0.0040360473 0.0024163371 0.0006474633 -0.0011387276 -0.0028836763 -0.0043702172 -0.005377769 -0.0063774747 -0.0063731760	-13. 6382 -9. 9670 -3. 9487 3. 0333 9. 1472 12. 0661 6. 0432 1. 9463	0.3673182462 0.3673187826 0.3673187614 0.3673187614 0.3673191402 0.3673176171 0.3673202131 0.3673203708 0.3673203708	0.000181862 0.000180813 0.000181688 0.000180901 0.000176344 0.000170342 0.000163701 0.000163736

Table 3.1 (Continued)

time sec	y(1/2,t) mm	P(t) N	WD N mm	E(t) N mm
U. 7142461538. 0. 7185770273. 0. 7227080200. 0. 7272390127. 0. 731567882. 0. 7359008789. 0. 7402318716. 0. 7445627451. 0. 7488437451. 0. 748843967. 0. 76313484629. 0. 7792104483. 0. 7792104483. 0. 7835413218. 0. 7835413218. 0. 7822033072. 0. 7963341806. 0. 8093651733. 0. 8051961660. 0. 8093270375. 0. 81818870375. 0. 8138580322. 0. 8138580322. 0. 81385803221. 0. 8311817646. 0. 8378437500. 0. 8441746235. 0. 8483036162. 0. 8483036162.	-0.0063929660 -0.0057958141 -0.0048422869 -0.00393969042 -0.0021340465 -0.0005379667 0.0010931385 0.0026461068 0.0040022926 0.005027672092 0.0059815643 0.0058223887 0.0058223887 0.0058223887 0.0058223887 0.0058233887 0.0058233887 0.0058233887 0.0058233887 0.0058233887 0.0058233887 0.0058233887 0.0058233887 0.0058233887 0.0058233887 -0.0037119524 -0.0037119524 -0.0037119524 -0.0037119524 -0.0037119524 -0.0037119524 -0.0037119524 -0.00371748413 -0.0037750641 -0.0037750641 -0.003750641 -0.003739883 0.0023339883	-4. 2764 -7. 0539 -11. 4074 -10. 9747 -7. 9718 -3. 6369 7. 5803 10. 2239 9. 9300 6. 6654 1. 3239 -7. 5117 -7. 5132 -7. 1577 -6. 5779 -2. 4323 2. 3643 6. 4982 8. 7290 8. 4290 -8. 4290 -8. 4308 -8. 4308 -8. 1716 -7. 8587 -7. 8587 -7. 8587 -7. 8587 -7. 6133 -1. 9776 -2. 1643 -3. 4067	0. 3675206700 0. 3675207284 0. 3675218225 0. 367521822397 0. 367522397 0. 367522397 0. 367522377 0. 3675223589 0. 3675223722 0. 3675233722 0. 3675234318 0. 3675234318 0. 3675234318 0. 3675234318 0. 3675234318 0. 3675234318 0. 3675234318 0. 3675234318 0. 3675234318 0. 3675234318 0. 3675234318 0. 3675245066 0. 3675245067 0. 3675245067 0. 3675245067 0. 3675245067 0. 3675251603 0. 3675251603 0. 3675251603 0. 3675251603 0. 3675251603 0. 3675251603 0. 3675251603 0. 3675251603 0. 3675251603 0. 3675251603 0. 3675251603 0. 3675251603 0. 3675251603 0. 3675251603 0. 3675251603 0. 3675251603	0. 0000162643 0. 000015072 0. 000013772 0. 0000137714 0. 00001477657 0. 0000147766 0. 0000147748 0. 0000144351 0. 0000133638 0. 0000133638 0. 0000134762 0. 00001328977 0. 0000127713 0. 0000124737 0. 0000124304 0. 0000124304 0. 0000124304 0. 0000124737 0. 0000124737 0. 0000124737 0. 0000127361 0. 0000115798 0. 0000113625 0. 0000113627 0. 0000113627 0. 0000113627 0. 0000113627 0. 00001073780 0. 00001073780 0. 0000107379 0. 0000107855 0. 0000107855
0.8571674824, 0.8614984731, 0.8638294678, 0.8701603413, 0.8744913340, 0.874891352001, 0.8874841928, 0.89181532001, 0.904770317, 0.9048080444, 0.9091389179, 0.91389179, 0.91389179, 0.91389179, 0.9221317768, 0.92244827693, 0.9321246357, 0.9321246357, 0.9321246357, 0.9321246357, 0.9481174946, 0.9524484873, 0.9634413462, 0.9634413462, 0.9634413463, 0.97543773174, 0.9784342051, 0.987960712, 0.9757579374,	0.0043772077 0.0043772077 0.0049472442 0.0051630763 0.0050226720 0.0043493804 0.0037834826 0.0027787234 0.0013980836 0.0003127749 -0.0009916937 -0.0022271623 -0.0033011786 -0.0041329339 -0.004648206 -0.0048633600 -0.0047269110 -0.0047269110 -0.0047269110 -0.0047269110 -0.0047269110 -0.002599607 -0.002599607 0.002599607 0.0021372307 0.0031486759 0.0031486759 0.0044760043 0.0044760043 0.0044760043 0.0044760043 0.0044382658 0.0013706179 0.002133339	7. 6103 7. 2743 4. 7100 1. 2183 -2. 6710 -7. 1590 -6. 8679 -1. 6348 2. 0123 5. 1020 6. 7387 6. 4149 4. 2929 1. 0367 -2. 0367 -2. 3943 -4. 2738 -1. 3673 -4. 2738 -1. 3673 -4. 2738 -1. 3673 -1. 3673 -1. 3673 -1. 3673 -1. 3743 -1. 3744 -1. 3746 -1. 1546	0. 3673264120 0. 36732667676 0. 3673268272 0. 3673268272 0. 3673268272 0. 3673270677 0. 3673270671 0. 3673274849 0. 3673274849 0. 3673274849 0. 3673274849 0. 3673274849 0. 3673274849 0. 3673274849 0. 3673278423 0. 3673278423 0. 3673278423 0. 3673278417 0. 3673278417 0. 3673281403 0. 3673281403 0. 3673281403 0. 3673281790 0. 3673281790 0. 3673281790 0. 3673281394 0. 3673281394 0. 3673281394 0. 3673281394 0. 3673281394 0. 3673281398	0. 000010424 0. 0000103833 0. 0000101781 0. 0000101036 0. 0000101036 0. 000097240 0. 000097383 0. 0000973007 0. 0000973007 0. 0000973007 0. 0000973681 0. 0000973681 0. 0000973681 0. 000097879 0. 0000087614 0. 000088073 0. 000088073 0. 000088073 0. 0000884878 0. 0000884878 0. 0000884878 0. 0000884878 0. 0000884878 0. 0000884878 0. 000088171 0. 000088171 0. 000088171 0. 000088171 0. 000088171 0. 000088171 0. 000088171 0. 000088171 0. 000088171 0. 000088177 0. 000088379 0. 000088379 0. 000088379 0. 000088379 0. 000088379 0. 000088379 0. 000088379 0. 000088379 0. 000088379

Table 3.2 Effect of the control gain \propto on the amplitude ratio a_n , the energy ratio e_n and the efficiency factor η for for initial displacement test results for test case 1

gain	n	t _n	y _n	a _n	En	e _n	η &
∝ N		sec	mm	mm/mm	N mm		
10	1	.1057	. 81548	. 81548	. 2573	. 836	30.08
	2	. 21077	.653619	.8015	.18131	.839	50.73
	3	. 31255	. 535909	.81991	.1241	. 827	66.28
20	1	.10791	.6218	. 622	.1485	. 635	59.65
	2	.21185	.4187	. 673	.0717	. 695	80.51
	3	. 31688	. 2766	.661	.031	. 657	91.58
40	1	.112	. 39	. 39	. 059	.40	86.41
	2	. 2205	.157	.40	.0094	. 399	97.45
	3	. 33	.062	. 395	.0014	. 386	99.62
80	1	.168	.064	.064	.0021	.076	99.43
	2	. 328	.008	. 125	.000024	.0081	99.9
	3	.433	.0053	. 662	.00	.00	100

108.........motion \rightarrow 0, no oscilation.

Test Case 2: Initial Velocity.

This case excites the first mode. Impulsive loads are common for mechanical structural elements like beams, yielding an initial kinetic energy to the beam. An impulse was simulated as an initial velocity. An example of such a simulation is $\partial y(x,0)/\partial t = .133\sin(\pi x/\ell)$ m/sec. Figure 3.3a shows the response of the middle of the beam for $\alpha = 0,10$, and 20 N. The curve for $\alpha = 0$ is the response of the free stable vibration. The frequency of this response is 9.654 Hz which is the first natural frequency of the beam. Table 3.3 shows the effect of α on the amplitude ratio $a_j = y_j / y_{j-2}$, energy ratio:

 $e_j = \sqrt{E_j / E_{j-2}}$ and the efficiency factor $\eta = (E(0) - E(t_j)) / E(0)$, where j is the amplitude number. Comparing the values of the amplitude ratio and the energy ratio at the same gain, in tables (3.2 and 3.3), they are very much close.

Figure 3.3b shows the required control force for α =10 and 20 N. The stabilizing effect of the control is evident again. The internal energy E(t) given by(3.9b) is plotted in Figure 3.3c for α = 0,10 and 20 N and can be compared with the work done by p(t) Figure 3.3d. The energy balance (3.9a) is satisfied for each α . In this test case; i.e. case of controlling the transient motion due to an initial velocity of the first model, the control algorithm could again successfully transform the stable system into an asymptotically stable system.

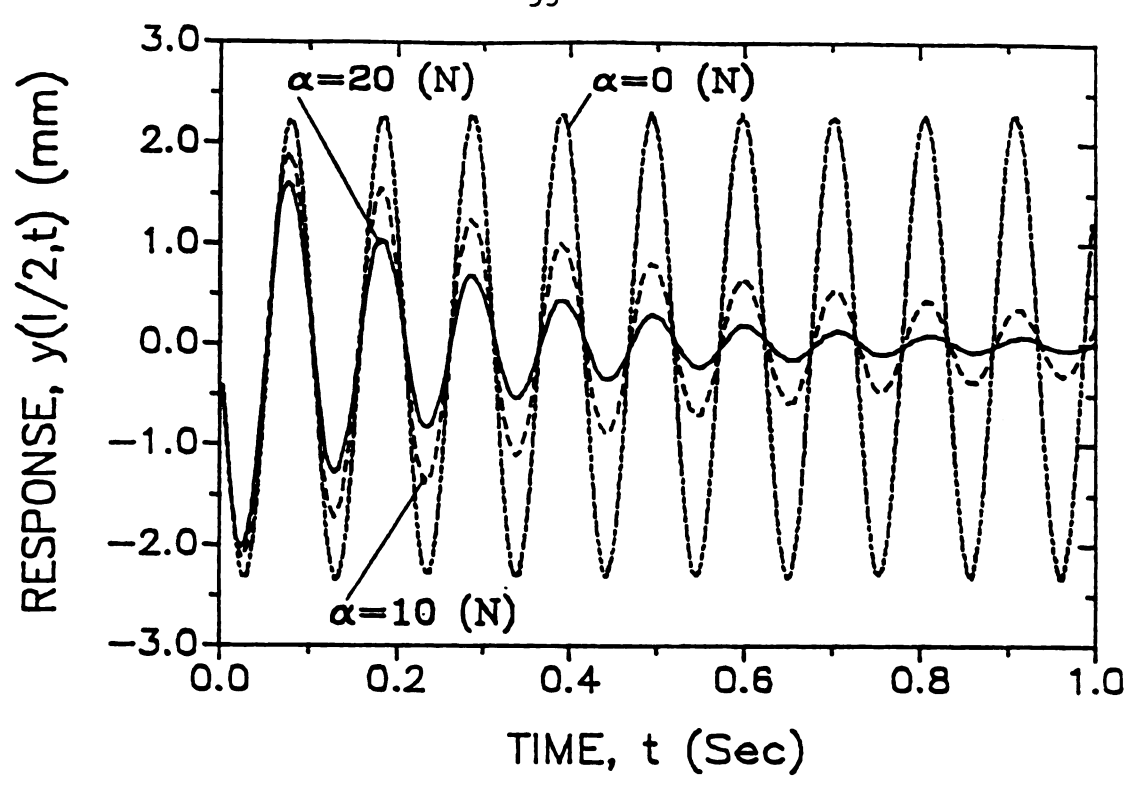


Figure 3.3a Response of the transverse vibration at $x=\ell/2$ for initial velocity test results for various control gains for test case 2

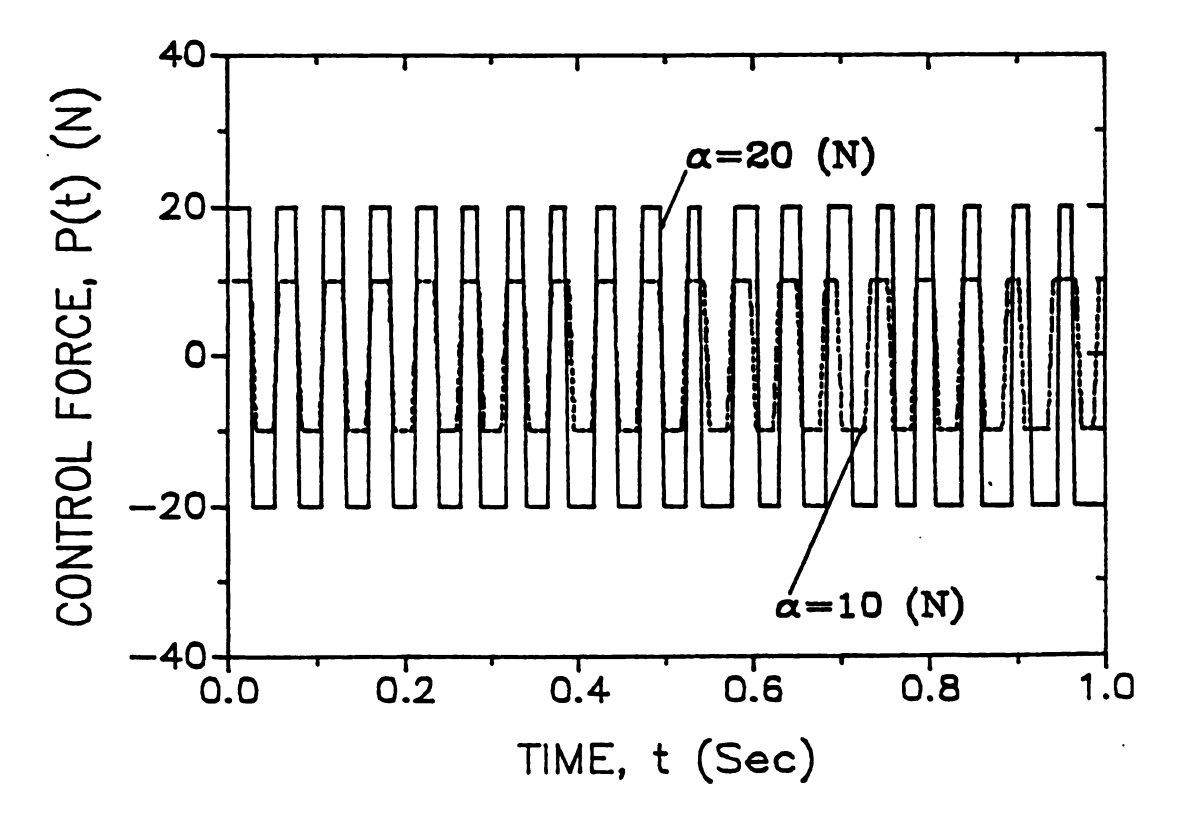


Figure 3.3b The required control forces, P(t) for test case 2

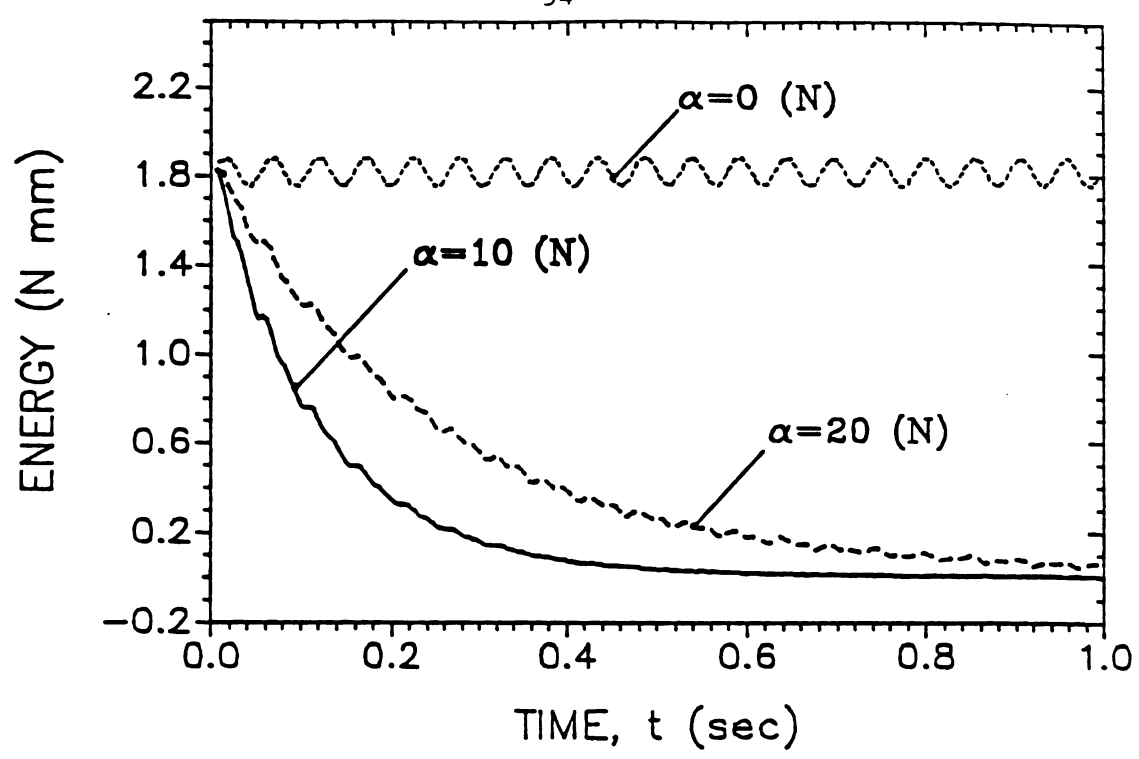


Figure 3.3c The internal energy of the system, E(t) for various control gains for test case 2

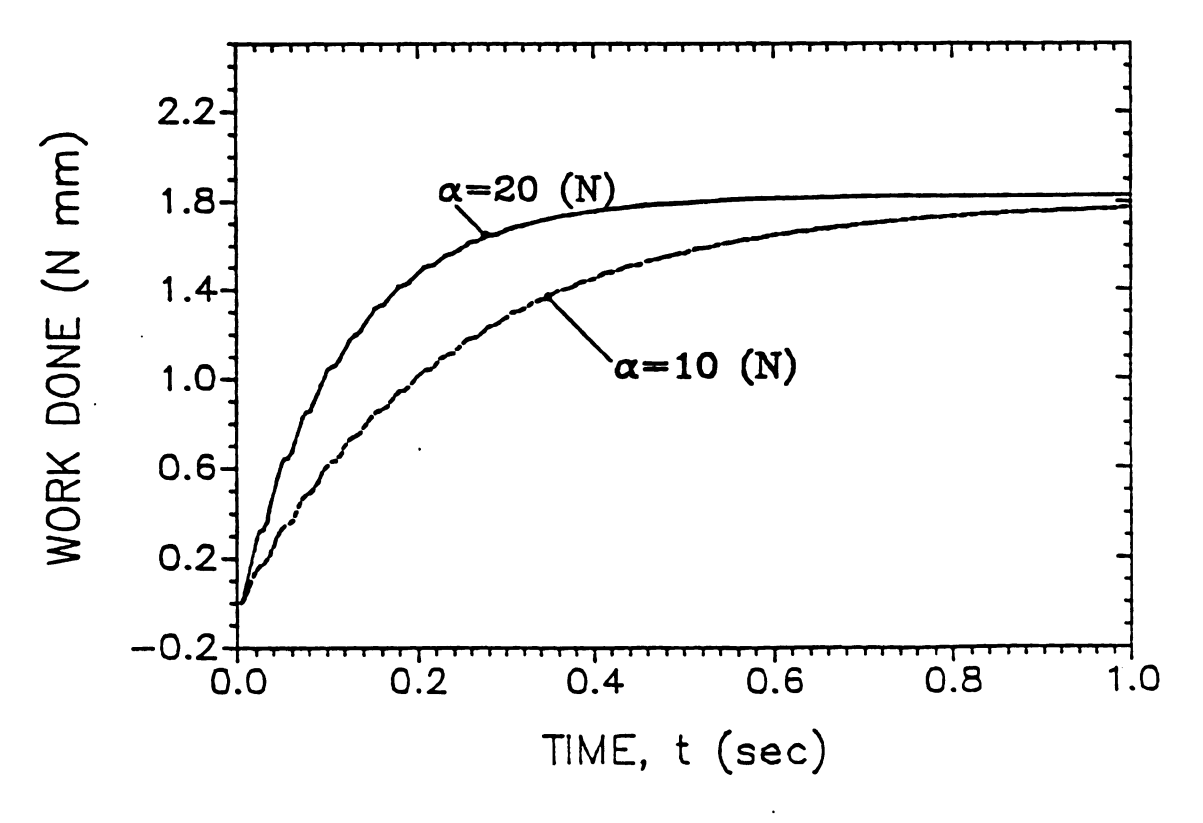


Figure 3.3d The work done by the control force, P(t)for various control gains for test case 2

Table 3.3 Effect of the control gain α on the amplitude ratio a_j , the energy ratio e_j and the efficiency factor η for initial velocity test results for test case 2.

gain	j	tj	Уj	a _j	Ĕj	e _j	η %
αN		sec	mm	mm/mm	N mm		
10	1	.02517	-2.1359		1.694		
	2		1.9036		1.3475		
	3	.12911	-1.7241	. 8072	1.1187	.812	40.5
	4	.18108	1.5475	.813	0.9055	.819	51.8
	5	. 23305	-1.39735	.8104	0.7411	.813	60.6
	6	. 2850	1.242	. 804	0.596	.811	68.3
	7	. 3370	-1.12196	. 803	0.4861	.81	74.1
20	1	.0235	-2.026		1.53		
	2	.07633	1.6037		0.965		
	3	.1291	-1.2994	.641	0.632	.634	66.4
	4	. 1819	1.03096	. 643	0.4048	. 647	78.5
	5	. 23468	-0.83564	. 643	0.26651	. 649	85.8
	6	. 2834	0.67515	. 654	0.17594	. 658	90.6

Test Case 3: Resonance.

In this case the system which is initially at rest is excited by applying a disturbing force $f(x,t) = .146 \sin \omega_1 t \text{ N/m}$, where ω_1 is the fundamental frequency (= 60.66 rad./sec). Figure 3.4a shows the response at $\alpha = 0,10,20$ and 40 N. For $\alpha = 0$, the growth is linear with t as is expected for resonance. For $\alpha = 20 - 40$ N the amplitudes are kept bounded, and the amplitude value decreases with the increase of the control gain α . Figure 3.4b shows the required control force. The internal energy of the system is shown in Figure 3.4c. For $\alpha = 0$ the internal energy increases unboundedly with t but for $\alpha = 20 - 40$ N it is kept bounded. Figure 4d shows the work done by p(t) and the energy balance of the system as given by (3.9c) for $\alpha = 20$ N. It should be noticed that the work done by p(t) is equal to the work done by p(t) Figure 3.4d and this limits the response amplitude.

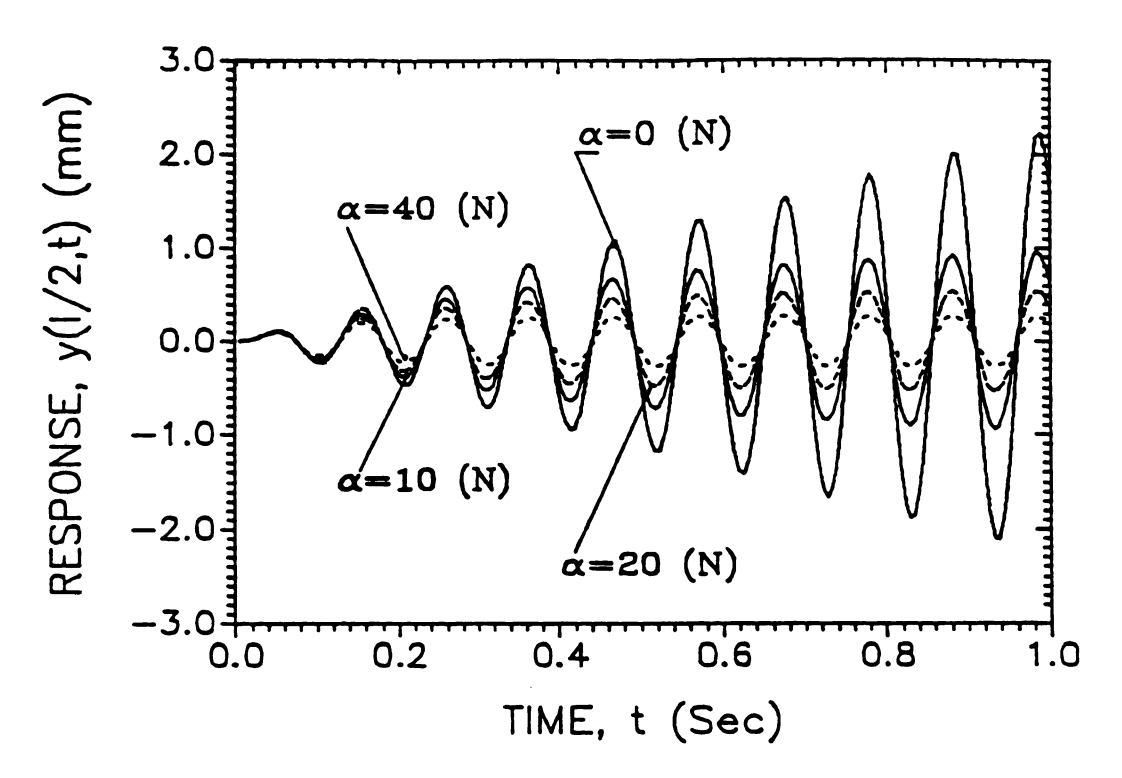


Figure 3.4a Response of the transverse vibration at x=1/2 for resonance excitation test results for various control gains for test case 3

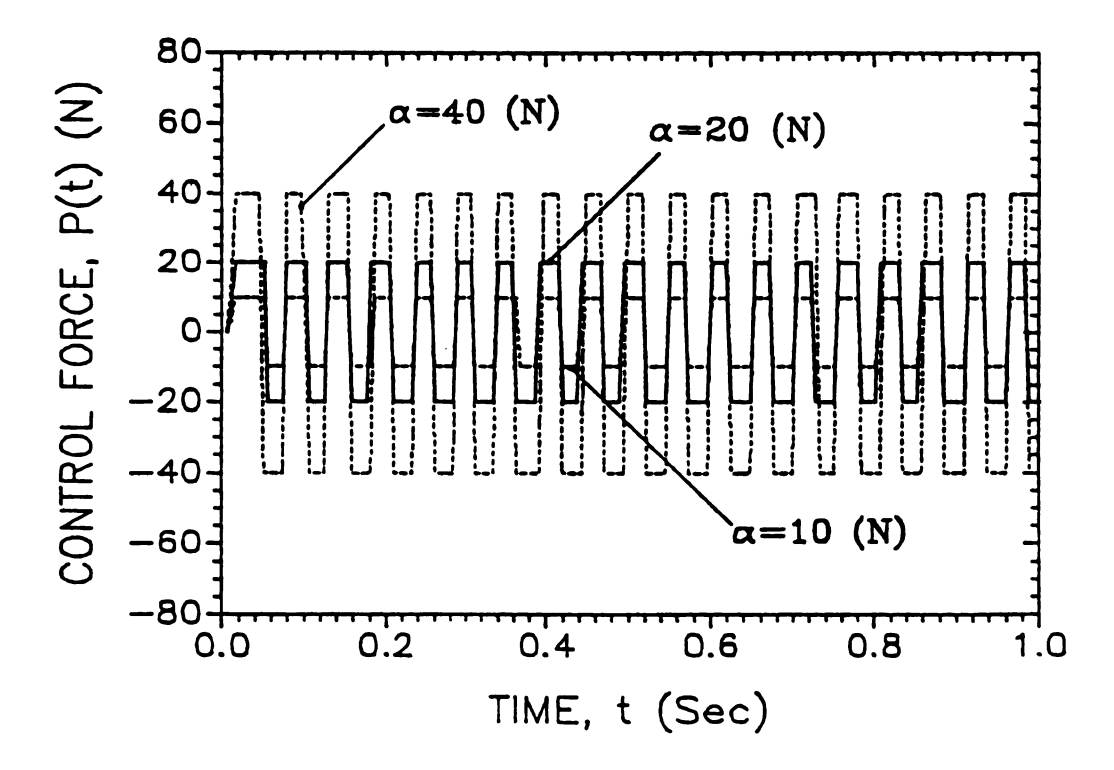


Figure 3.4b The required control forces, P(t) for test case 3

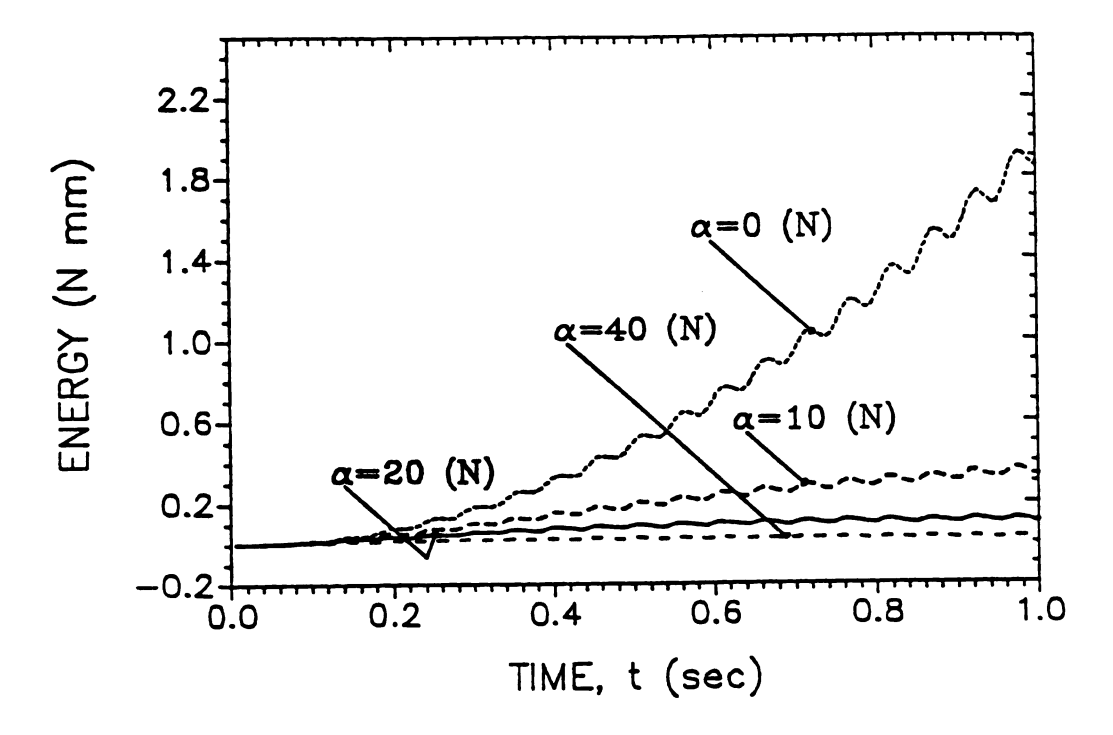


Figure 3.4c The internal energy of the system, E(t) for various control gains for test case 3

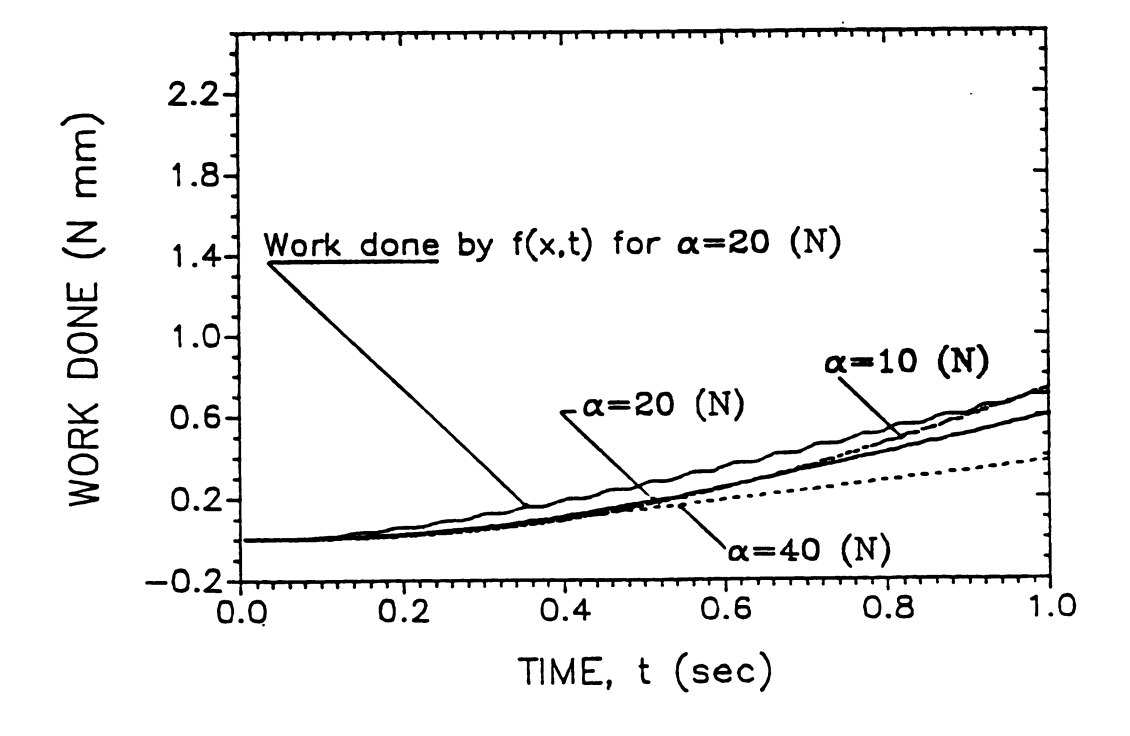


Figure 3.4d The work done by the control force, P(t)for various control gains for test case 3

Test Case 4: Steady State Time Response.

To study the steady state time response of the beam, a damping term should be added to the LHS of (2.15a). The damping model chosen is the structural damping (3.7). The basic property of structural damping is that the amplitudes of normal modes of vibration are attenuated at rates which are proportional to the oscillation frequencies. The structural damping of a DPS is found to be consistent with the model [19]:

By -
$$CB^{1/2}y_{t} + \rho A y_{tt} = 0$$

Where C is the damping coefficient and B is the operator EIy_{XXXX} defined on an appropriate domain and $B^{1/2}$ is the unique positive definite square root of B. Therefore (2.15a) becomes

EI
$$\frac{\partial^4 y(x,t)}{\partial x^4}$$
 - $C \frac{\partial^3 y(x,t)}{\partial x^2 \partial t}$ - $\frac{\partial}{\partial x} \left[p(x,t) \frac{\partial y(x,t)}{\partial x} \right]$ + $\rho A \frac{\partial^2 y(x,t)}{\partial x^2}$ - $f(x,t)$, $0 < x < \ell$ (3.10)

In this case the forcing function,

$$f(x,t) = 4.38 \sin(\omega_1 t) N/m$$

where ω_1 is the fundamental natural frequency (= 60.66 rad/sec), and C = .267 kg m/sec which was chosen to produce fast steady-state response not as a model of the experimental test system. Figure 3.5a shows the time response of the closed-loop system for zero initial

conditions. For $\alpha=0$, due to the passive damping the amplitude is limited to 1.55mm. For $\alpha=40$ N two control actions are considered, the first is that for t>0 the control is turned on and the second is that the the control is turned on for $t\geq 1.115$ sec. In both cases the amplitude is reduced from 1.55 mm to .545 mm. Figure 3.5b shows the control forces p(t) versus t. The internal energy is shown in Figure 3.5c for both cases. The internal energy for $\alpha=0$ is constant for $t\geq 1.1$ due to the passive damping. For $\alpha=40$ N the largest dissipation is due to the active control action as shown in the figure. From figures 3.5a and 3.5c we conclude that the desired steady state response may be obtained regardless of the time the control action starts. The open-loop steady state internal energy is .958 (N mm) and the closed loop steady state internal energy is .13 (N mm) which yields a steady state $\eta=86.64$ %.

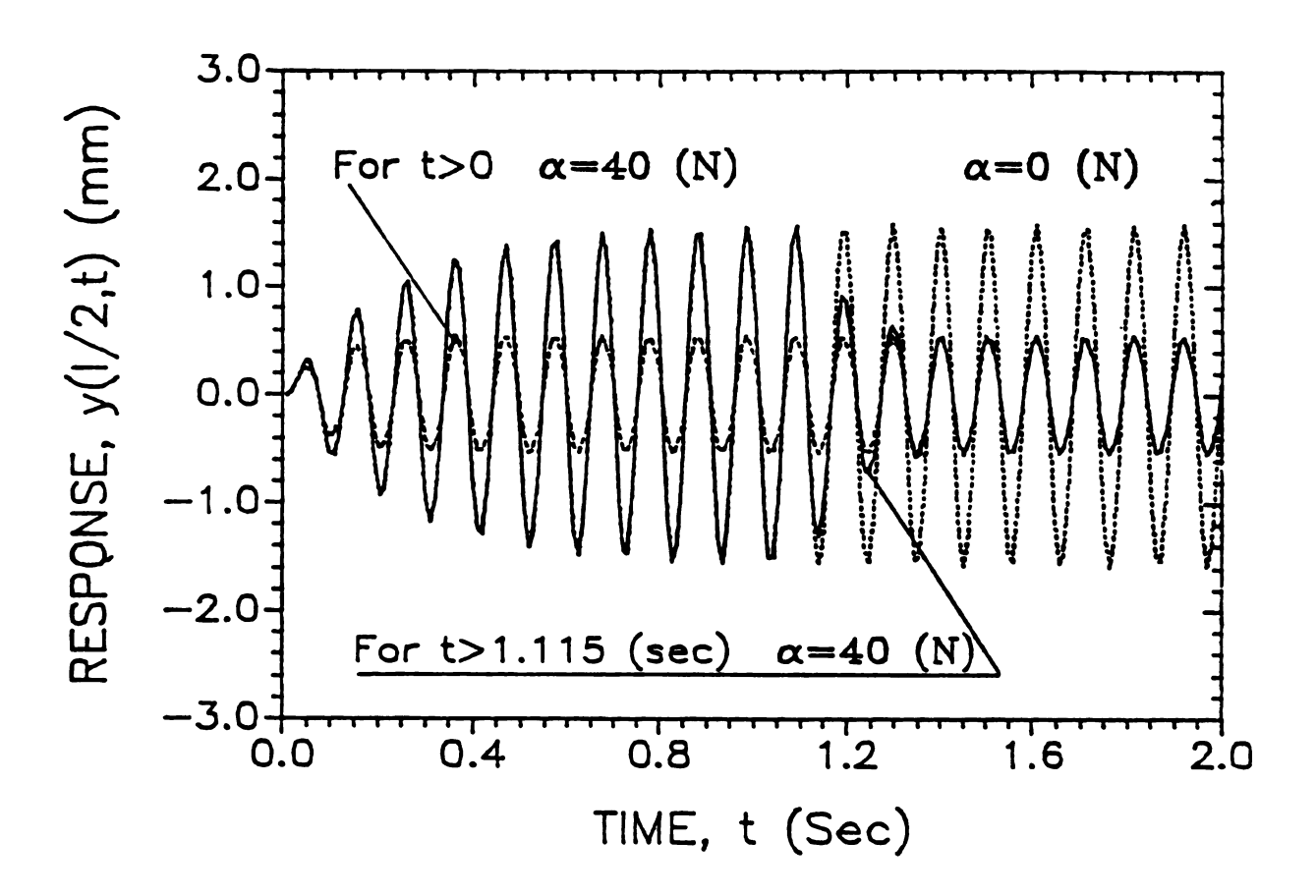


Figure 3.5a Response of the transverse vibration at $x=\ell/2$ for steady-state excitation test results for various control gains for test case 4

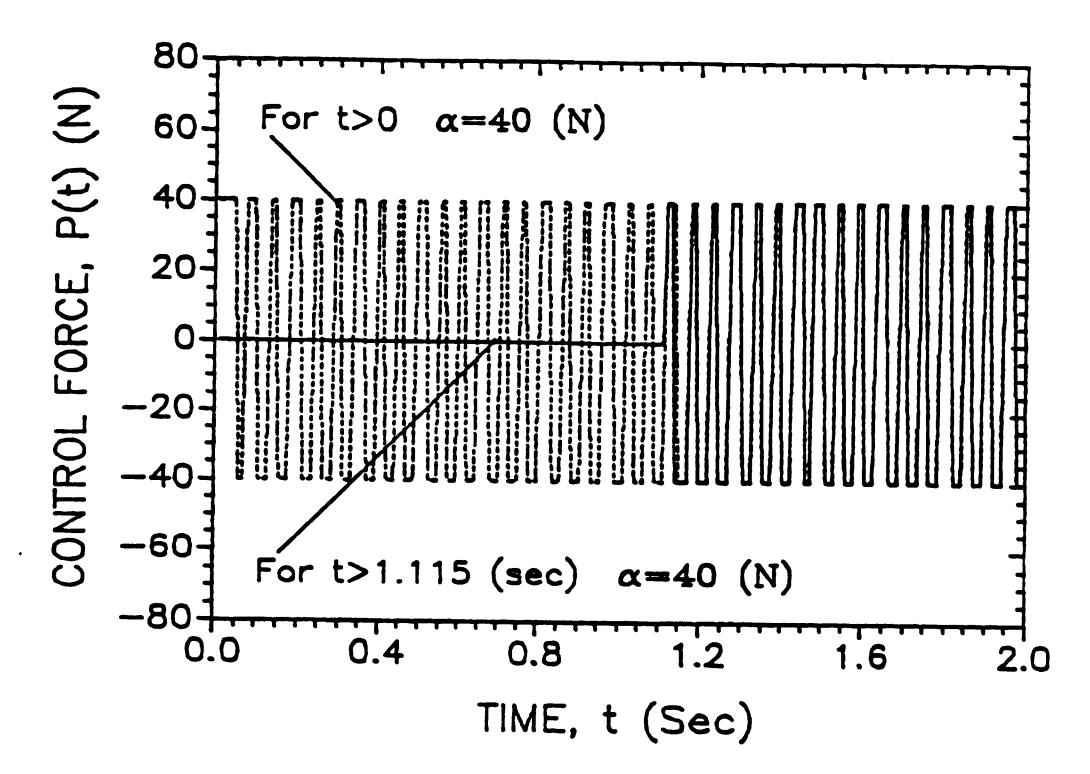


Figure 3.5b The required control forces, P(t) for test case 4

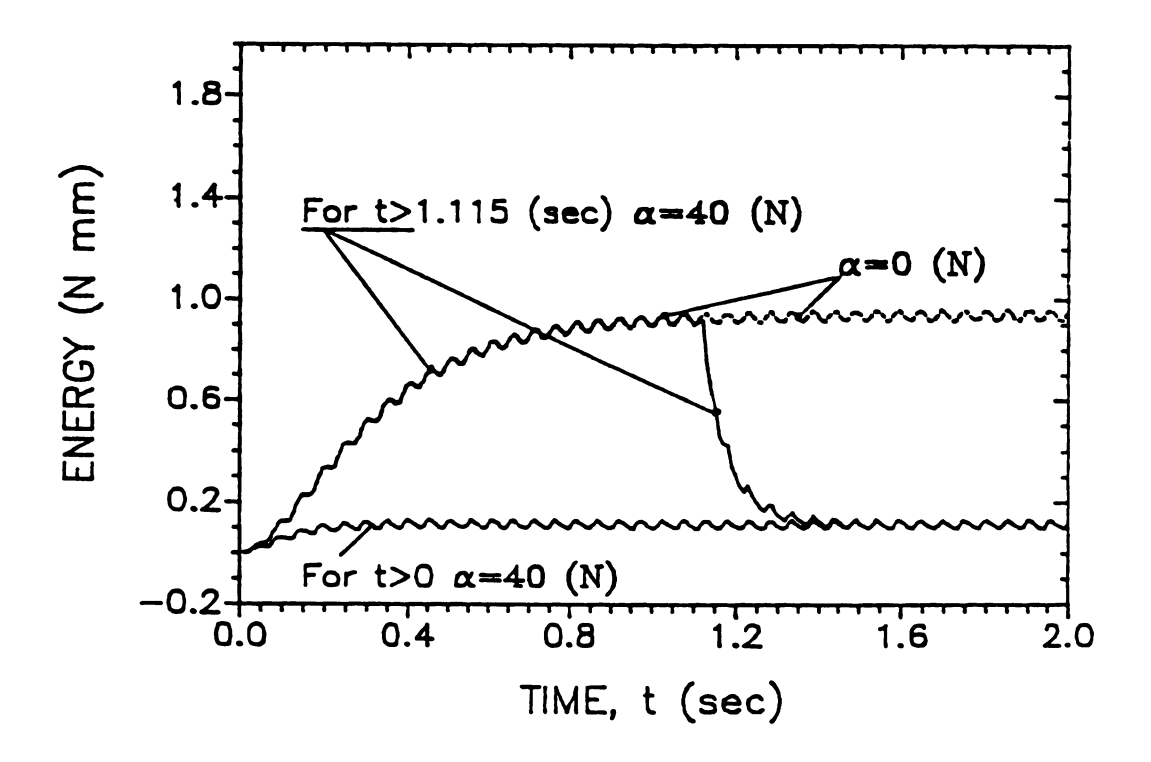


Figure 3.5c Effect of the control action on the internal energy of the system for test case 4

Test Case 5: Initial Displacement of an Infinite Number of Modes.

In this test case the initial data is given by y(x,0) = 21.527x(x-l) mm where x is in meters. This case excites an infinite number of modes. The control action is set "on" for internal energy $E(t) \geq .3 E(0)$. Figure 3.6a shows the response for $\alpha = 0$, 10, and 30 N. Since the control action is based on internal energy; The amplitudes of $\alpha = 10$, 20 and 30 N dropped to .8mm. for $E(t) \geq .3E(0)$ for each α . It is the equality starts to be satisfied at $t = t_1$, one can see from Figure 3.6b that $E(t_1)=.3E(0)$ is satisfied after 3/4 of a cycle for $\alpha = 30$, and after 4 1/2 cycles for $\alpha = 10$ N. The internal energy and the work done are shown in Fig.(3.6c) in which the energy balance is satisfied for each α . Table 3.4 shows the effect of α on a_n , a_n and a_n in the first three cycles for each α .

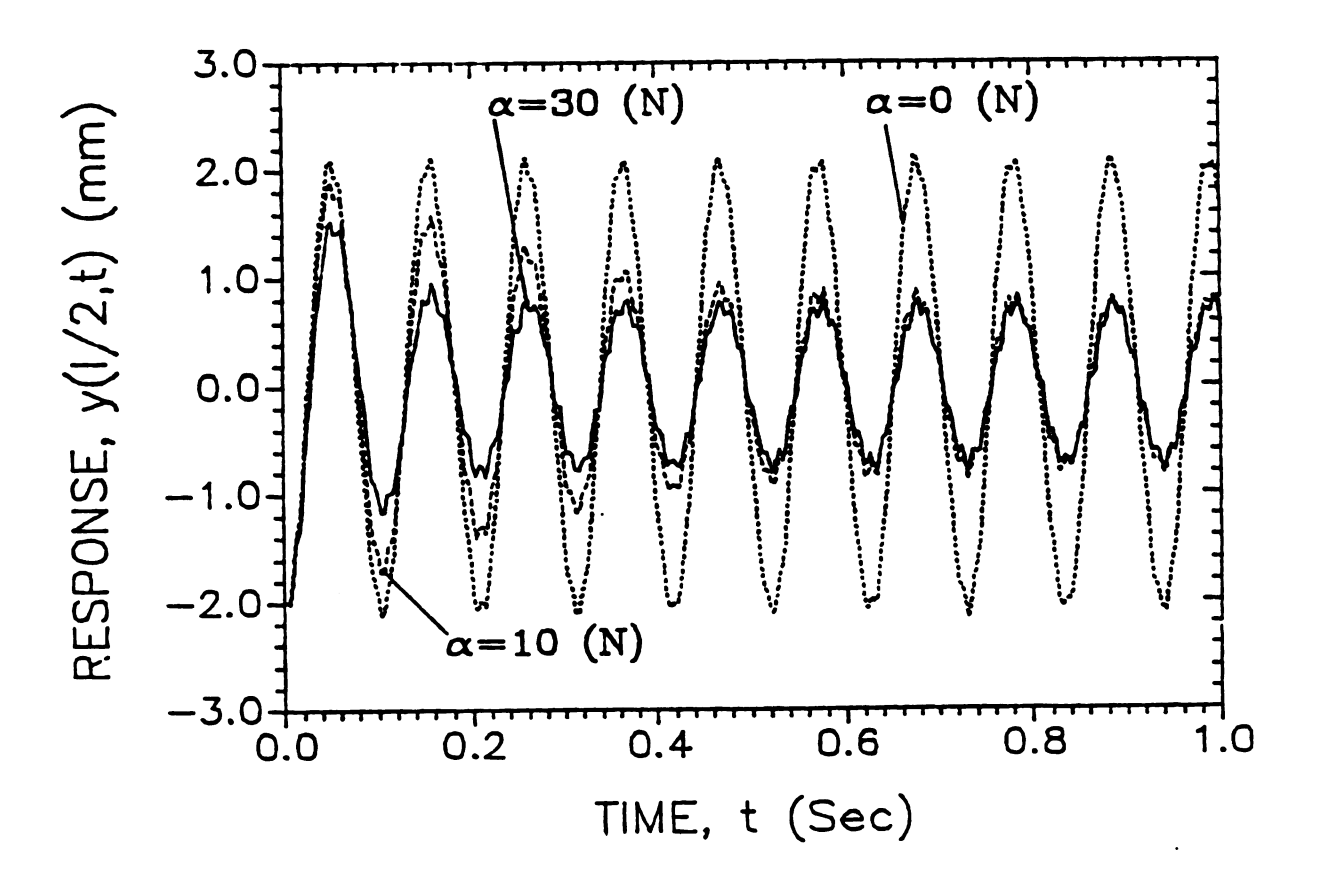


Figure 3.6a Response of the transverse vibration at $x=\ell/2$ for initial displacement of an infinite number of modes for various control gains for test case 5 .

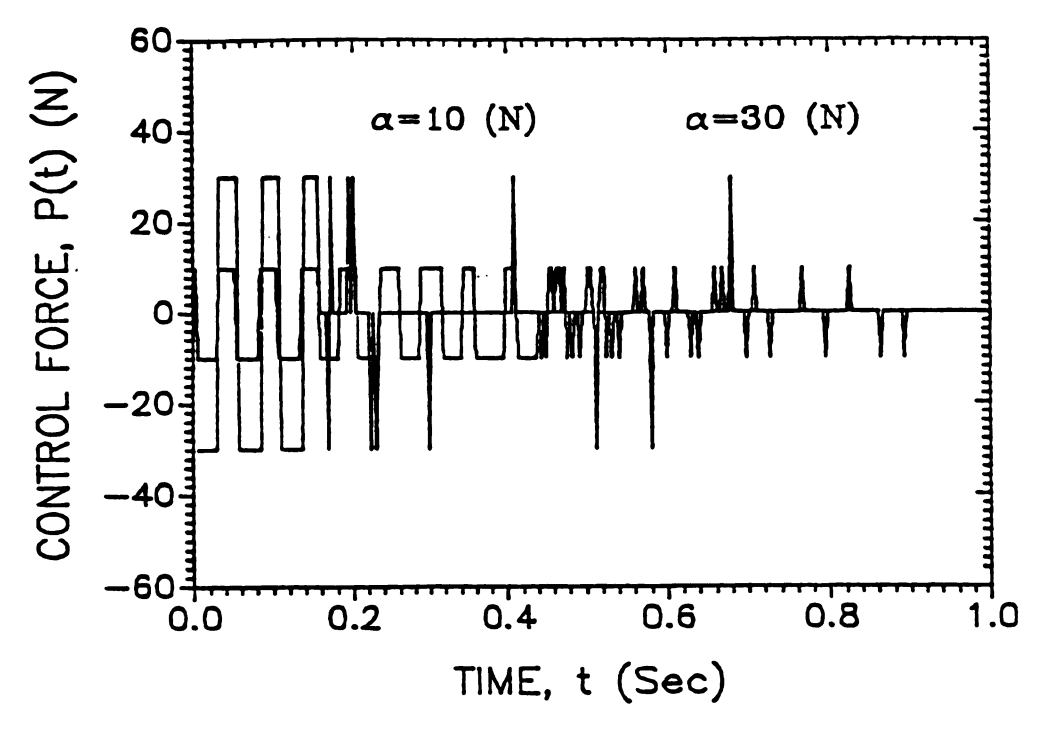


Figure 3.6b The required control forces, P(t) for test case 5

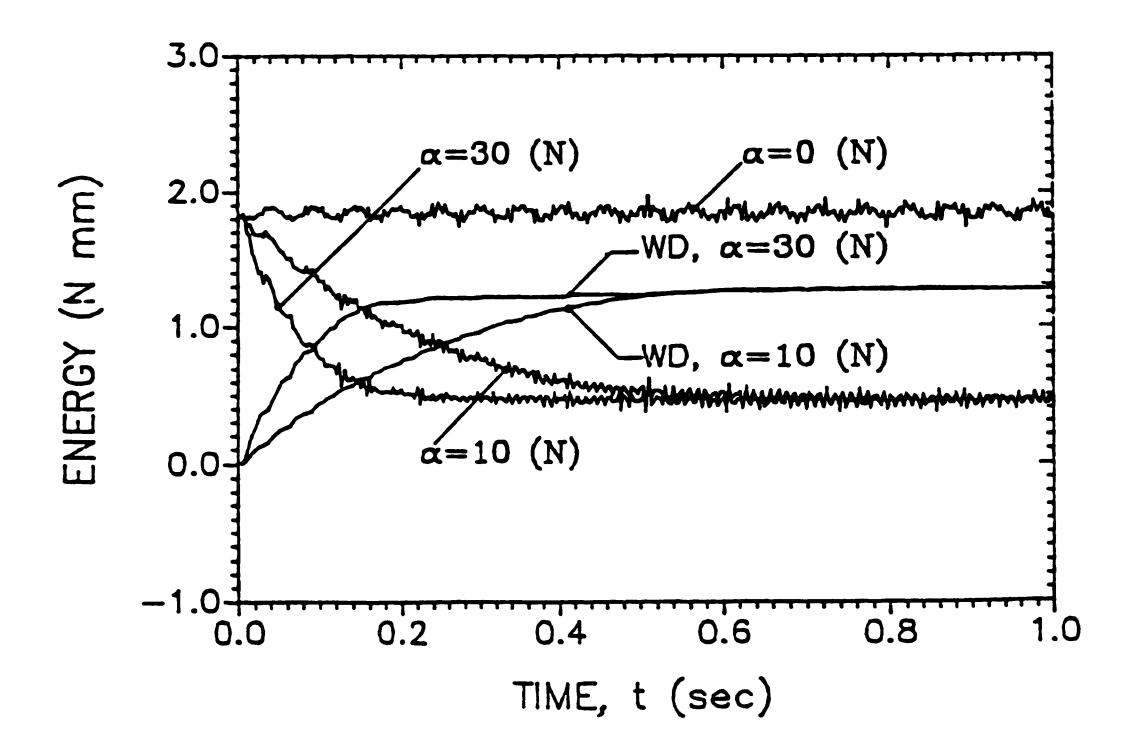


Figure 3.6c Internal energy and work done for test case 5

Table 3.4 Effect of the control gain α on the amplitude ratio a_n , the energy ratio e_n and the efficiency factor η for initial displacement for an infinite number of modes for test case 5.

gain	n	t _n	y _n	a _n	En	e _n	η \$
∝ N		sec	ma	TRIPA / TRIPA	N man		
10	1	.103	-1.741	. 8705	1.343	0.86	25.8
	2	. 2135	-1.37	. 7869	0.9272	0.831	48.77
	3	. 3110	-1.17	. 854	0.6818	0.857	62.33
20	1	.103	-1.418	. 709	0.983	0.737	45.7
	2	. 2038	-0.993	. 70	0.580	0.768	67.95
	3	. 311	-0.8427	. 848	0.438	0.864	75.8
30	1	.103	-1.174	. 587	0.759	0.647	58.1
	2	. 2038	-0.84	.715	0.508	0.818	71.9
	3	.311	-0.777	.925	0.427	0.917	76.4

Test Case 6: Initial Impulse Excitation of an Infinite Number of Modes.

The impulse in this case excites an infinite number of modes.

This impulse may be simulated as an initial velocity of the form

 $\partial y(x,0)/\partial t = 1.094x(l-x)$ m/sec

where x in meter, $0 \le x \ge l$. In this case, because the numerical differentiation process for estimating $\partial u(l,t)/\partial t$ causes numerical instability when the energy level is less than 0.0026 E(0), the control action is set "on" for internal energy $E(t) \ge 0.0026 E(0)$. (Figures 3.7a, b and c) show the response of the middle of the beam, the control force and the internal energy and the work done versus time for $\alpha = 0$, 10 and 30 N respectively. It is clear from figures 3.7 b,c that $E(t_1) = .0026 E(0)$ is satisfied in less than $5\frac{1}{2}$ cycles for $\alpha = 30$. Also the energy balance is satisfied for all $t \ge 0$ as shown in Figure 3.7c.

Table 3.5 shows the effect of control gain α on the amplitude ratio a_j , the energy ratio e_j and the efficiency factor η . It is clear from table 3.5 that for certain α , the amplitude ratio

 $a_j = y_j / y_{j-2}$ and the energy ratio $e_j = \sqrt{E_j / E_{j-2}}$ are equal up to the first decimal point, and these ratios decrease with increase of α , where j is the amplitude number. In this test case the control action could reduce the intial impulse energy to .0026 of its initial value in less than $5\frac{1}{2}$ cycles for $\alpha = 30$ N.

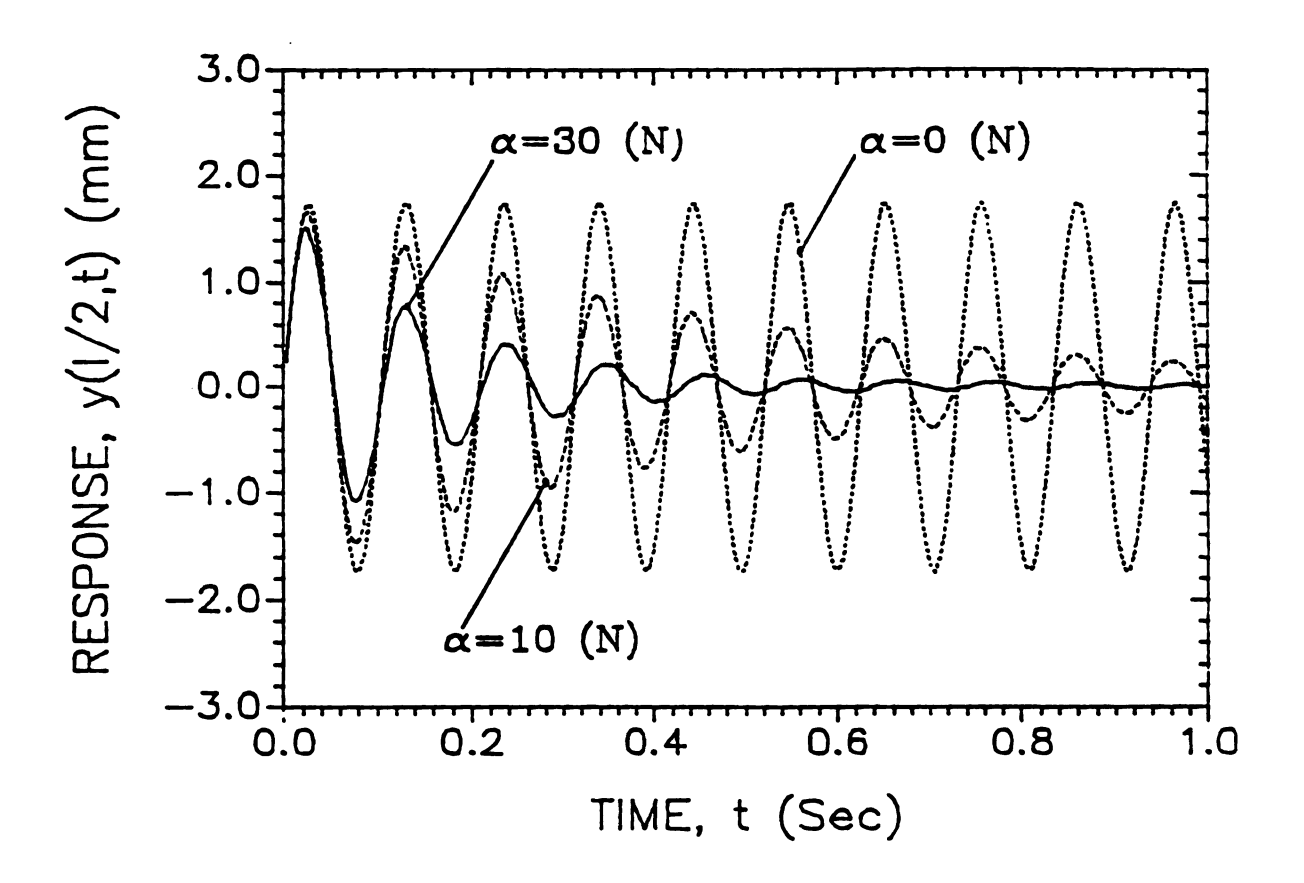


Figure 3.7a Response of the transverse vibration at $x-\ell/2$ for initial impulse of an infinite number of modes for various control gains for test case 6

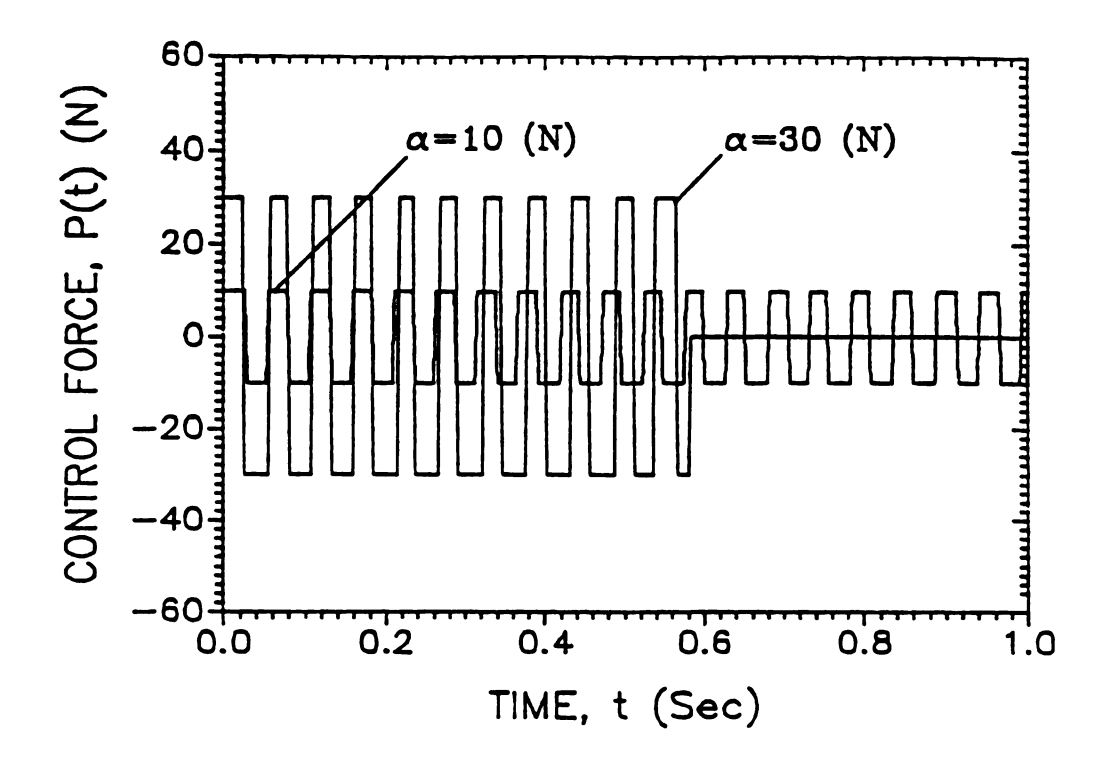


Figure 3.7b The required control forces, P(t) for test case 6

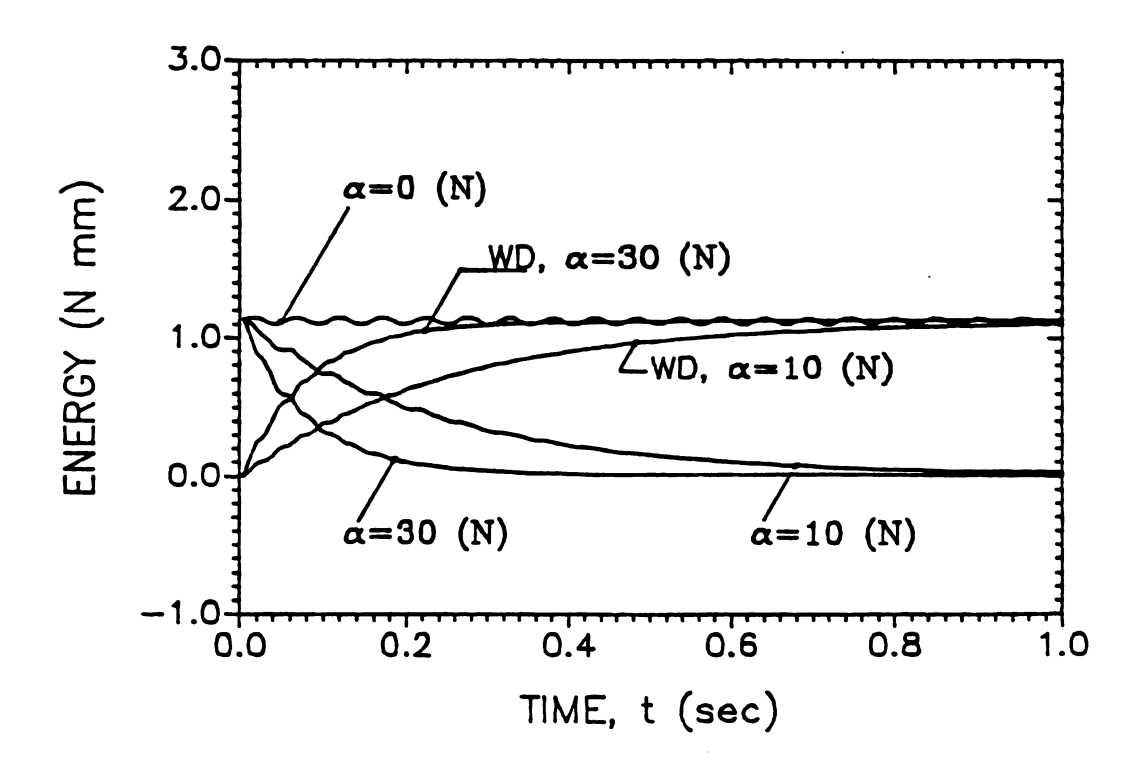


Figure 3.7c Internal energy and work done for test case 6

Table 3.5 Effect of the control gain α on the amplitude ratio a_j, the energy ratio e_j and the efficiency factor η for initial impulse excitation of an infinite number of modes for test case 6.

ain : N	ţ	t _j sec	y j	*j	Ij V —	• j	ηξ
0		··········	±1.74		1.125		0
10	1	.025	1.651		1.0178		9.53
	2	.0771	-1.4923	.8576	0.82119	.854	27.0
	3	.129	1.333	. 807	0.6624	.807	41.12
	4	.181	-1.1927	.80	0.5364	. 808	52.32
	5	.233	1.0781	.8087	0.4328	. 808	61.53
	6	. 285	-0.9746	.818	0.3498	.8075	68.91
	7	.337	0.8657	. 803	0.2819	.8071	75.02
20	1	.0219	1.576		0.942		16.27
	2	.0771	-1.276	.733	0.6011	.731	35.02
	3	.12911	1.023	.65	0.3906	.644	65.28
	4	.181	-0.8172	. 64	0.2556	.625	77.28
	5	. 2298	0.6606	.646	0.170	.659	84.89
	6	.285	-0.541	.662	0.1085	.651	90.36
	7	.3402	0.4301	.651	0.0701	. 642	92.99
30	1	.021	1.519		0.862		23.34
	2	.0771	-1.0885	. 623	0.438	.624	61.07
	3	.1291	0.778	.512	0.2271	.513	79.81
	4	.181	-0.553	. 508	0.120	. 523	89.33
	5	.233	0.4039	.519	0.0630	.526	94.4
	6	.02882	-0.2912	. 526	0.0327	.522	97.09
	7	.343	0.211	.522	0.0175	.527	98.44

Test Case 7: Internally Unstable System.

This test case is considered to give more insight in order to understand the control and to show that it can transform an internally unstable system into an asymptotically stable one. The system is internally distabilyzed by replacing a positive C in (3.10) by a negative value, C = -.00445 Kg m/sec. An initial displacement, $y(x,0) = 1.5 \sin(\pi x/l)$ mm, which is the first eigenfunction of the beam is applied. Figure 3.8a shows the response of the middle of the beam, y(l/2,t) versus time for $\alpha = 0$, 10, 20 and 100 N. In Figure 3.8a the curve for $\alpha = 0$ (control is off) is the response of the free unstable, self excited vibration. The frequency of this response is 9.654 Hz which is the the first self excited frequency of the beam.

The frequency of the response For $\alpha=0$ varies with time within one cycle of oscillation. It oscillates about the frequency of the uncontrolled ($\alpha=0$) system, therefore every half cycle of the response curve, there are two different zones: slow and fast. Figure 3.8b is a plot of the response and the control force for $\alpha=40$ N. In Figure 3.8b t and t are the time of any point $x \in l$ taken to reach the equilibrium position from the maximum amplitude of oscillation and from the equilibrium position to the maximum amplitude of oscillation respectively. It should be noticed from Figure 3.8b that during t and t, P(t) is compression and tension respectively which gives a physical interpretation of the control mechanism, e.g., when the distance between the beam supports tends to get longer, the control force is compression and vice versa. In this case the

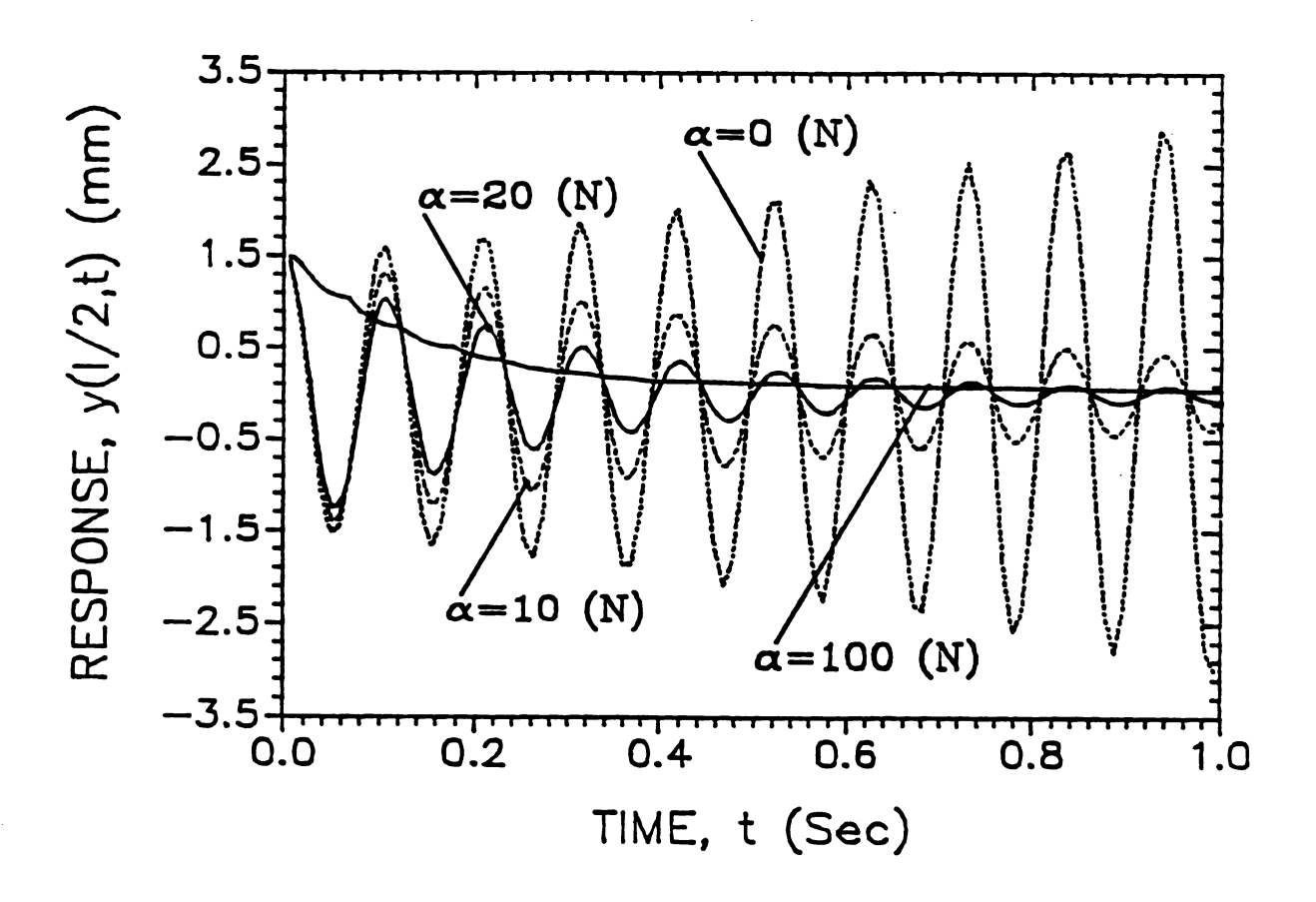


Figure 3.8a Response of the transverse vibration at x-2/2 for internally unstable system test results for various control gains for test case 7

numerical values of t_c and t_t give the frequencies ω_c =7.35 Hz and ω_t =11.36 Hz respectively, i.e., during half of a cycle of the transverse vibration, the frequency of oscillation varies from ω_c to ω_t . This fluctuation shows that there are softening and stiffening actions due to the parametric force p(x,t) generated by the control action P(t).

Figure 3.8c shows the required control force versus time for α -10, 20 and 100 N. The internal energy E(t) and the work done by the control force p(t) are plotted versus t for the same control gains α in Figure 3.8d. An efficiency factor $\eta = (E(0)-E(t))/E(0)$ giving the fraction of the energy dissipated due to the control action during the first cycle of oscillation, t_1 has been considered in order to judge the efficiency of the approach in the first cycle. Table 3.6 shows the effect of the control gain α on the amplitude ratio a_j , the energy ratio e_j and the efficiency factor η . In this test case, the control algorithm could successfully transform the initially internally unstable system into an asymptotically stable system without exciting any other modes which might be excited easily since the system is internally unstable and for α -100 N the vibration monotonically decreases with time.

This chapter has shown the effectiveness of the control law in controlling beam transverse vibration through investigation of stability, transient motions and controlled response from external disturbances. The closed-loop system which was derived in chapter 2 from the Liapunov function for the beam, was reduced to a nonhomogeneous wave equation for u(x,t) subject to the non homogeneous

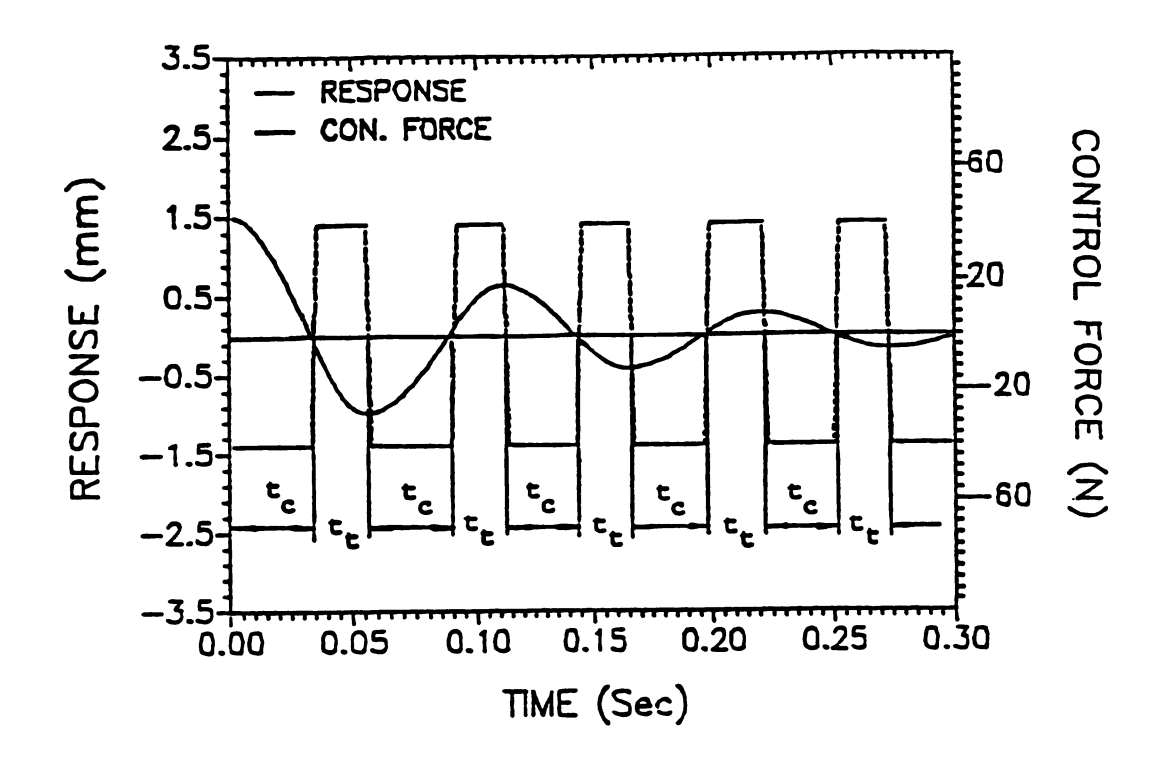


Figure 3.8b Curves of response and control force for $\propto -40$ N for test case 7

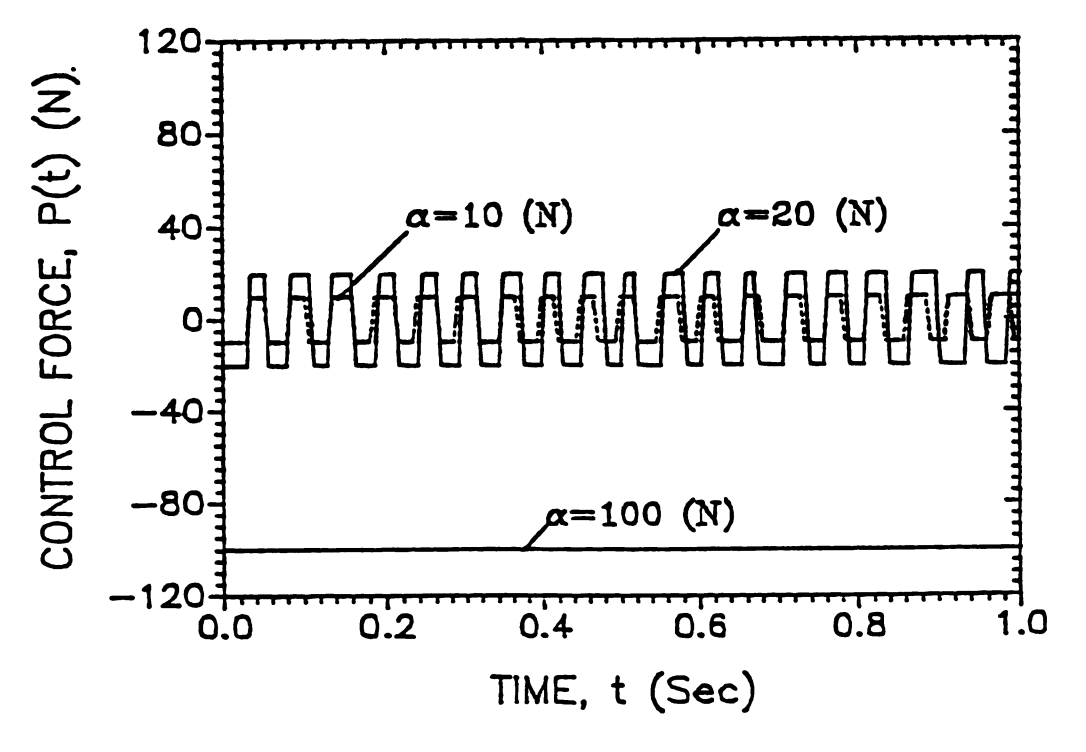


Figure 3.8c The required control forces, P(t) for test case 7

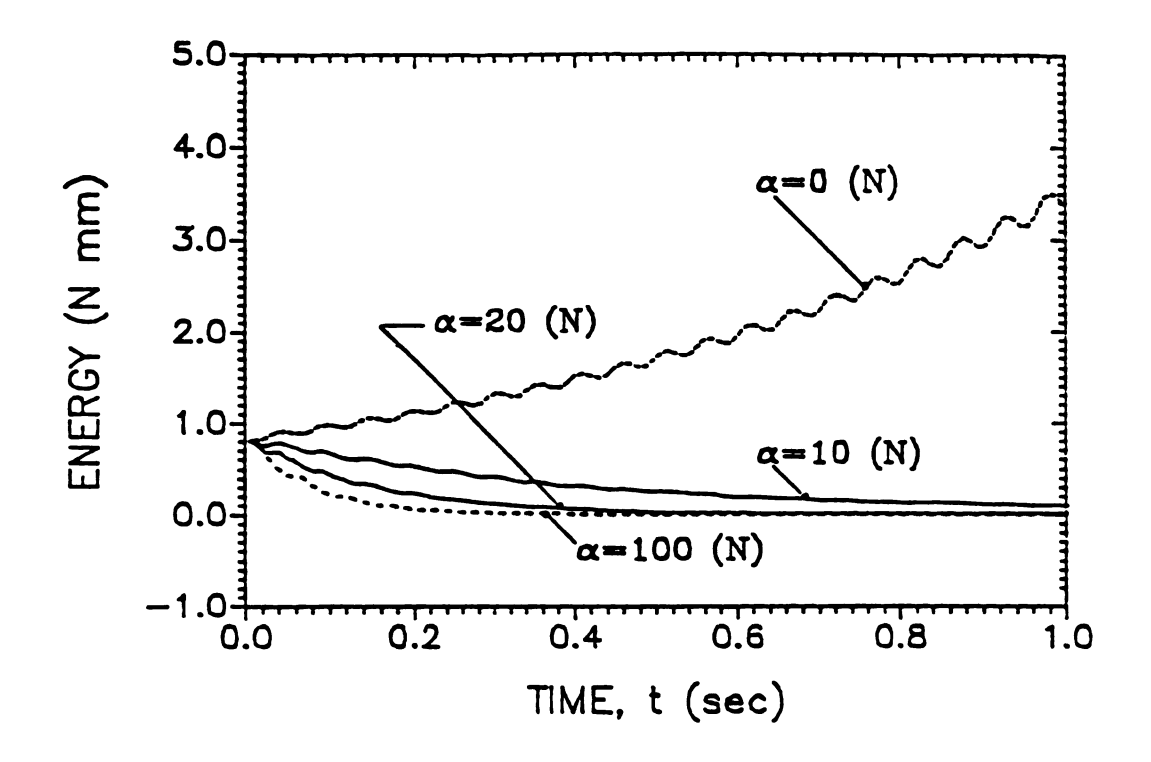


Figure 3.8d Internal energy for test case 7

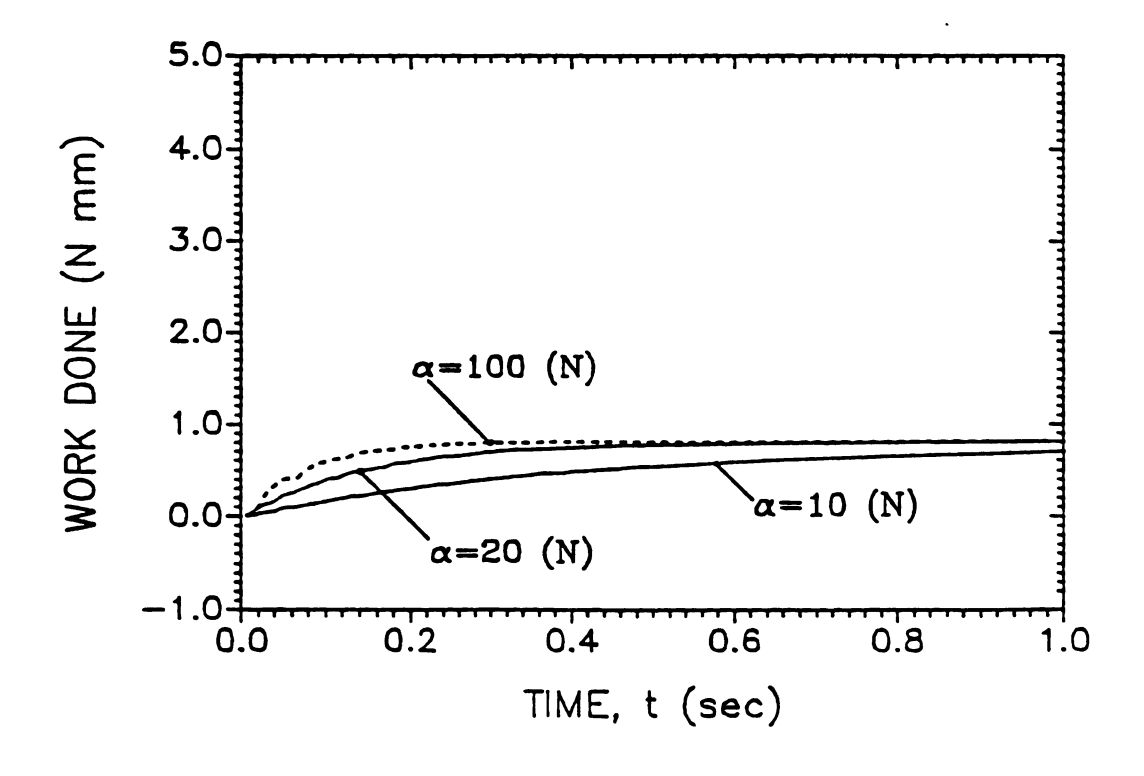


Figure 3.8e The work done for test case 7

Table 3.6 Effect of the control gain \propto on the amplitude ratio a_j , the energy ratio e_j and the efficiency factor η for for internally unstable system for test case 7.

gain	j	tj	Уj	^a j	^E j	e j	η &
α N		sec	mm	man/mm	N mm		
			· · · · · · · · · · · · · · · · · · ·		· · · · · · · · · · · · · · · · · · ·		
10	1	.0527	-1.41477		.74872		8.47
	2	. 1039	1.31884	. 8792	.651616	. 892	20.3
	3	.157538	-1.235227	.8731	. 57022	. 87	30.29
	4	. 2086977	1.13517	.861	.481039	. 86	41.19
	5	. 259857	-1.06915	. 8655	.429797	. 868	47.46
	6	. 31345	0.98863	.871	.3701688	. 877	54.75
	7	. 36461	-0.92952	. 8694	.3276178	.873	59.95
20	1	.0527	-1.26749		. 596791		27.04
	2	.106379	1.041047	.694	.403597	.702	50.66
	3	.157538	-0.873227	. 689	.287831	. 694	64.81
	4	. 211134	0.72176	. 693	. 199689	. 703	75.59
	5	. 262293	-0.610207	. 699	.142664	. 704	82.56
	6	. 31588	0.50948	. 706	.09699	.697	88.26
	7	. 367048	-0.42654	. 699	.070878	. 705	91.34

boundary conditions which could be solved analytically using finite Fourier transform and a nonlinear fourth order parabolic equation in y(x,t) which was approximated by finite difference method.

The simulation was run on a prime 750 computer at the Albert H. Case Center for Computer-Aided Design at Michigan State University. The beam chosen for the test had dimensions and material properties appropriate for the laboratory tests which will be given in chapter 4 and the simulations indicated asymptotically stable response. Test cases 5 and 6 for infinite number of modes demonstrated most of the initial energy was removed in the early oscillating cycles. Test cases 3 and 4 showed resonant amplitude could be limited by this control.

The single mode test results demonstrated:

- 1) asymptotically closed-loop stable transient response for $\alpha < 40$ N and monotonically decreasing response for control gain $\alpha = 108$ N.
- 2) the closed-loop control reduced the resonant response amplitude.

For test results exciting an infinite number of modes the control action successfully:

1) reduced the amplitude from 2 mm to 0.8 mm for control gains 10, 20 and 30 N for energy based control; i.e. control was set "on" for $E(t) \ge .3E(0)$ for the initial displacement $y(x,0) = 21.527 \ x(x - l)$ mm where x in m.

2) reduce the initial impulse energy due to an initial velocity given by $\partial y(x,0)$ / $\partial t = 1.094(\ell - x)$ m/sec where x in m, to .0026 of its initial value for control gain $\alpha = 30$ N.

In both transient single mode and infinite number of modes the closed connection between the energy ratio \mathbf{e}_n and the amplitude ratio \mathbf{a}_n for low values of control gain α was clear. For low α it was clear that the amplitude ratio \mathbf{a}_n and the energy ratio \mathbf{e}_n were almost constant and equal for the first three cycles and depend only on α . This observation has not been previously reported because none has used this control before.

CHAPTER 4

EXPERIMENTAL FACILITIES, PROCEDURES AND RESULTS.

A prototype control system was constructed to evaluate the performance of the active parametric vibration control system on a simply supported beam (Figure 4.1). The beam chosen for the experimental tests has dimensions that give reasonable natural frequencies. This chapter discusses the experimental control evaluation in three main sections. In section 4.1 the construction of the simply supported beam test stand is presented. The actuator mechanisms and sensors and their associated circuits are presented in section 4.2. Experimental results are given in section 4.3. The modelled beam is compared with the ideal beam with respect to the modal frequencies and the modulus of elasticity in section 4.4. Significant increases in stability of the test beam were measured which demonstrated the feasibility of employing active parametric vibration control. The experimental results presented here will be compared with simulation results in chapter 5.

4.1 Simply-Supported Beam Test Stand

In this section, the construction of the beam test stand to assess control performance is described. The test stand had the following requirements:

- 1- External damping due to frictions in the joints of the moving parts should be minimized.
- 2- The actuators and sensors should have minimum interaction with the beam dynamics.
- 3- The effect of gravity on the transverse and longitudinal vibration should be eliminated.

Figure 4.1 shows the prototype active vibration controller.

The dimensions and physical properties for the steel beam are:

$$\rho = 8304 \text{ kg/m} [.31b/in]$$

$$l = .61 m [2ft]$$

A = 50.8mm width x 1.588mm thickness [2in x .0625in]

To eliminate the friction in the hinge junctions of the beam supports while achieving near-zero bending moment at the ends of the beam, i.e. $y_{xx}(0,t) = y_{xx}(l,t) = 0$; the end conditions were approximated using very thin steel shims of thickness .01 inch which were soldered in slots at the ends of the beam and tightly fixed to the supports.

To realize the axial movement of the simply-supported beam end, while keeping minimum interaction between the beam dynamics and the supports; the other end of the corresponding shim was fixed in a rigid

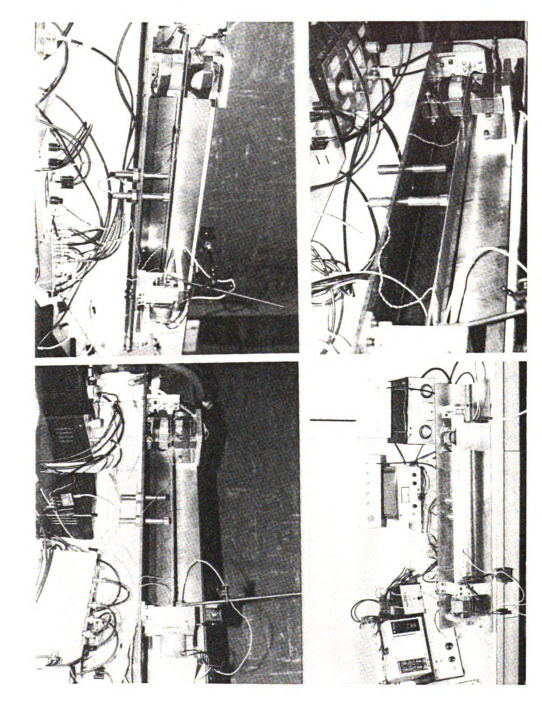
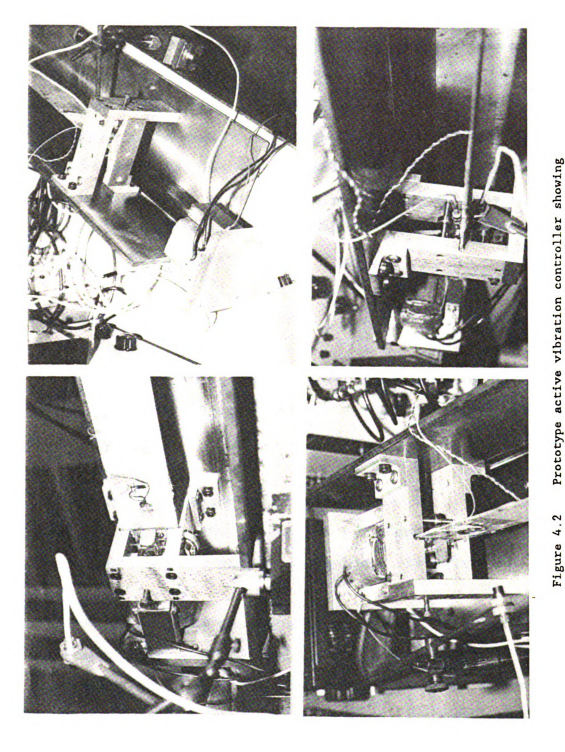


Figure 4.1 Prototype active vibration controller showing the simply-supported beam test stand and the main instrumentation devices

cross shaped section of plexi-glass (to reduce inertia) which was supported on three deep groove ball bearings (to allow only axial motion with minimum friction). To ensure proper contact between the bearings and the plexi-glass support, one of the bearings was made adjustable through a screw which drives two swivelling brackets and tightened when adjusted. A steel strip of dimension $1.5 \times 3.5 \times .06$ in. fixed by screws at the other end of the plexi-glass support, which could be attracted by the electromagnet to implement the active control as shown in Figure 4.2. The maximum control force applied by the magnet was up to 90 N for .01 in. gap. The supports of the beam were fixed through brackets to a machined 6.5 x 6.5 x 35.5 in. right angle which was fixed to a heavy cast iron test stand through heavy duty C-clamps. To excite the beam, two identical electromagnets were fixed to the frame through brackets and centered at 82.55 mm. pair of magnets could excite the first five modes of the beam efficiently. The effect of gravity on the transverse and longitudinal vibrations was eliminated by allowing both y(x,t) and u(x,t) to be in the horizontal plane.



re 4.2 Prototype active vibration controller showing the end motion sensors and the structure of the moving beam end and the control actuator

4.2 Active Control Prototype

In this section the experimental procedure and the measured quantities are presented. This section is divided into five subsections. Subsection 4.2.1 describes the main instrumentation circuits, and subsections 4.2.2a and 4.2.2b describe the end beam acceleration and displacement measurements respectively. The transverse displacement measurement is given in subsection 4.2.3. The beam excitation and the control actuators are presented in subsections 4.2.4 and 4.2.5 respectively.

4.2.1 Main Instrumentation Circuits

To evaluate the performance of the control law derived in chapter 2 from the Liapunov function for the beam, the following circuits constructed:

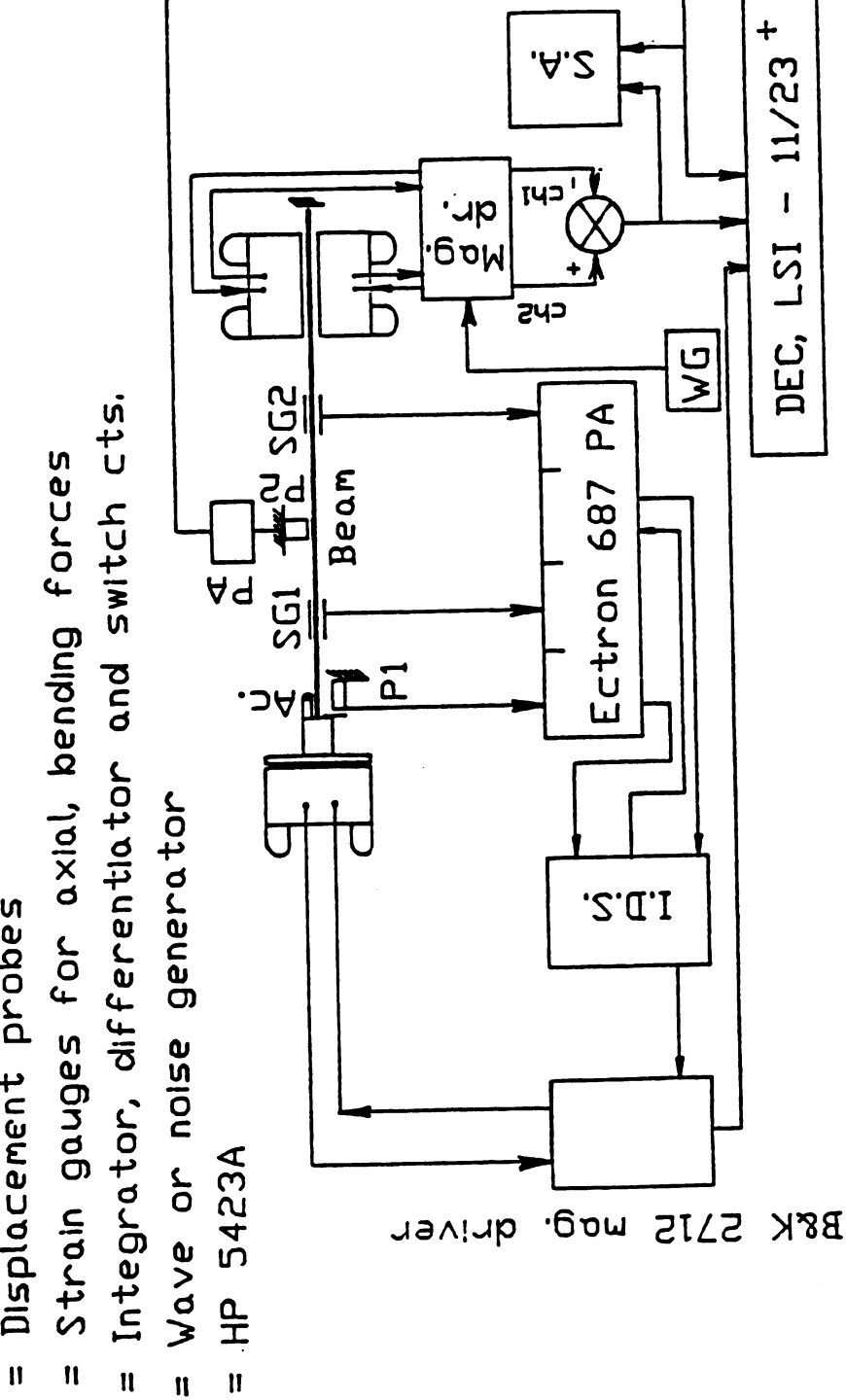
- a) The transverse vibration measurement circuit.
- b) Beam excitation and the exciting force circuits.
- c) Beam control actuator circuits to implement the control law.

The transverse vibration was measured using an inductive noncontacting displacement probe. The beam excitation circuit consisted of a pir of electromagnets driven by a custom built magnet amplifier driven by two wave functions or by a random noise generator. The exciting force was measured using a strain gauge bridge circuit. The control actuator was an electromagnet on the end of the beam excited by a magnet derive amplifier driven by custom built analog circuits. The analog circuits consisted of an integrator if the end beam motion was observed by an

accelerometer or a differentiator if the end beam motion was observed by a noncontacting displacement probe. The output signal from either the integrator or the differentiator represented the end beam velocity $(\partial u(l,t)/\partial t)$. This velocity was fed into an analog switch deriving the power amplifier that supplied current to the control electromagnet. Figure 4.3 shows the measurement circuits and control flow diagram.



11



Measurement and control flow diagram Figure 4.3

4.2.2 End Beam Motion Measurement

The control law derived in chapter 2 from the stability analysis using the direct method of Liapunov gave the relation between beam end velocity and the control force. A control force opposing the velocity for all t > 0 was shown to yield asymptotic stability. Two different methods to accurately observe the beam end velocity were necessary. It was found in the transient motion test experiments that the observed signal level produced by the accelerometer was too small at low frequencies to be distinguished from the noise. At low frequencies, the displacement of the end of the beam was measured by one of the inductive noncontacting displacement probes to improve the signal-to-noise ratio.

4.2.2a End Beam Acceleration Measurement.

The closed-loop control law based upon observing the end beam velocity and applying the actuating force accordingly. Because there was no available velocity transducer, the acceleration was measured and integrated by an analog integrator. Integrating acceleration is a smoothing process, which reduces high frequency noise.

The end beam acceleration was measured with a piezoelectric accelerometer and amplifier by PCB PiezoTronics, Inc. model 482A10. The measured signal was fed into the analog integrator (Figure 4.4). The output velocity was amplified and fed into an analog switch; which controlled the power amplifier type 2712 by Bruel & Kjaer which drove the control electromagnet.

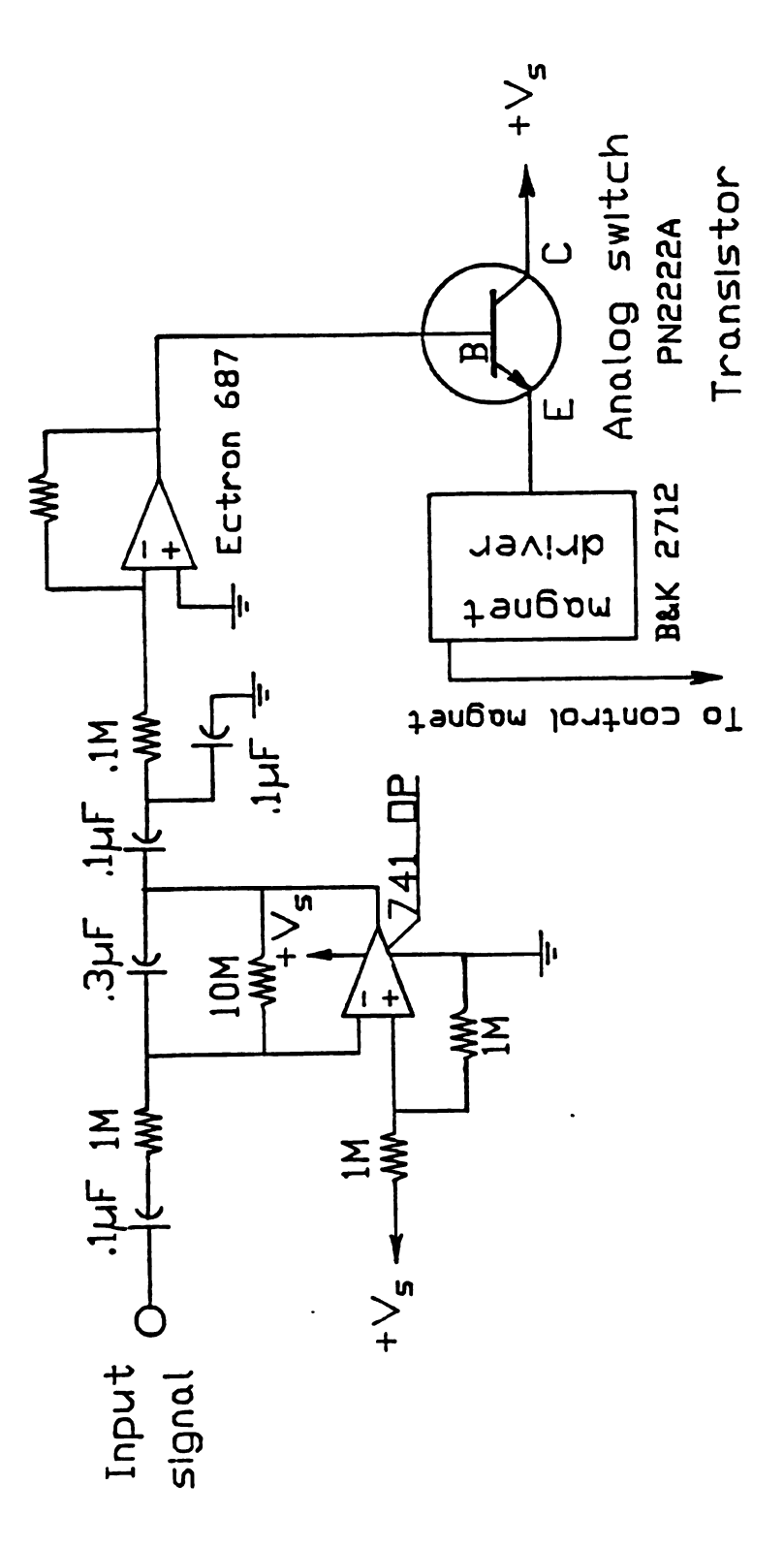


Figure 4.4 Integrator and analog switch circuit

To find the bandwidth of the integrator, the transfer function of the integrator was measured over 0-200 Hz using the HP dynamic analyzer as shown in Figure 4.5a which showed that the integrator was acceptable over 20 - 200 Hz. Figures 4.5 b,c show two test signals at 20 Hz and 200 Hz and their integrator outputs which verify the frequency response result.

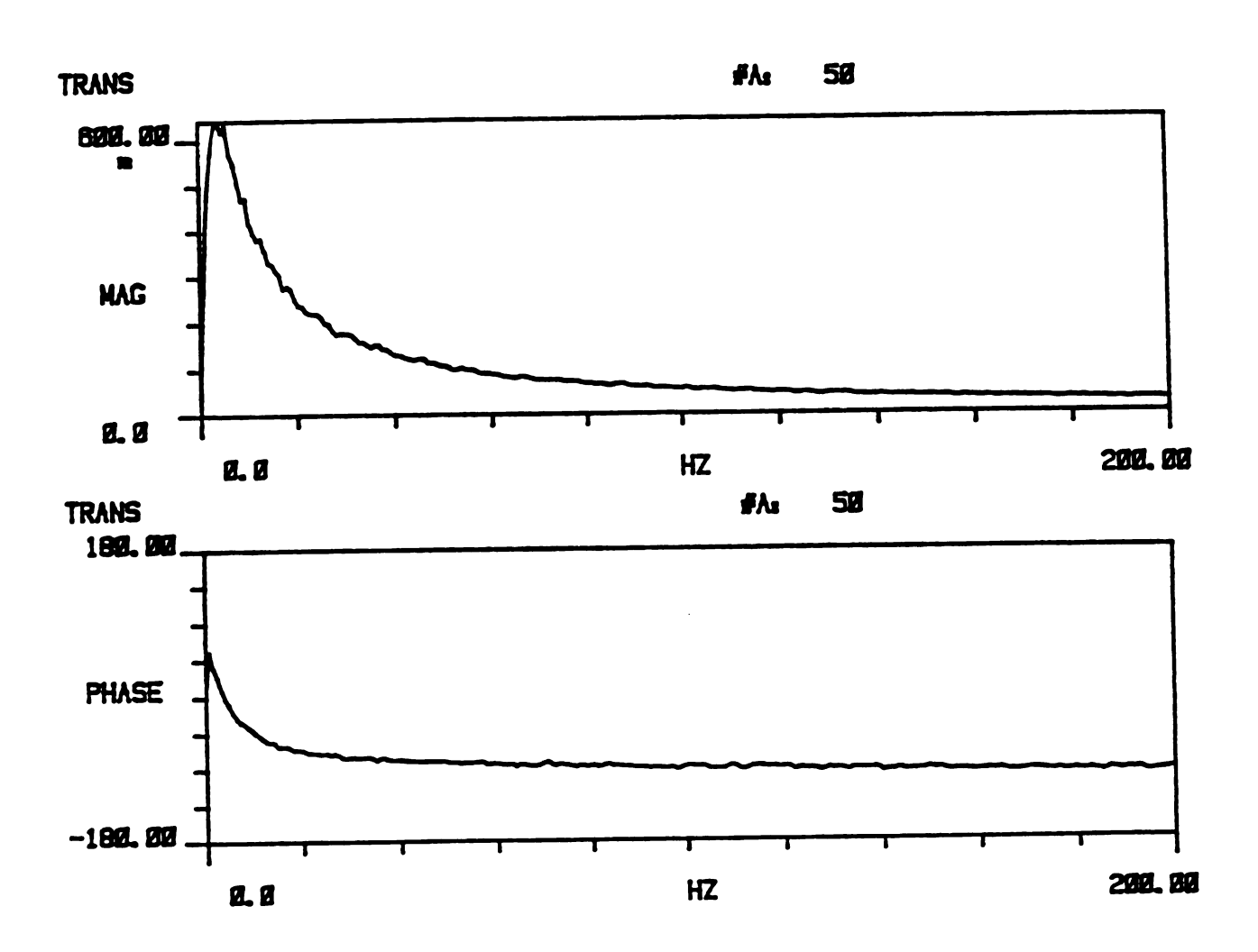


Figure 4.5a Integrator transfer function test results

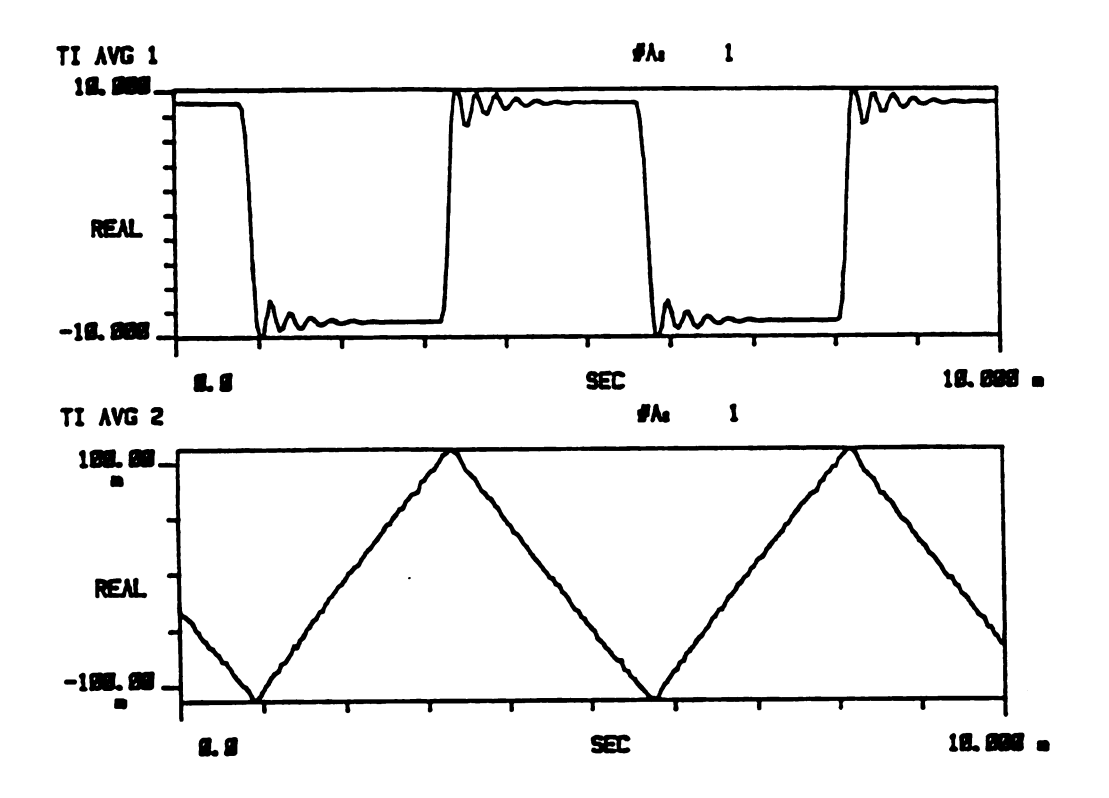


Figure 4.5b Integrator test signal results at 20 HZ

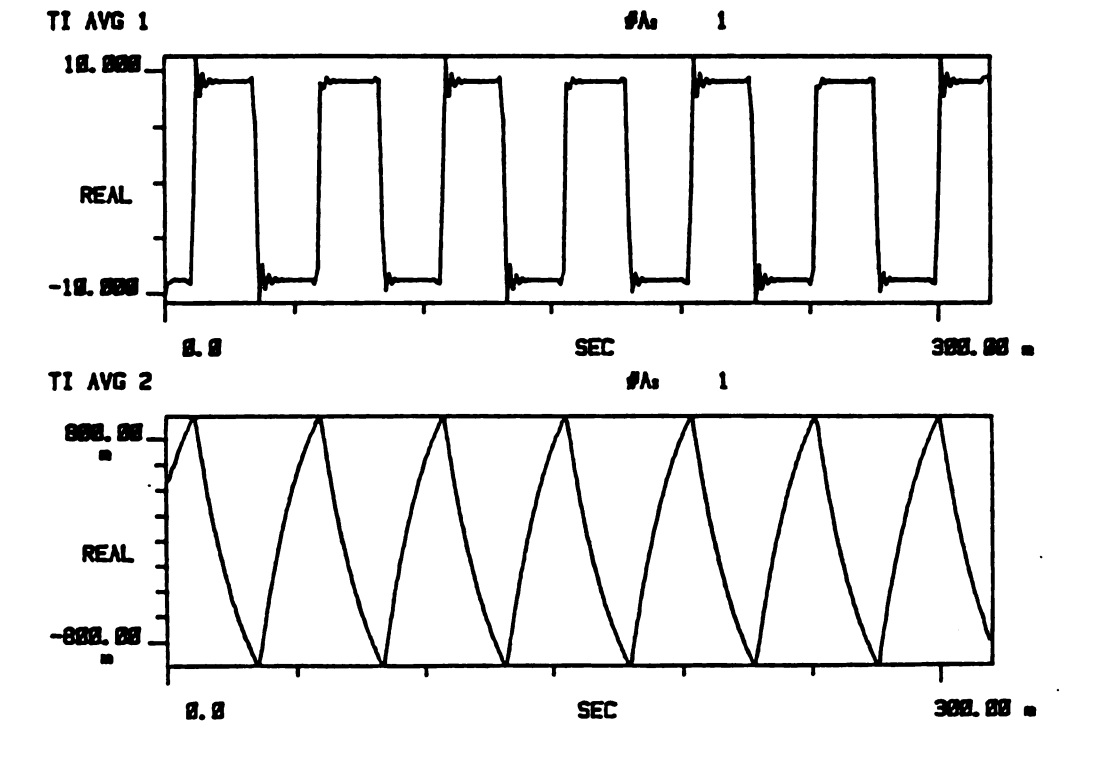


Figure 4.5c Integrator test signal results at 200 HZ

4-2.2b End Beam Displacement Measurement.

In the transient tests, an efficient way to find the beam end velocity by observing the displacement was required. The displacement was measured using inductive noncontacting probe model KD 2400 by Kaman Sciences and the observed signal was fed into the analog differentiator showed in Figure 4.6. The resulting velocity signal was fed into the analog switch as in the integrator circuit. To find the bandwidth of the differentiator, the transfer function of the differentiator was measured from 0 to 50 Hz using the HP dynamic analyzer as shown in Figure 4.7a. This test showed that the differentiator was acceptable over a frequency range of (5- 25 Hz). Figure 4.7b shows a test signal at 20 Hz and the corresponding differentiator output.

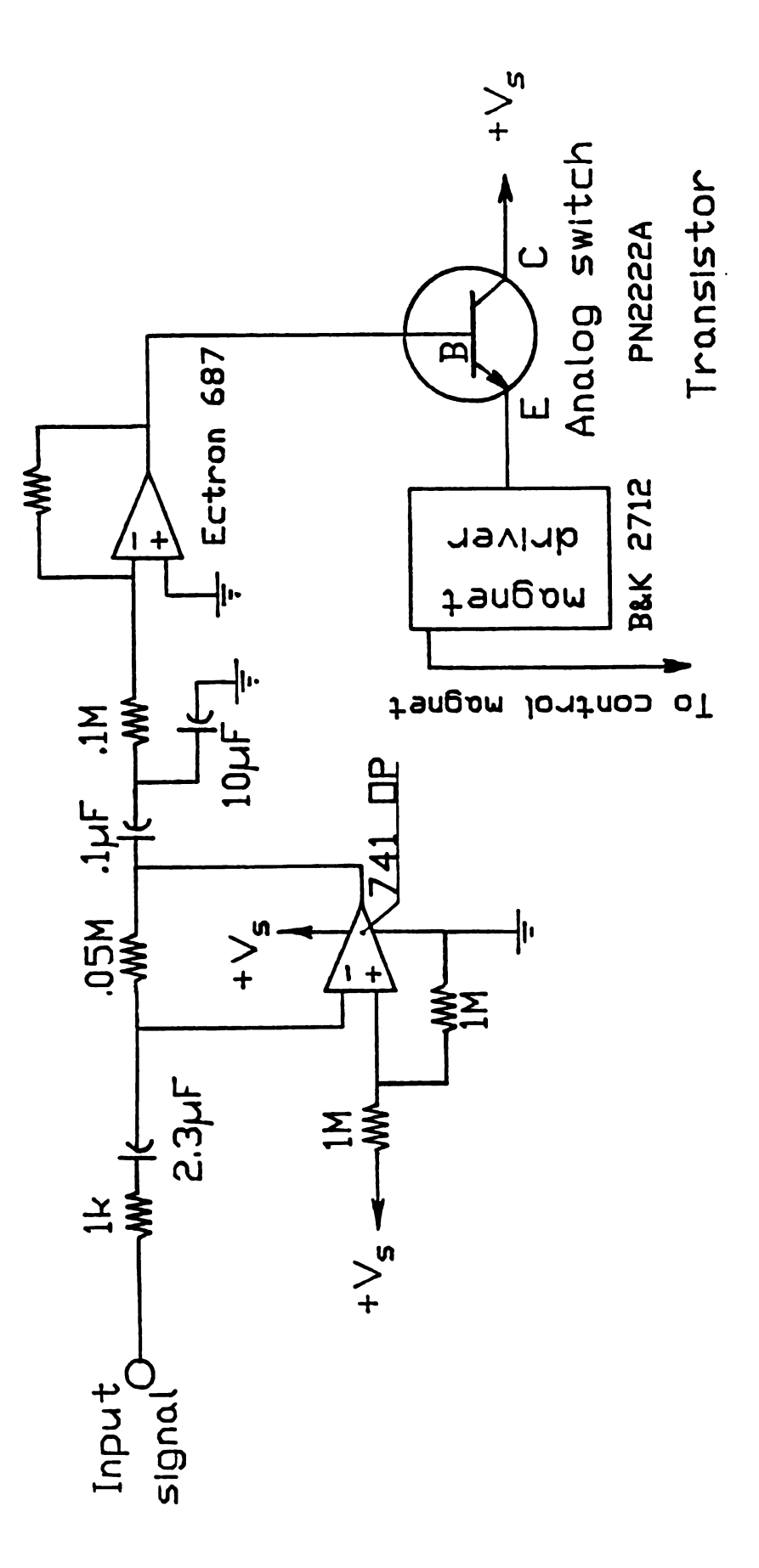


Figure 4.6 Differentiator and analog switch circuit

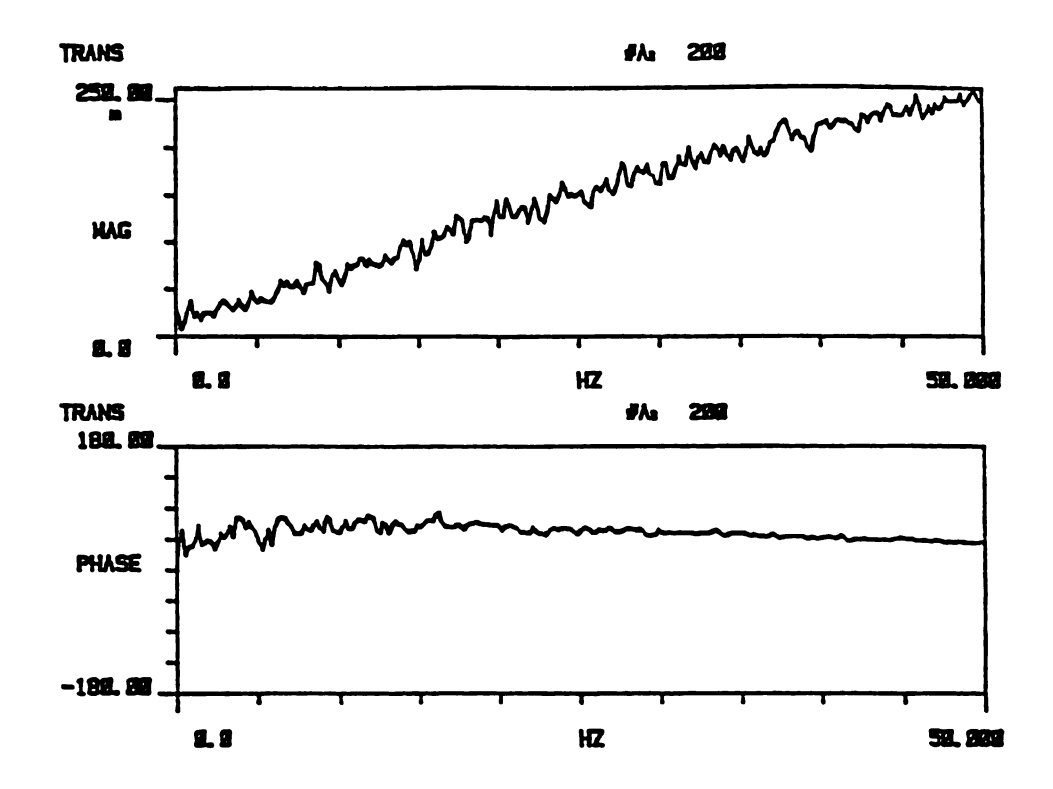


Figure 4.7a Differentiator transfer function test results

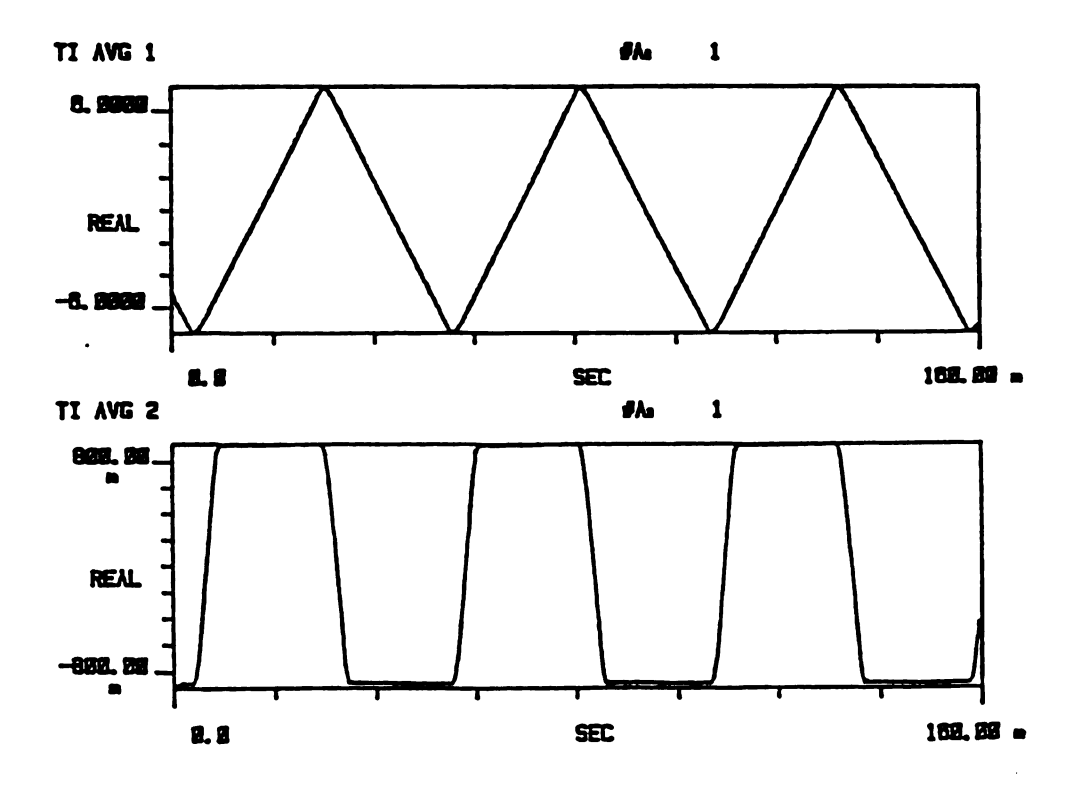


Figure 4.7b Differentiator test signal results at 20 HZ

4-2.3 Transverse Displacement Measurement.

To evaluate control power, the transverse displacement of the beam was measured using an inductive noncontacting displacement probe model KD2400 by Kaman Sciences Corporation, located at 367.2 mm from the stationary end of the beam. This position was chosen to avoid nodes in the first five modes. The output signal was fed into the signal amplifier then into DEC LSI/23⁺ after removing the DC component as shown in Figure 4.3. The sensor had a sensitivity of .23 mm/V with a resolution of .25 V (appendix Al) yielding a measurement range of 0-2.5 mm and accuracy ± 0.06 mm.

4.2.4 Beam Excitation.

To achieve minimum interaction between the beam dynamics and the beam excitation force, two identical electromagnets opposing each other and located at 82.55 mm from the stationary end of the beam were used. The two electromagnets were driven either by a function generator (Wavetek Model 180) or random noise generator (HP 54410 A and 5423 A). The exciting force was calibrated using strain gauge (type EA-13-125BT-120 by Micro-Measurements group, INC.) the maximum force available was 5 N and the strain gauges had a sensitivity of 1.5 N/V for a linearized magnet output range of 0-.75 N with resolution of .08 N. The exciting force calibration procedure and the strain gauge arrangement are given in appendix A2.

4.2.5 Control Force Measurement

The axial force produced by the control electromagnet was calibrated using a full strain gauge bridge (type EA-13-125BT-120 by M-M). The strain gauges had a sensitivity of 36.1 N/V for magnet drive output up to 90 N with resolution of .75 N (appendix A2).

4-3 Experimental Test Results and Discussions.

The prototype control system presented in the previous sections was constructed to obtain experimental data to evaluate the performance of the control law derived in chapter 2 by using the direct method of Liapunov for the beam. In this section the experimental procedure and the results of three test cases representing the stability due to transient and steady state motion are presented and discussed. The significant increase in stability of the test beam demonstrates the feasibility of employing active parametric vibration control. The experimental results presented will be compared with the simulation results in chapter 5.

In the following test cases the control force P(t) was set "on" for negative end beam velocity and "off" elsewhere (Figure 3.2). The control gain here is the amplitude of the control force α . The locations of the sensors and actuators are shown in (Figure 4.8).

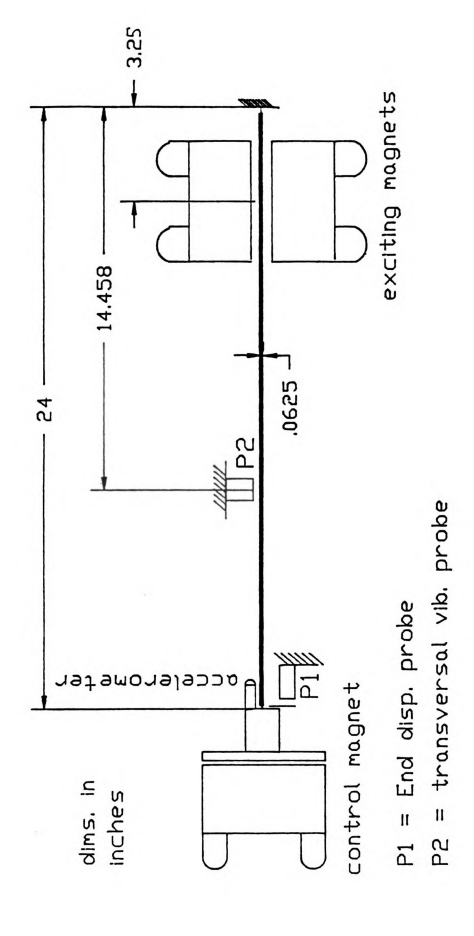


Figure 4.8 Sensors and electromagnets locations

Test Case 1: Transient Motion.

This case is similar to an initial value problem in which an initial displacement, velocity or both were given to the beam. To realize this, the beam was excited at the desired mode until reached a steady state, then the excitation was turned "off" and the control at a test gain α was turned "on" until the vibration decayed. Data was recorded from a time just before the excitation was turned "off". Figures 4.9-4.12 show the real time record of the transient motion for control gain $\alpha = 0$, 10.63, 13.98 and 58.67 after being converted into physical values using the calibration formulas given in the appendices. Figure 4.9 shows the results of the transient response for the uncontrolled beam. In figures 4.9a, 4.10b, 4.11a and 4.12a the response curves are marked "2" while the excitation signals are marked "1". The excitation signals where plotted with the response curves just to give an idea when the excitation was turned off". In Figures 4.10b, 4.11b, and 4.12b the amplitudes of the control force decrease with the decay of the response, that is because the control law uses the end beam velocity (which is more or less proportional to the response) of the observed signal to apply the control action P(t). Table 4.1 summarizes the experimental test results of the transient case for the control action on the amplitude of the cycles number 1,5,10,15,20 and 48. By comparing figures 4.9 with 4.12a and from table 4.1, the amplitudes were reduced with the increase of the control gain α ; e.g. for n = 48, the amplitude reduced from .40 mm to .16 mm, for control gain $\alpha = 58.67$ N.

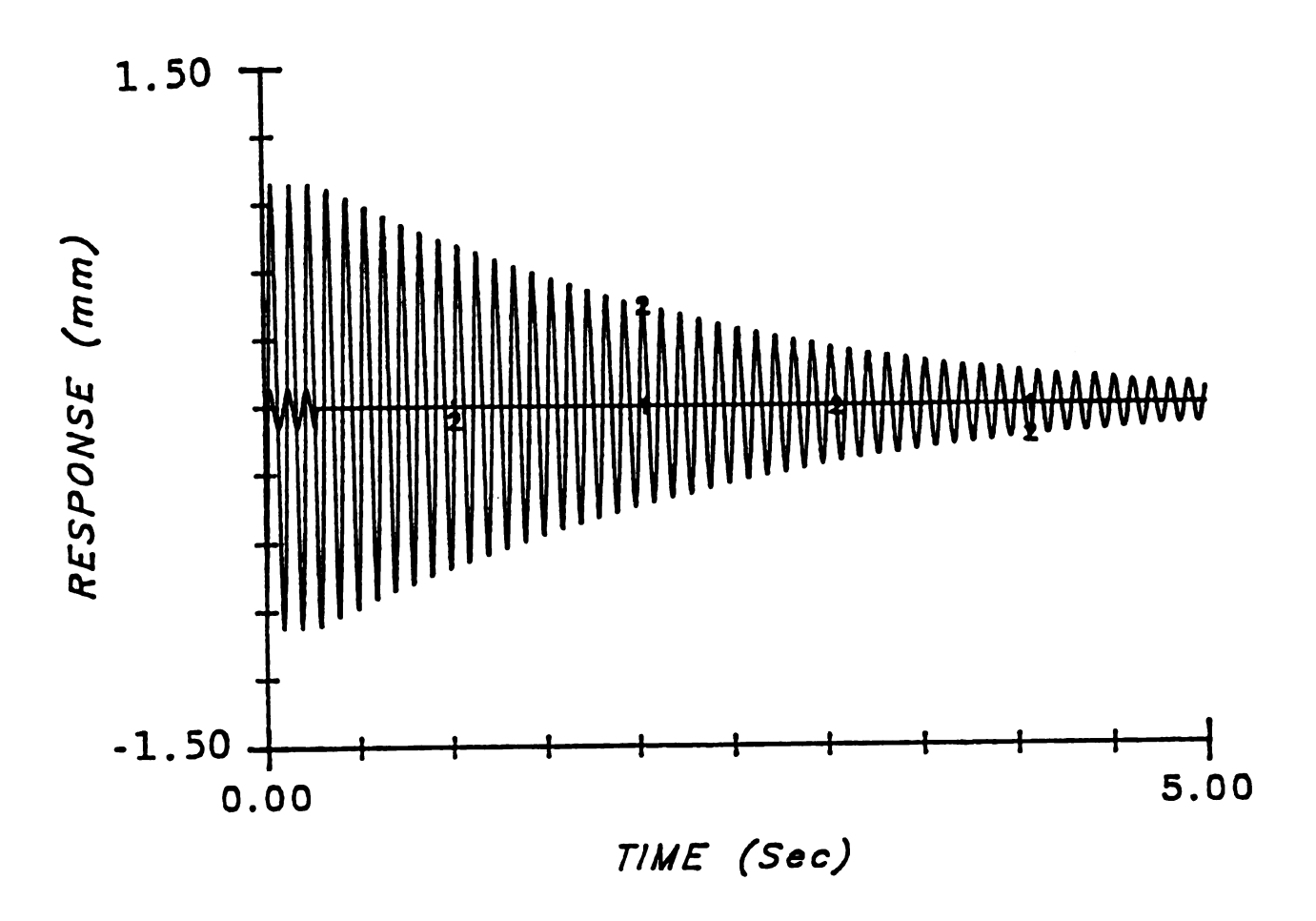
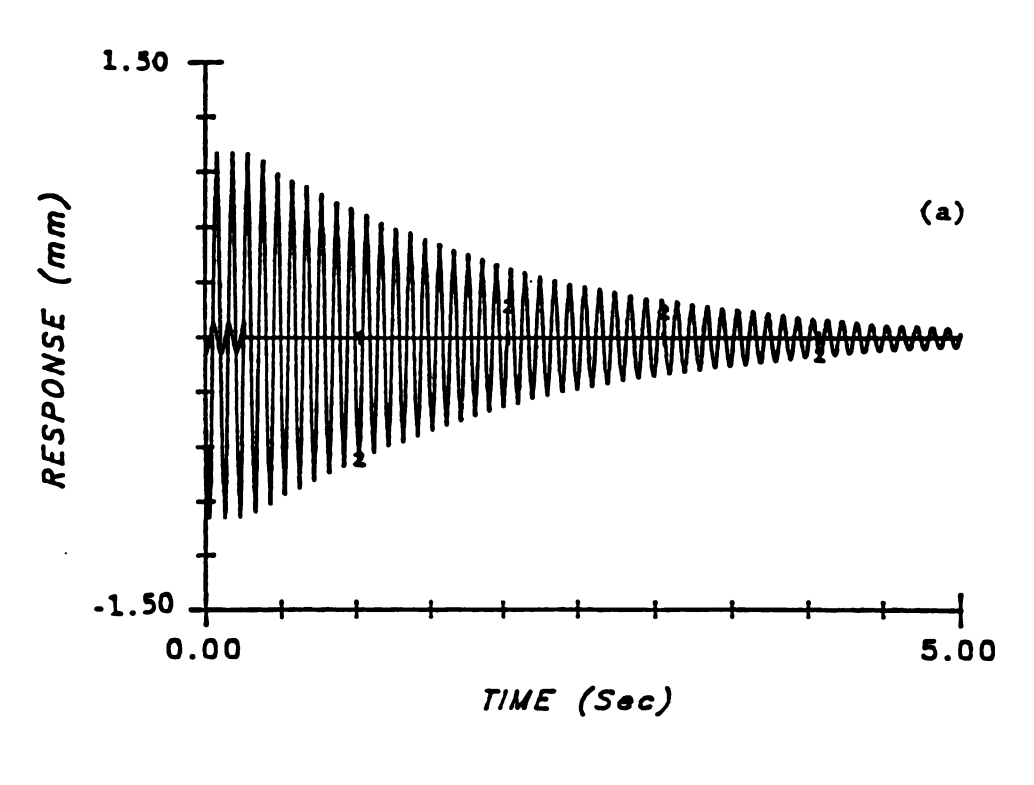


Figure 4.9 Transient response first-mode test results at x = 367.2 mm for the uncontrolled beam



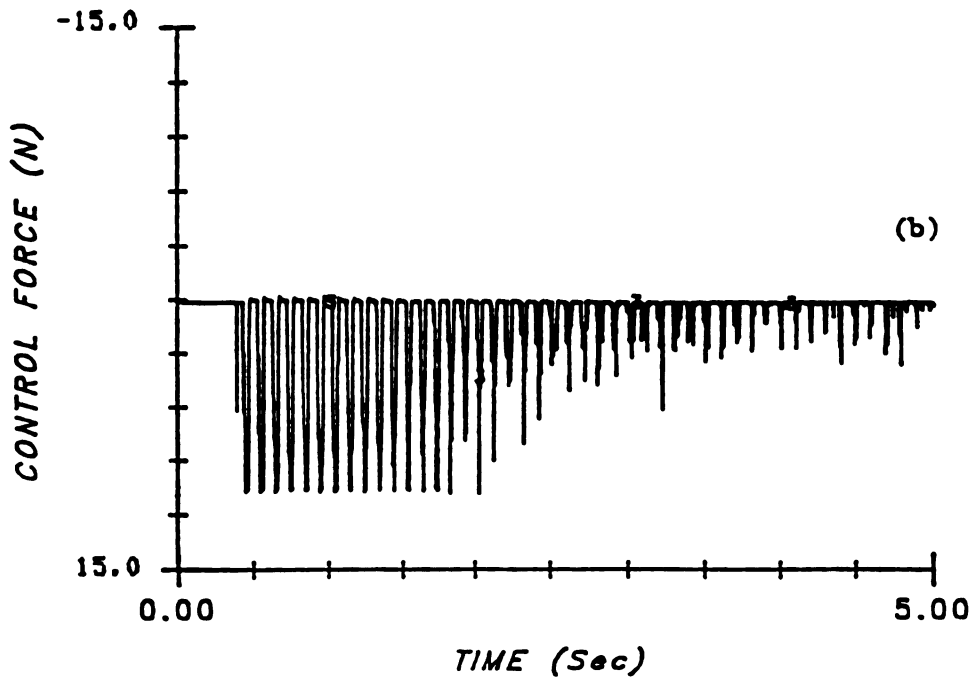
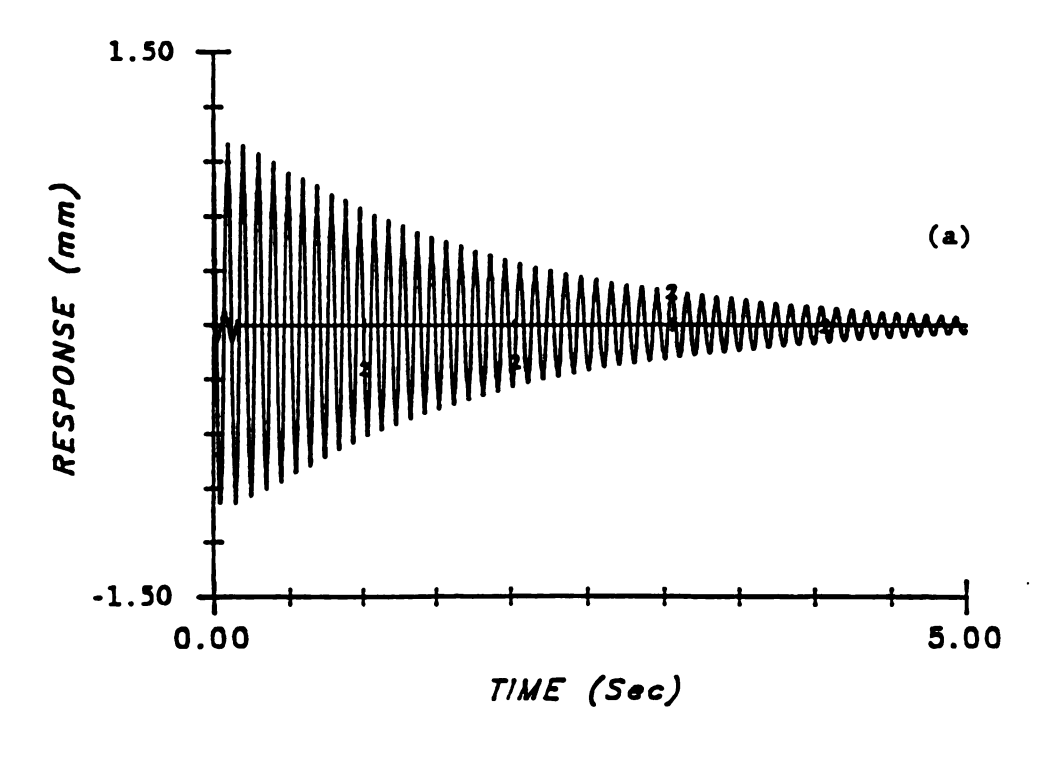


Figure 4.10 Transient vibration, first-mode test results for control gain $\alpha = 10.63$ N. a) the response at x = 367.2 mm b) the control force P(t)



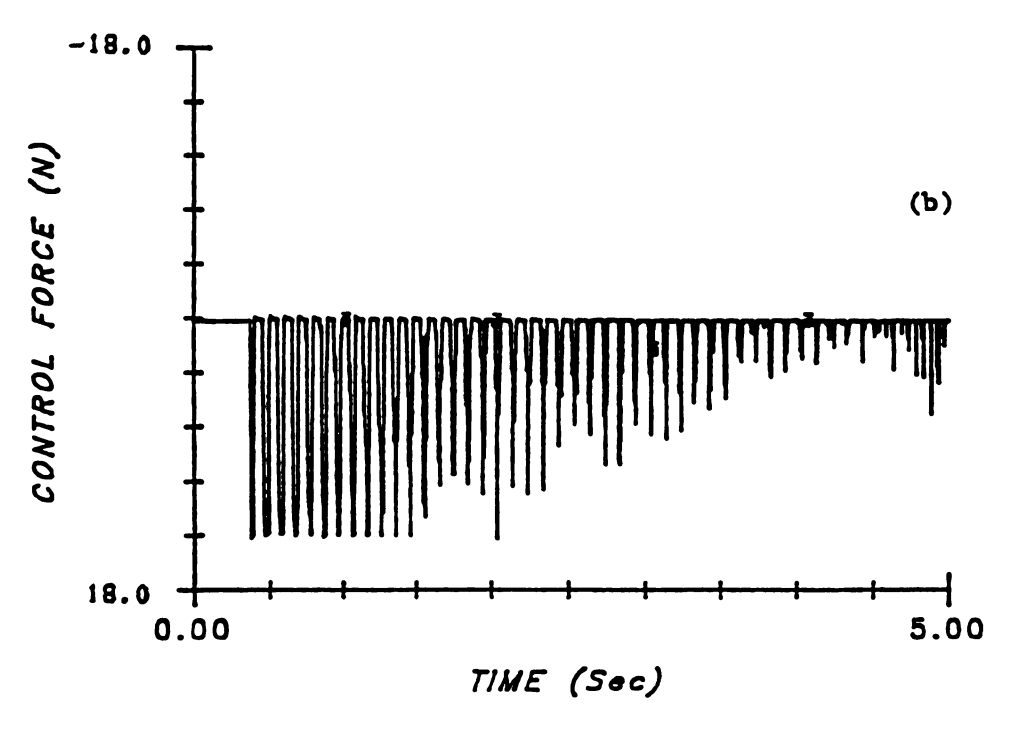
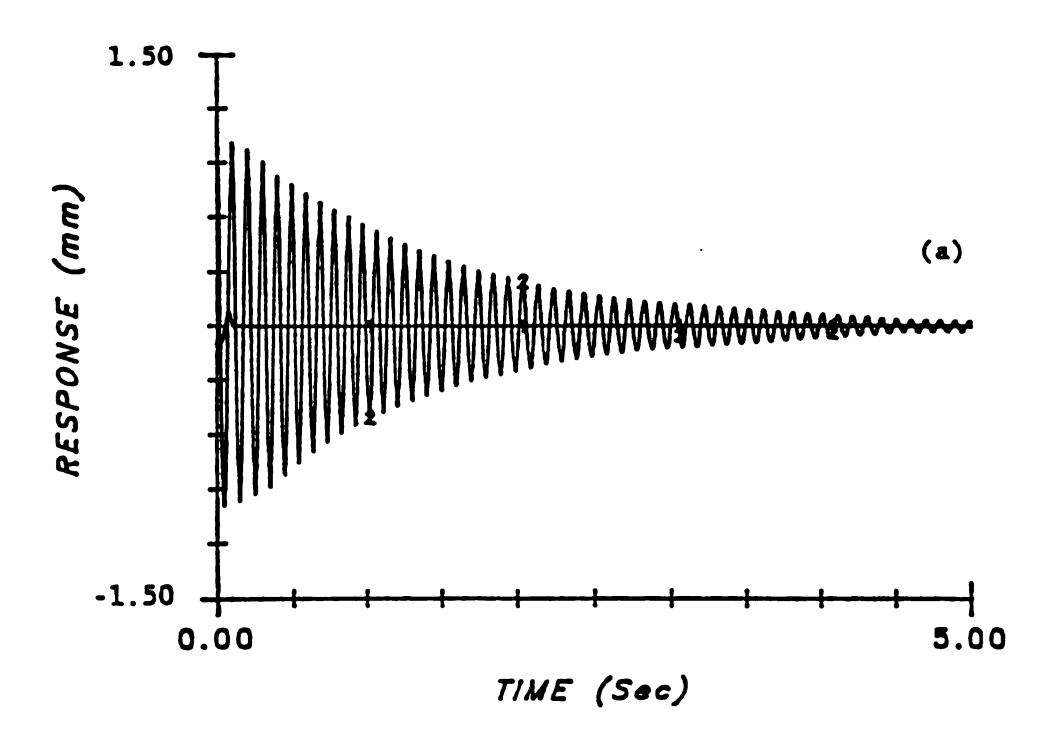


Figure 4.11 Transient vibration, first-mode test results for control gain $\alpha = 13.98$ N. a) the response at x = 367.2 mm

b) the control force P(t)



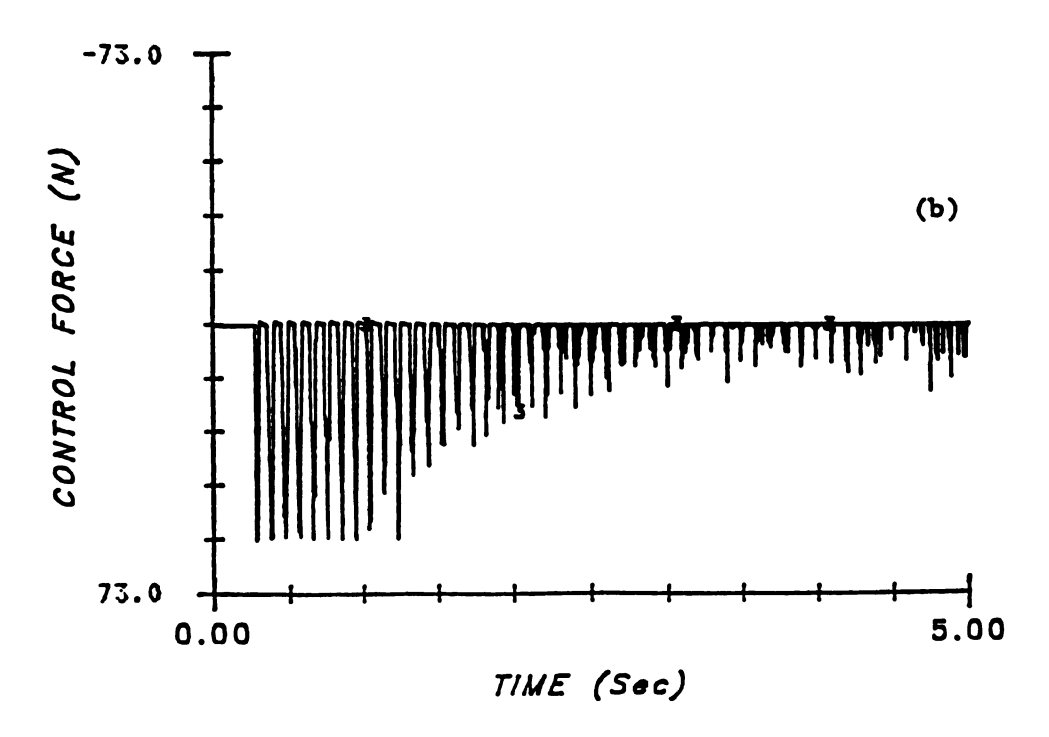


Figure 4.12 Transient vibration, first-mode test results for control gain at $\alpha = 58.67$ N.

a) the response at x = 367.2 mm

b) the control force P(t)

Table 4.1 Effect of the control gain on the transient motion amplitudes test results.

gain ∝		Amplitu	de (mma) at	n =		
N N	1	5	10	15	20	48
00.00	1.10	1.0	0.88	0.78	0.71	0.40
10.63	1.10	0.98	0.84	0.74	0.65	0.27
13.98	1.10	0.97	0.83	0.73	0.64	0.24
58.67	1.10	0.90	0.79	0.67	0.59	0.15

Test Case 2 Steady State Resonant Response

The most severe working conditions for a mechanical structure is when it is excited with a harmonic force having one or more frequencies equal to one or more of its eigenvalues, and it is the role of the active control to limit the resonant amplitudes. In this case the results of the effect of the control action on the steady-state resonant amplitudes are presented and discussed. Subsections (a) and (b) discuss the effect of the control action on the resonant amplitude due to single mode and two-mode excitations respectively. In both subsections the obtained results showed the efficiency of the control law in limiting the steady state resonant amplitudes.

a) One-Mode Excitation:

to obtain a steady-state resonant response, the wave generator was adjusted to provide a magnitude and frequency (which corresponded to the first or the second natural frequency of the beam) of the sinewave signal to drive the exciting power amplifier, after a while the beam responded with the steady-state resonant amplitude for the uncontrolled beam. To obtain the steady-state resonant amplitude for the controlled beam; the previous step was done first while the control was "off", then control action at certain gain a was set "on" until the steady-state amplitude for the controlled beam was obtained. This procedure was repeated up to five times and the average of the steady-state resonant amplitude was obtained. Table 4.2 shows the experimental test results of the effect of the control gain on the steady-state first-mode amplitude.

The control action could reduce the resonant amplitude from 1.26 mm to 1.0 mm for $\alpha = 12.55$ N and to .73 mm for $\alpha = 28.2$ N. It was expected to observe some increase in the resonant frequency caused by the stiffening effect of the control force, but this did not happen.

Figures 4.13a, b and c show the steady-state second-mode test results of a complete record of the exciting force, the response and the control force for control gain $\alpha = 35.46$ N for the steady-state second mode. These Figures show the relationship between the exciting force, the response and the control force at any instance during the time record. The control force is applied during the period while the beam tends to get shorter, and zero while it tends to get longer which demonstrates the control action mechanism, which was explained before in chapter 3, (test case 7). Table 4.3 shows the experimental test results of the effect of the control gain on the steady state second-mode response. It is clear from table 4.3 that the steady state amplitude is reduced from 1.42 mm for $\alpha = 0$ to .72 mm for $\alpha = 60$ N. A subset of the measured displacement, exciting force and control force histories for the steady-state second mode test results for $\alpha = 35.46$ N will be shown in appendix B.

b) Two-Mode Excitation:

As mentioned in the beginning of test case 2, that the most severe working conditions for a mechanical structure is when it works under the effect of an exciting force having a frequency equal to one of the eigenvalues of the structure. A more dangerous situation is when the exciting force has more than one frequencies that are equal

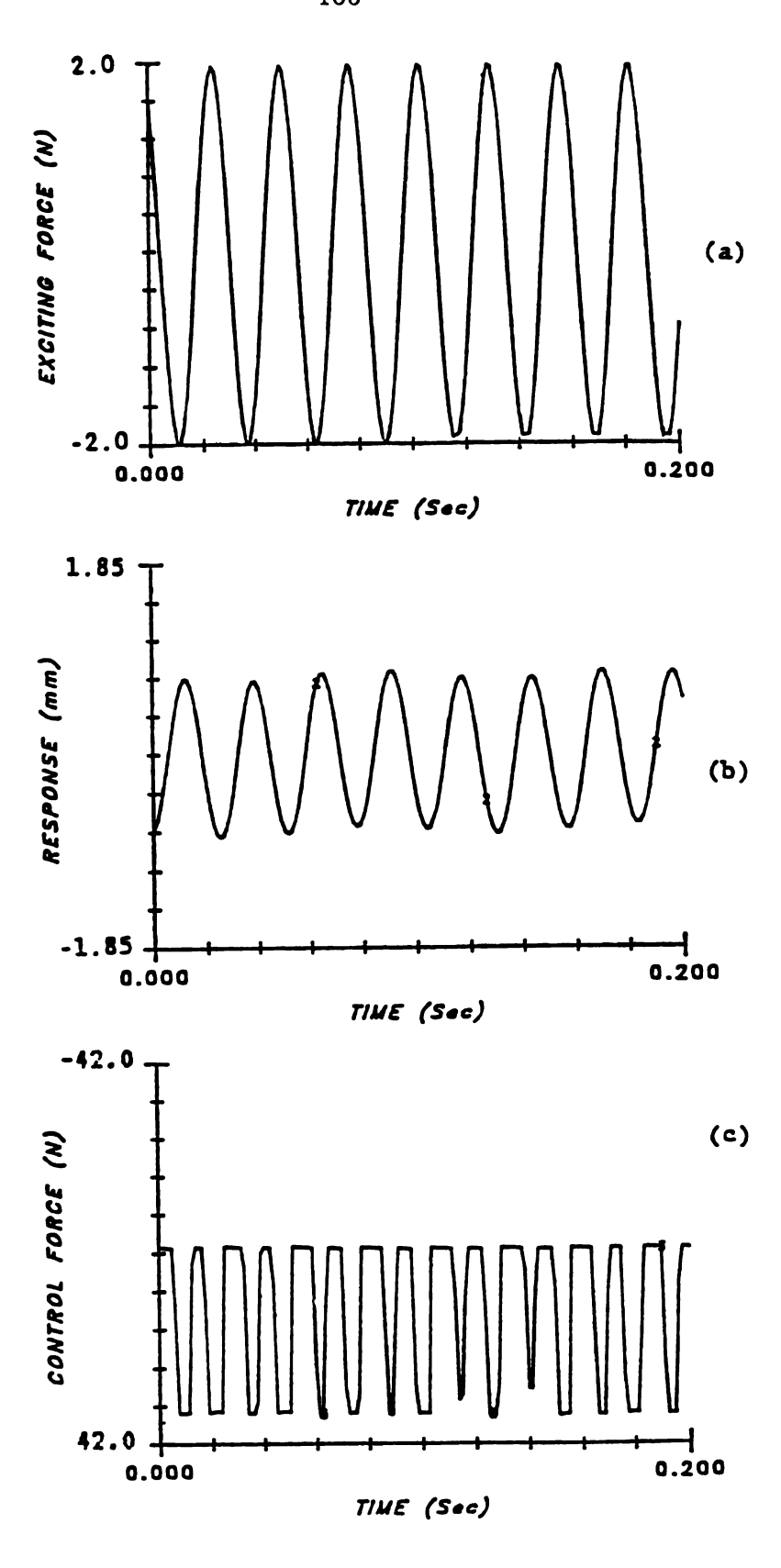


Figure 4.13 Steady state second-mode test results for α = 35.46 N.

- a) the exciting force.
- b) the response at x = 367.2 mm.
- c) the control force

Table 4.2 Effect of the control gain on the steady state first mode response for test case 2.

gain ∝ N	amplitude mm	frequency Hz	exciting amplitude
00.00	1.26	9.412	0.22
12.55	1.00	9.412	0.22
28.20	0.73	9.412	0.22

Table 4.3 Effect of the control gain on the steady state second mode response for test case 2.

gain,	amplitude	frequency	exciting amplitude
α N	THE REAL PROPERTY.	Hz	n
00.00	1.42	37.65	1.95
35.46	1.04	37.65	1.95
60.0	0.72	37.65	1.95

to the eigenvalues of the structure. The two-mode excitation case is considered to demonstrate the efficiency of the control law to limit resonant amplitudes resulting from two-mode excitation. The exciting force was due to two sinsoidal waves having frequencies of the first and second modes and were added together then fed to the magnet drive power amplifier. The time domain data for various control gains will be given in appendix C. Since the time domain data due to mixed modes is difficult to demonstrate the efficiency of the control law , the FFT of the steady-state response for various control gains are plotted in Figure 4.14. Table 4.4 summarizes the two-mode excitation test results for various control gains. In this test case, the amplitude of the first-mode was reduced from .95 mm to .55 mm and that of the second-mode was reduced from .8 mm to .65 mm for $\alpha = 50$ N, which demonstrates the effectiveness of the control action in limiting the resonant amplitudes resulting from the two-mode excitation.

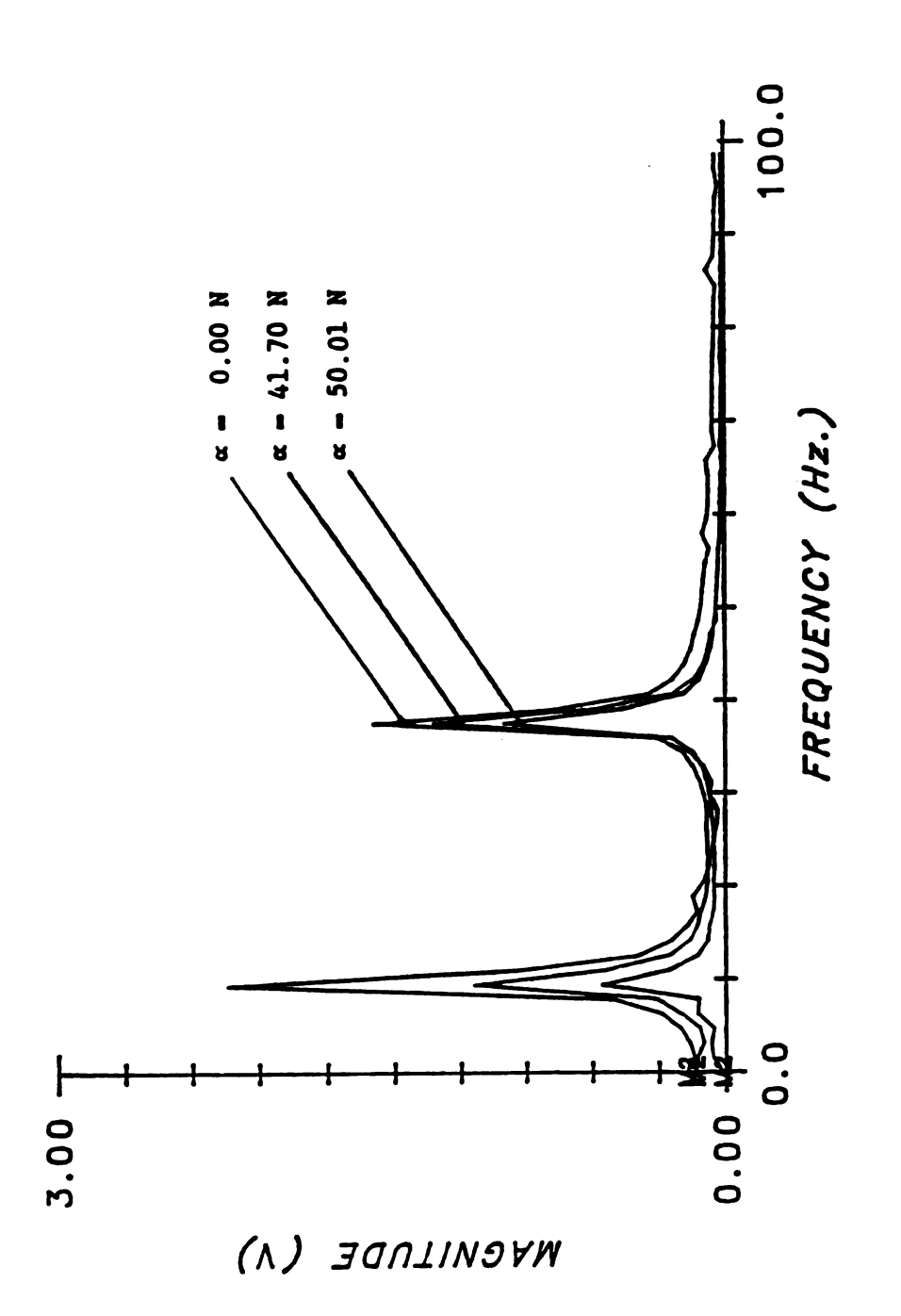


Figure 4.14 FFT of the steady state response of the two-

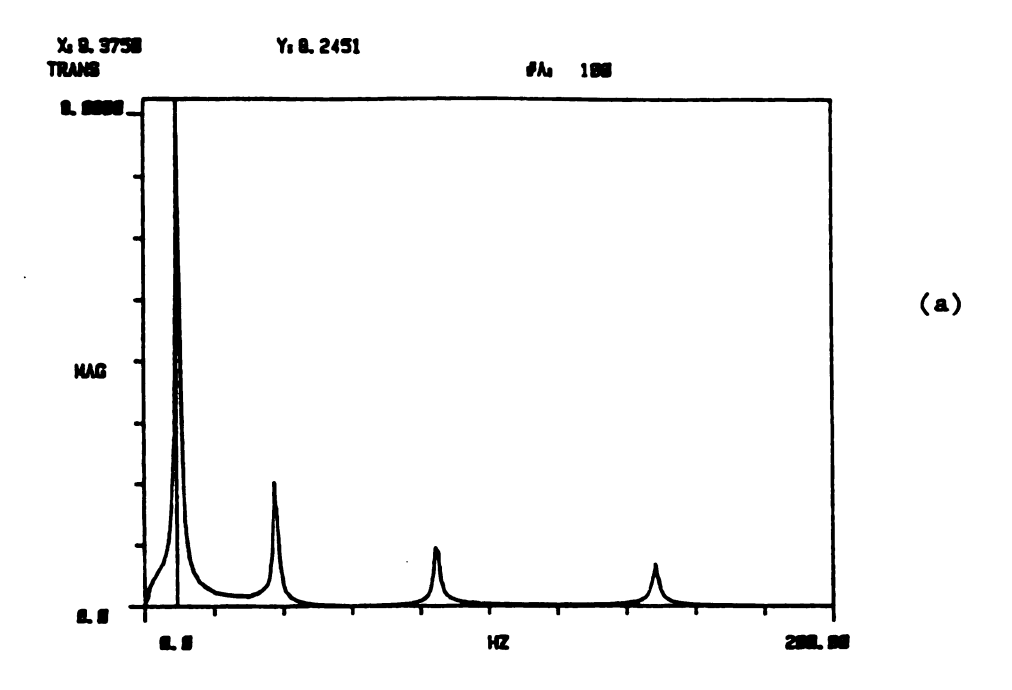
mode test results

Table 4.4 Effect of the control gain on the steady state two-mode response for test case 2.

gain ∝ N		resį	oonse	excitation		
		amplitude	frequency Hz	amplitude N	frequncy Hz	
00.0	mode	1	0.95	09.39	0.288	09.393
00.0	mode	2	0.80	37.57	0.537	37.57
1.71	mode	1	0.68	09.39	0.288	09.3
L. / L	mode	2	0.73	37.57	0.537	37.57
0.0	mode	1	0.55	09.39	0.288	09.393
, . 0	mode	2	0.65	37.57	0.537	37.57

Test Case 3 Random Noise Excitation.

The behavior of the beam under one and two-mode excitation were presented in test case 2, in which the excitation were pure sinewaves. The more practical case is when the beam is exposed to a force that carries all the possible frequencies (including the eigenvalues of the beam) within a bandwidth. The resulting response in this case will cover all the possible resonant amplitudes within that bandwidth. The results presented in this test case were for a random excitation with 200 Hz bandwidth. Since the excitation was random, the given results were the average of 100 records. Figures 4.15a and 4.15b show typical test results done by the HP structural analyzer for $\alpha = 0$ and 13 N. A replot of the test results done by the HP analyzer is given in figure 4.16 for $\alpha = 0$, 13, 48.4 and 88.5 N. Table 4.6 summarizes the most important results in this test case. It can be shown by the aid of figure 4.16 and table 4.6 that when the gain increased the amplitude of the first mode was reduced from 8.25 V/V to 4.87 V/V for α - 88.52 while the amplitude of fourth mode was reduced from .66 V/V to .56 for the same gain. Also the table shows that the resonant frequencies of the controlled beam were increased slightly from those of the uncontrolled beam; e.g. the first mode frequency was 9.38 for α - 0 was increased to 10.156 for α - 13 N. This increase in frequency was expected since the control action was applied in one direction i.e. tension force only.



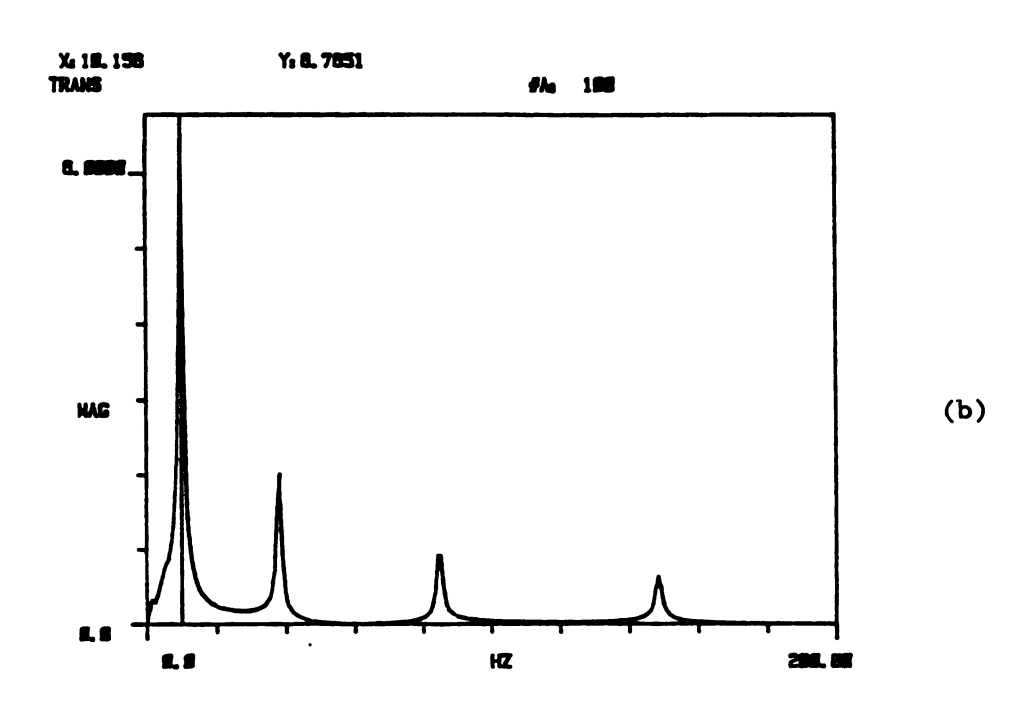


Figure 4.15 Typical test results of the transfer function of the beam. The displacement sensor located at x = 367.2 mm and the exciting force applied at x = 82.55 mm.

a) the transfer function for $\alpha = 0$

b) the transfer function for $\alpha - 13 \text{ N}$

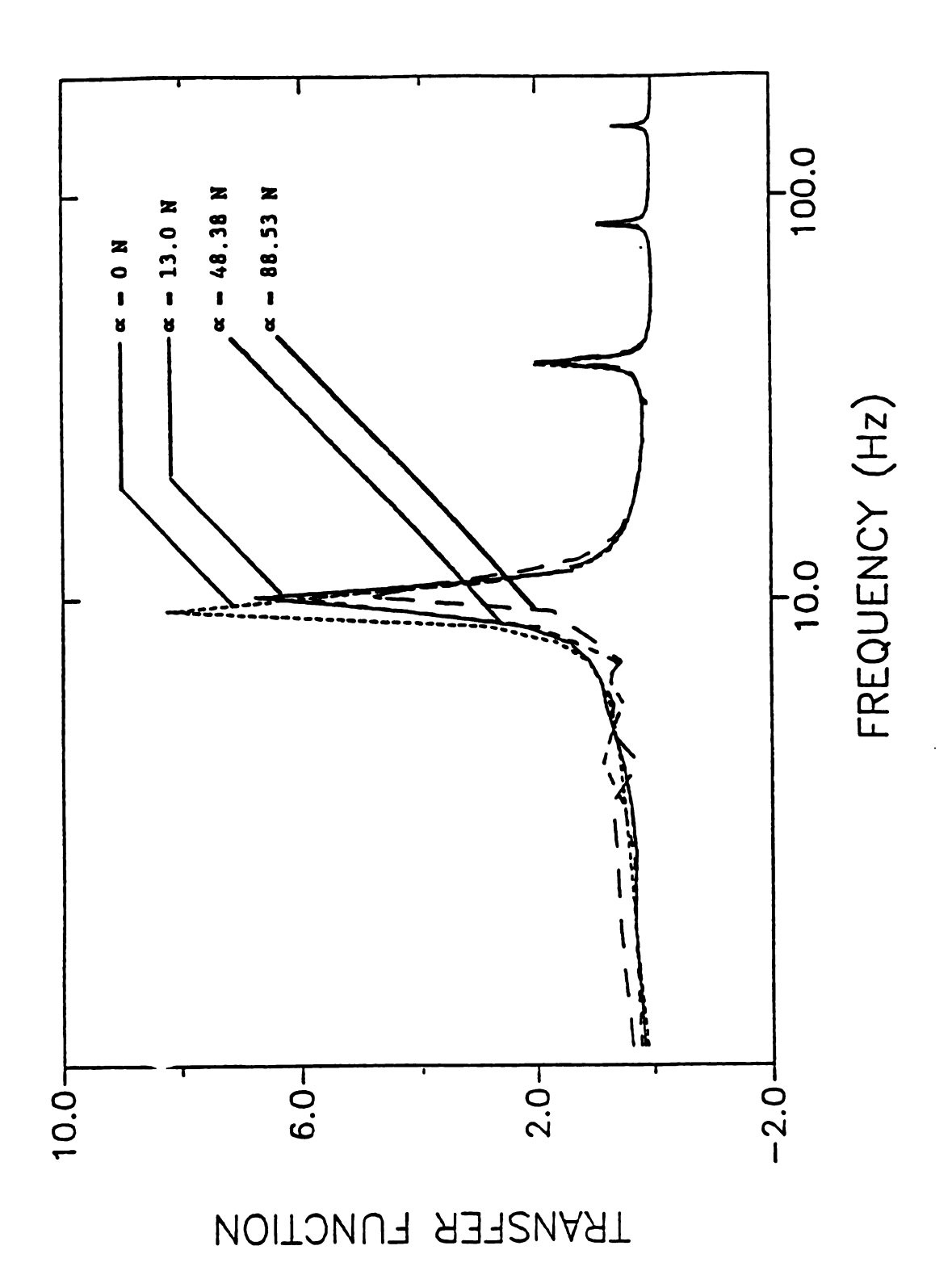


Figure 4.16 Random noise excitation test results for the controlled beam for various control gains

Table 4.5 Effect of the control gain on the transfer function at the first four modal frequencies for the random noise excitation test results.

gain ∝		transfer	function,	frequency	at mode no.
N		1	2	3	4
00.0	freq. Hz	9.375	37.50	84.375	148.48
00.0	TF. V/V	8.2451	2.0272	. 9467	.6598
13.007	freq. Hz	10.156	37.50	84.375	148.48
13.007	TF V/V	6.7651	2.0272	. 9466	. 6597
48.3836	freq. Hz	10.156	38.281	85.156	149.22
48.3030	TF V/V	6.0847	1.9039	. 7974	. 5857
	freq. Hz	10.156	38.379	85.094	149.23
88.527	TF V/V	4.8709	1.3171	. 7299	. 5612

4.4 Comparison of the Uncontrolled Ideal Beam With the Modelled Beam With Respect To Natural Frequencies and Young's Modulus

To see how well the modelled beam agrees with the ideal beam, the experimental modal frequencies f_i and the Young's modulus E of the modelled beam were compared with those of the ideal beam. The ideal natural frequencies f_i of the uncontrolled beam were calculated from the relation:

$$\dot{\tilde{\mathbf{f}}}_{\mathbf{i}} = \frac{\mathbf{i}^2 \pi}{2 \ell^2} \sqrt{\frac{\dot{\tilde{\mathbf{f}}}}{\rho \mathbf{A}}} \qquad \text{Hz} \tag{4.1}$$

where \dot{E} = 210 GN/m² is Young's modulus of the ideal beam. Also Young's modulus E of the modelled beam was evaluated at the first four modes using the experimental modal frequencies f_i in the relation:

$$E - \left(\frac{2f_i}{\pi}\right)^2 \left(\frac{\ell}{i}\right)^4 \left(\frac{\rho A}{I}\right) N/m^2$$
 (4.2)

The difference between the ideal and experimental natural frequencies and Young's modulus are less than 5% and 10% respectively (table 4.6) which shows good agreement between the ideal and the modelled beam.

In this chapter; the active control prototype, the test set up and the experimental test results were given and discussed. Although the control action acted in tension only, the significant increase in stability of the test beam demonstrated the feasibility of employing

Table 4.6 Comparison of the uncontrolled natural frequencies and Young's modulus of the ideal beam with those of the modelled beam.

		mode no., i					
	1	2	3	4			
Ť _i Hz	9.73	38.93	87.58	155.71			
f _i Hz	9.375	37.50	84.375	148.48			
% err	3.65	3.67	3.66	4.64			
E GN/m ²	195.00	194.9	194.9	191.0			
% error	7.14	7.19	7.19	9.05			

active parametric vibration to control the motion due to initial data and dynamic external disturbances. The comparison of the uncontrolled modal natural frequencies and the Young's modulus for the modelled beam with those of the ideal beam showed good agreement. In chapter 5 comparison between the simulation test results and the experimental test results will be presented and discussed.

CHAPTER 5

COMPARISON OF EXPERIMENTAL WITH SIMULATION RESULTS

The simulation results showed the effectiveness of the approach in controlling the beam transverse vibration with respect to the stability, the transient motions and the dynamic motions due to external disturbances. Unfortunately, there are no published study on the active parametric control beam transverse vibration; therefore it was important to verify the effectiveness of the approach experimentally. The experimental test results showed significant increase in the stability and demonstrated the feasibility of employing active parametric vibration to control the transverse motion of the beam. In this chapter some considerations needed for the comparison between the experimental and simulation results will be presented, then two comparison test cases representing transient and steady-state motions will be presented and discussed. The comparison results showed good agreement between the experimental and numerical test results.

5.1 Comparison Considerations.

The experimental transient and steady-state cases given in chapter 4 were used in the comparison with the numerical simulation. In each comparison test case, the simulation was adjusted to agree with the experimental test conditions. Therefore the following factors were taken into account when adjusting the simulation:

- 1) The control forces in the experimental tests were applied in one direction; i.e. tension forces only; as was mentioned in chapter 4.
- 2) Although the control forces in the experimental tests were a bang-bang control; i.e. "on" and "off"; they were proportional control; i.e., the control amplitudes decreased with the decrease of the horizontal end velocity of the beam.
- 3) The damping of the uncontrolled beam which effected the response of the beam. The damping sources were due to the structural damping, friction in the bearings and the air resistance to the transverse vibration.

Factors 1 and 2 reduced the efficiency of the experimental control, and the simulation was modified to account for these deficiencies. For factor 1 the simulation was modified to allow only tension control forces. For factor 2 the simulation was modified by choosing the modification control factor ϵ (Figure 2.2) in which the control forces of both the simulation and the experiment were close. For factor 1 the following method was used to model the damping of the uncontrolled beam.

5.1.1 Damping Model for the Uncontrolled Beam.

The damping model chosen for the simulation was the same one given in chapter 3, equation (3.10). The reason of choosing that damping model is that the amplitudes of normal modes of vibration are attenuated at rates which are proportional to the oscillation frequencies [39]. Equation (3.10) includes the damping coefficient C

which must be estimated. The procedure for the evaluation of C for the test beam is to excite the test stand beam at its first natural frequency until steady-state is reached. The excitation was then turned "off" and the displacement at x = 367.2 mm recorded and converted using the calibration formula (A.1). A simulation using equation (3.10) was given an initial displacement y(x,0) = 1.161 sin mm and the response (y(x,t)) for various trial values of C was obtained. The C value which gave the closest simulation to the experimental response was found to be .01558 Kg m/sec. This behavior will be shown when comparing the experimental with results simulated results for the transient case for no control force ($\alpha = 0$) in table 5.2.

5.1.2 Open-loop Modal Frequencies.

The first four open-loop modal frequencies of the test beam were obtained using the HP dynamic analyzer. A random noise of bandwidth of 200 Hz was used to excite the uncontrolled beam and the transfer function obtained. The corresponding simulated results were obtained by giving equation (3.10) initial displacement:

$$y(x,0) - \sin \frac{i\pi x}{\ell}$$
 mm

with mode number i = 1,2,3 and 4. The corresponding simulation natural frequencies were obtained from these responses. Table 5.1 shows the first four open-loop natural frequencies of the experimental and simulated results of the beam. The maximum error is 4.05 %.

Table 5.1 Open-loop natural frequencies of the experimental and simulated results of the beam.

Mode No.	F	requency Hz	Error &
node No.	Exp.	Num.	
1	9.375	9.6543	2.97
2	37.5	39.02	4.05
3	84.375	86.587	2.62
4	148.48	145.84	1.78

5.2 Comparison Cases.

The above factors 1-3 accounted for through adjusting the simulation conditions to agree with the experimental test conditions.

Two comparison cases will be presented and discussed.

Comparison Case 1: Transient Motion

The details of the experimental test procedures and response time history for the transient motion for the first mode for various control gains were presented and discussed in chapter 4. A damping coefficient C - .01558 Kg m/sec and an initial displacement y(x,0) -1.161 sin TX were used in the simulation. The comparison between the experimental and the corresponding numerical amplitudes, n for various control gains and control modification factor, & will be given The amplitude of control forces in the in this subsection. experimental test results which were shown in Figure 4.10b, 4.11b and 4.12b decreased with the decrease of the amplitudes of the response, therefore the simulation was modified to account for this effect by changing ϵ . Table 5.2 shows the experimental and numerical results for various control gains. The simulated values in table 5.2 were calculated for $\epsilon = 2.4 \times 10^{-3}$ m/sec. The difference between the numerical and experimental test results is less than 12 % which shows good agreement between the experimental and numerical results for transient motion of the first beam mode.

Table 5.2 Experimental and simulation results for transient motion of the beam for $\epsilon = 2.4 \text{x} 10^{-3}$ m/sec

			Amplitude (mma) at n =				
	gain ∝ N	1	5	10	15	20	48
Exp .	00.00	1.10	1.0	0.88	0.78	0.71	.40
Num.	00.00	1.10	1.0	0.87	0.76	0.67	. 38
% error		0.0	0.0	1.14	2.56	5.63	5.00
Ехр .	10.63	1.10	0.98	0.84	0.74	0.65	. 27
Num.	10.63	1.10	0.98	0.84	0.72	0.63	. 26
% error		0.0	0.62	0.00	2.70	3.07	3.70
Exp.	13.98	1.10	0.97	0.83	0.73	0.64	. 24
Num.	13.98	1.10	0.98	0.83	0.71	0.62	. 231
% Error		0.0	1.03	0.00	2.73	3.13	3.80
Exp.	58.67	1.10	0.90	0.79	0.67	0.59	.15
Num.	58.67	1.10	0.91	0.74	0.61	0.52	. 132
% Error		0.0	1.11	6.33	8.95	11.86	12.00

Comparison Case 2: Steady-State Motion.

Comparison of steady-state experimental and numerical first-mode test results required a representative excitation force distribution. The exciting force was simulated as a trapezoid centered at x = 82.55 mm and having an area equal to the exciting force amplitude, F_e . The base length of the trapezoid was equal to the magnet length 88.9 mm (3.5 in) and the top length was equal to 76.2 mm (3 in), therefore the height of the trapezoid was:

$$w = \frac{2 \times 1000}{(88.9 + 76.2)}$$
 F_e = 2.698 N/m for F_e = .2227 N. (table 4.2)

It was found that for low control gains the experiment and simulation control forces were close for $\epsilon=1.2 \times 10^{-3}$ and for high control gains they were close for $\epsilon=3 \times 10^{-5}$. Figure 5.1 shows the effect of the control gain on the steady-state amplitude simulation results for damping coefficient C=.0155 Kg m/sec and for $\epsilon=1.2 \times 10^{-3}$, 3×10^{-4} , $3.\times 10^{-5}$, and $3.\times 10^{-8}$. Also plotted in Figure 5.1 the experimental results for control various gains. Table 5.3 shows the experimental and numerical results for selected control gains and ϵ . The difference between the numerical and experimental test results is less than 11 % which shows good agreement between the experimental and numerical results for the steady-state motion.

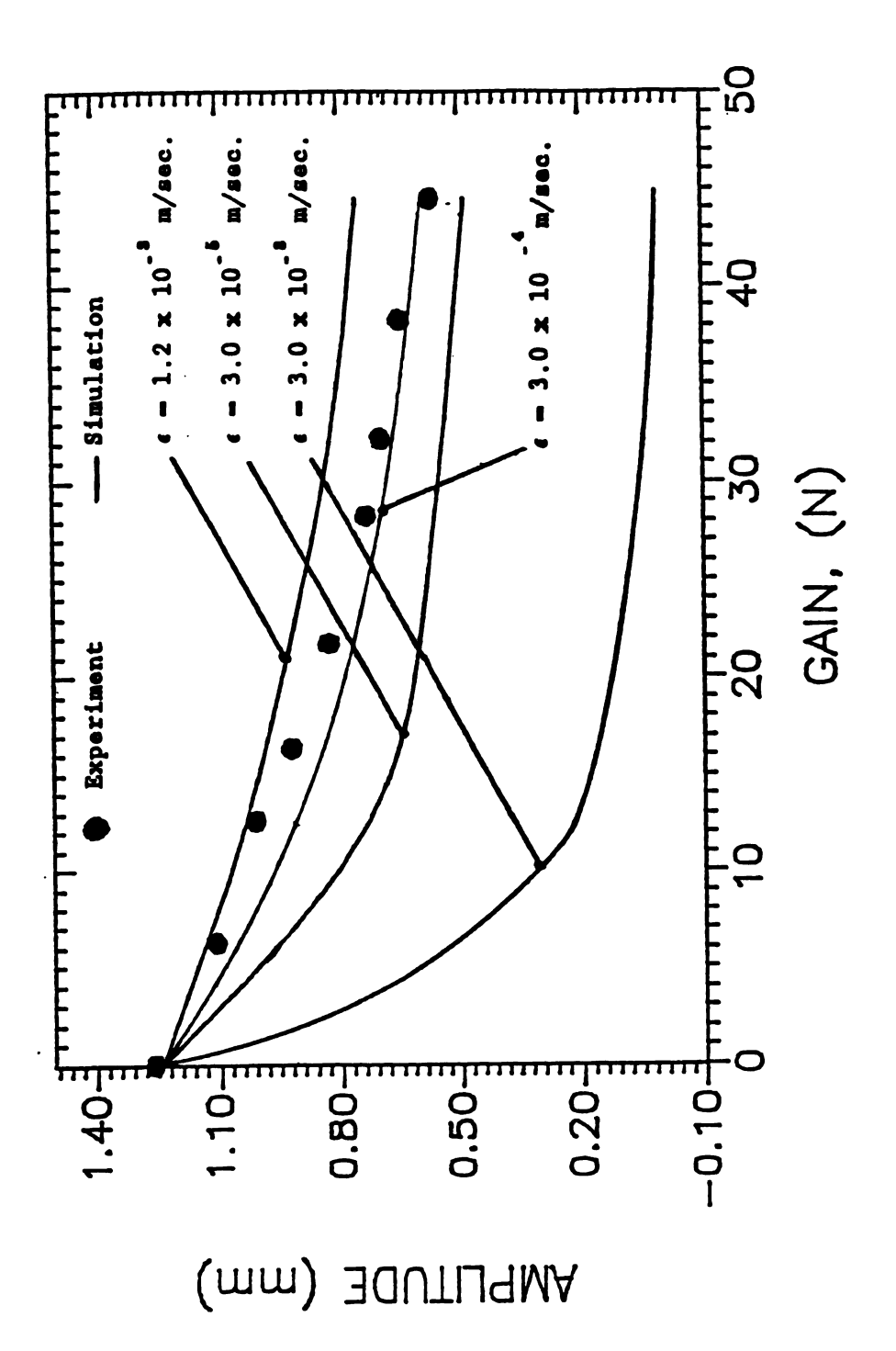


Figure 5.1 Results of experiment and simulation for steady-state first mode response for comparison case 2

Table 5.3 Experimental and analytical amplitude test results for the steady-state motion of the beam.

Gain, N	0.0	12.56	28.21	44.48	€ m/sec
Exp. (mm)	1.26	1.00	0.73	0.57	
Num. (mm)	1.24	1.03	0.85	0.753	1.2x10 ⁻³
	1.24	0.97	0.67	0.61	3.0x10 ⁻⁴
	1.24	0.73	0.56	0.483	3.0x10 ⁻⁵
	1.24	0.20	0.09	0.0001	3.0x10 ⁻⁸

The results for the transverse vibration of a beam under the action of the active parametric control have not been previously reported in the literature. In this chapter some considerations for the comparison between the experimental and simulation were presented. These considerations included the damping model and the nature of the experimental control forces. Based on these considerations two comparison cases representing transient and steady-state motions were presented and discussed. The simulation results agreed with the experimental results with error up to 12-11 % for the transient and the steady-state response.

CHAPTER 6

SUMMARY AND CONCLUSIONS

The active parametric control theory was presented and applied to control the transverse vibration of a modified, nonlinear, dynamic, simply-supported Bernoully-Euler beam. The mathematical formulation of the open-loop system equations of motion was derived using the extended Hamilton's principle. More importantly, the functional found after application of Hamilton's principle is a valid Liapunov functional. Closed-loop stability was then investigated using the direct method of Liapunov and the control algorithm for asymptotic stability was found.

The control law was tested analytically and experimentally. The closed-loop system model derived from Hamilton's principle was reduced to a nonhomogeneous wave equation for the longitudinal vibration u(x,t) subject to nonhomogeneous boundary conditions and a parabolic equation for the transverse vibration y(x,t). The wave equation was solved analytically using the finite Fourier transform. The nonlinear fourth order parabolic equation for the transverse vibration y(x,t) was solved approximately using the finite difference method.

A prototype control system was designed and constructed to demonstrate and verify the approach and to evaluate its performance. Both the simulation and the prototype control system were tested and compared to evaluate stability of transient vibration and resonant amplitude due to external disturbances. The methods used for measuring

the motion of the end of the beam, showed that an inductive, non-contacting, proximity probe has satisfactory noise immunity for observing displacement at frequencies up to 50 Hz and the accelerometer is less noise sensitive at higher frequencies. Comparison of the simulation with experiment results showed good agreement with errors less than 12 % and 11 % in transient and steady state tests respectively.

The active parametric control approach was found to be an efficient method to reduce vibration due to external disturbances. The control algorithm is easy-to-implement. No truncation is required in the control algorithm. It enables a single force to control all modes of the beam based on observation of one velocity and does not suffer from the spillover problems.

Further work may be directed toward the design and implementation of a double acting force actuator to increase the efficiency of the approach, the digital realization of controller feedback, the combination of observing both the displacement using proximity probe and the acceleration of the end of the beam and the analytical solution of the closed-loop system.

This work is the first time the direct method of Liapunov has been used to derive a parametric active control law. This easy-to-implement, single-input single-output control law was tested analytically and experimentally and stabilized the beam in transient and steady-state tests without suffering from spillover induced instability.

APPENDICES

APPENDIX A

Displacement And Forces Measurements And Calibrations

APPENDIX A1

Displacement Sensor Calibration

The displacement sensor used was inductive, non-contacting proximeter model Kd2400 manufactured by Kaman Sciences corporation. One sensor consisting of a detector and detector driver was used in tests. The sensor was fixed to the frame through a long threaded sleeve which was tightened to the frame. The position of the sensor was chosen to detect the first five modes. The sensor was calibrated in its mount on the prototype controller test stand. At varying distances from the stationary detector, the gap between the detector head and the test beam was measured with feeler gages and the sensor output voltage measured. These calibration measurements were then plotted and a least squared error fit to a first order polynomial obtained over the measurement range used during the prototype controller tests (Figure A1). The deduced relationship between the displacement y_d in mm and the probe output x_n in V is given by:

$$y_d = 0.4233 + 0.233 x_p mm$$
 (A.1)

This polynomial fit was subsequently used in the test data conversions.

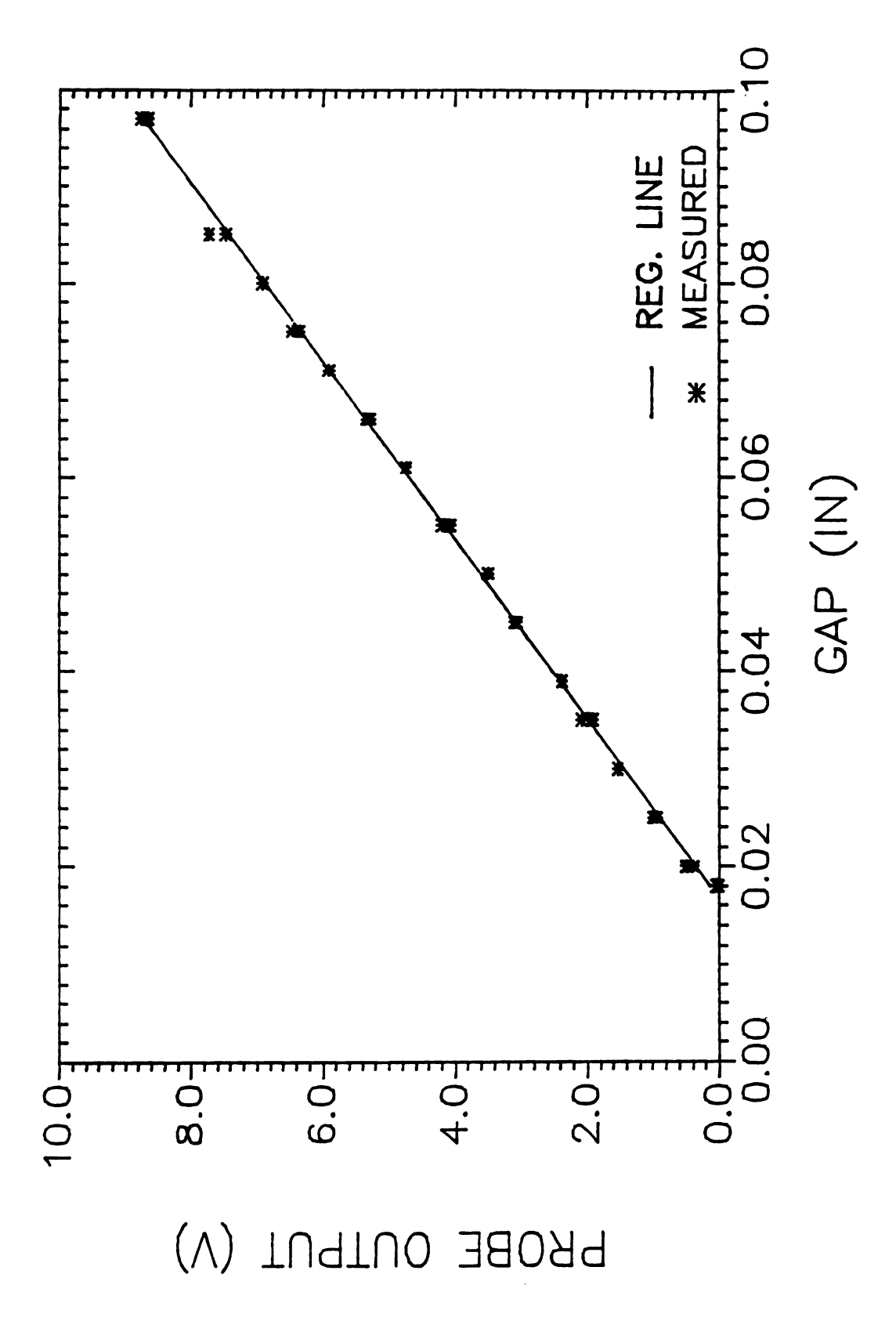


Figure Al Displacement sensor calibration results

APPENDIX A2

Forces Measurements and Calibrations

A2-1 strain Gauge Orientation and Configuration:

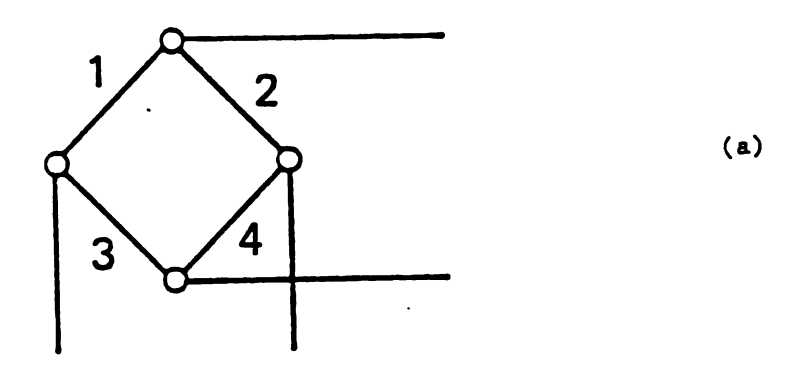
The following circuits were used in measuring the axial force and the exciting force.

1) Control Force measurement:

The axial control force applied by the control magnet was measured by a four-arm strain gauge bridge which compensates for temperature and bending effects. Figure A2 shows the strain gauge orientation and the bridge configuration.

2) Exciting force measurement:

The exciting force was applied by using two identical magnets one of them pulls the beam for the positive part of the exciting signal and the other for the negative part. The exciting force was measured by a four-arm strain gauge bridge which compensates for temperature, axial and torsional effects. Figure A3 shows the strain gauge orientation and the bridge circuit.



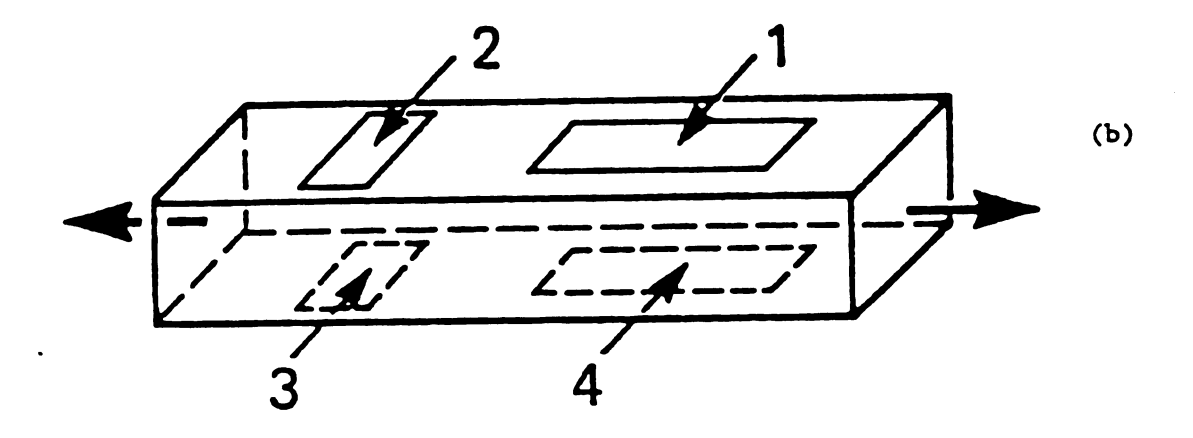
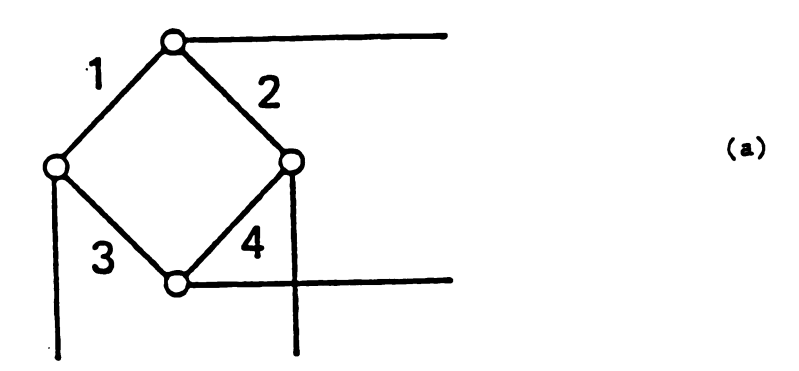


Figure A2 Four-arm strain gauge bridge for measuring the control force.

- a) bridge circuit.
- b) strain gauge orientation



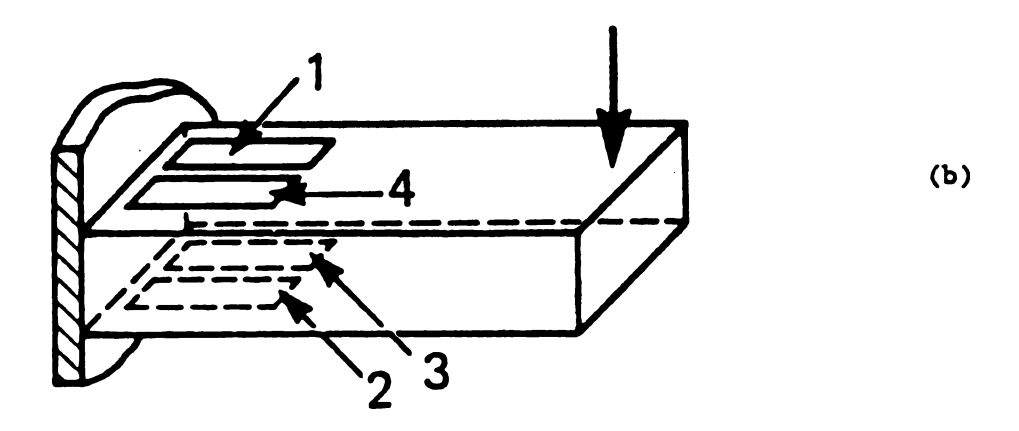


Figure A3 Four-arm strain gauge bridge for measuring the exciting force.

- a) bridge circuit.
- b) strain gauge orientation.

A2-2 Force Calibration:

In this section; the calibration procedures are presented and the calibration constants are deduced for both the exciting and the control forces.

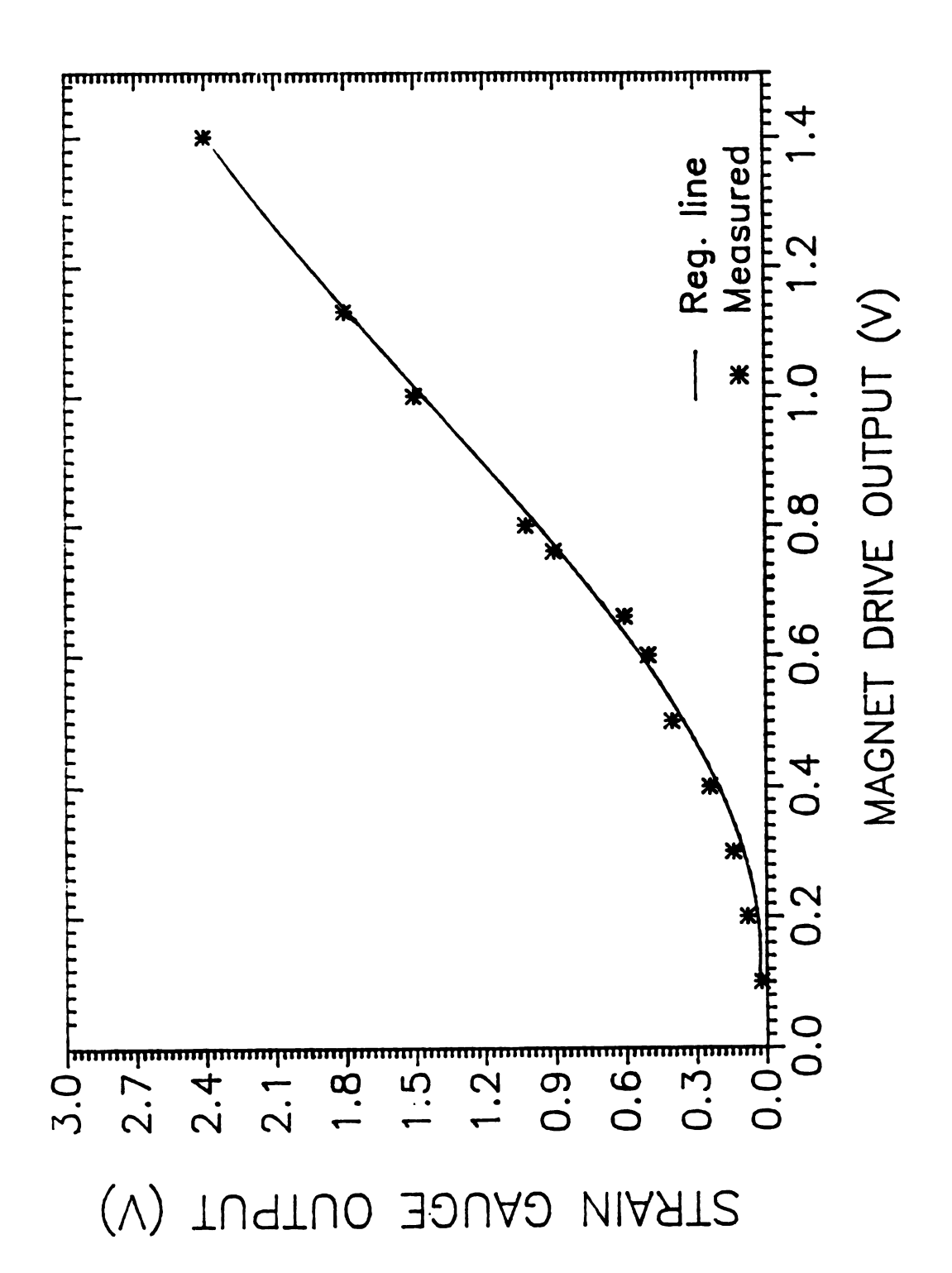
A2-2.1 Control force calibration:

The beam was taken out and clamped firmly by a machine vise. Weights were hung by a wire through holes at the end of the beam and the corresponding strain gauge output signals were recorded. Figure A4 shows a typical results of that calibration. Then the beam was mounted back on the test support and the control magnet was excited by the power amplifier. Both signals from the strain gauge and the power amplifier outputs were recorded and plotted using a least square approximation as shown in Figure A5. The relationship between the strain gauge output in volts; y_s and the control force magnet drive power amplifier output; x_c in volts is given by (using the least square approximation):

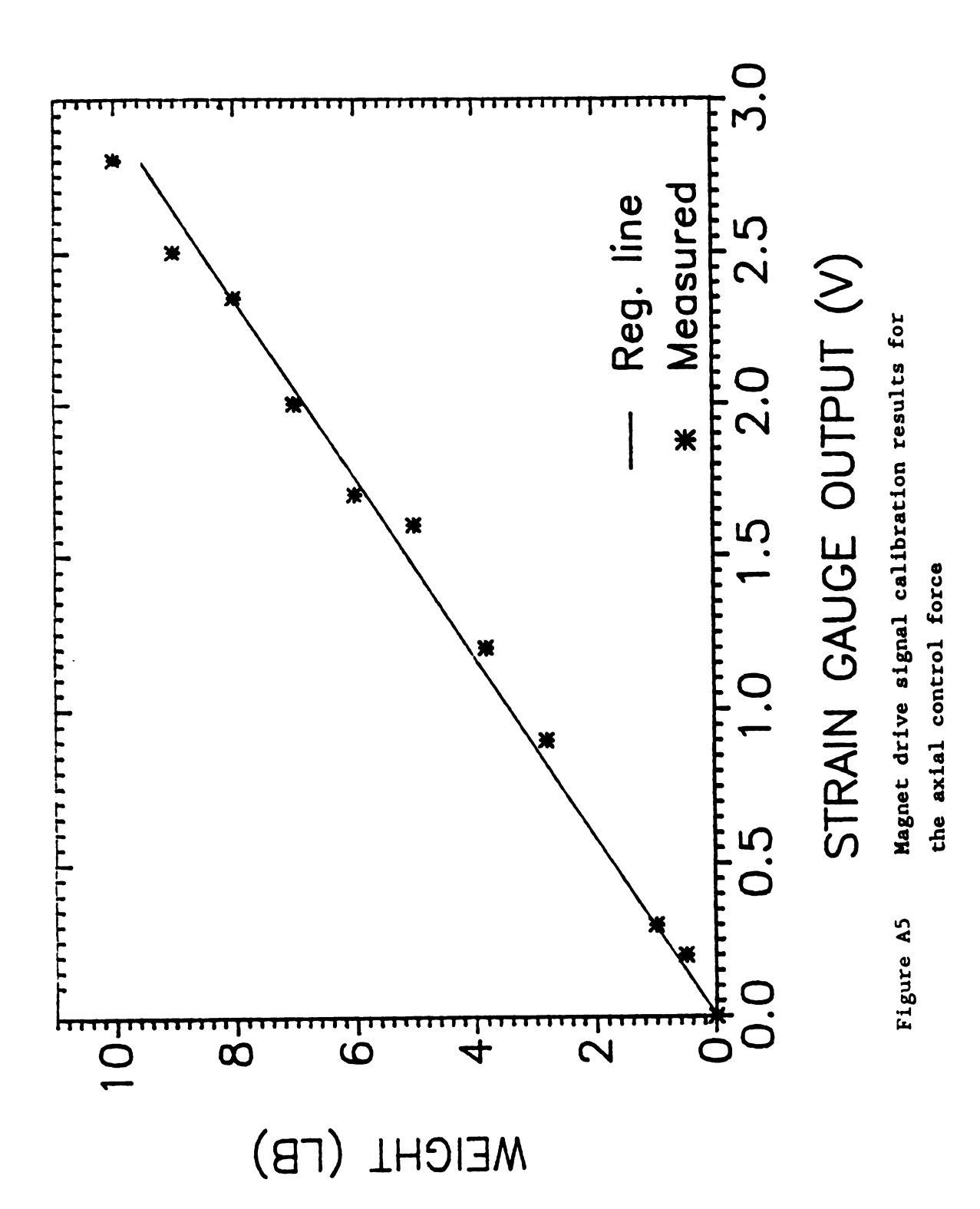
$$y_s = .0061x_c + 1.5056x_c^2$$
 V (A.2)

and the relationship between the weight which were applied axially; y_w in pounds and the strain gauge output is (using the least square approximation):

$$y_w = 3.413 \ y_s$$
 LB (A.3)



Strain gauge calibration for the axial control Figure A4



from (A.2) and (A.3) the control force, y_w can be calculated by knowing the control magnet drive signal; x_c :

$$y_w = 3.413 (1.2 x_c - 0.3241 x_c^2 + 0.5119 x_c^3)$$
 LB

$$= 18.218 \times_{c} - 4.92 \times_{c}^{2} +7.771 \times_{c}^{3} N$$
 (A.4)

A2-2.2 Exciting Force Calibration:

First the outer bracket which supports the outer exciting magnet was taken out and the whole set up was turned 90 degree. Dead weights were mounted at the point of application of the exciting force and the corresponding strain gauge output signals were recorded. A typical plot of the calibration results is shown in Figure A6. The set up was put back again and one of the magnets was excited by the exciting power amplifier. Both signals from the strain gauge and the power amplifier outputs were recorded and plotted using the least square approximation as shown in Figure A7. The relationship between the strain gauge output in volts; y_s and the exciting magnetic drive power amplifier output; x_e in volts is given by:

$$y_s = 0.02998x_e + 0.22966x_e^2 V$$
 (A.5)

The relationship between the weights; $\mathbf{y}_{\mathbf{w}}$ in pounds and the strain gauge output; $\mathbf{y}_{\mathbf{s}}$ is:

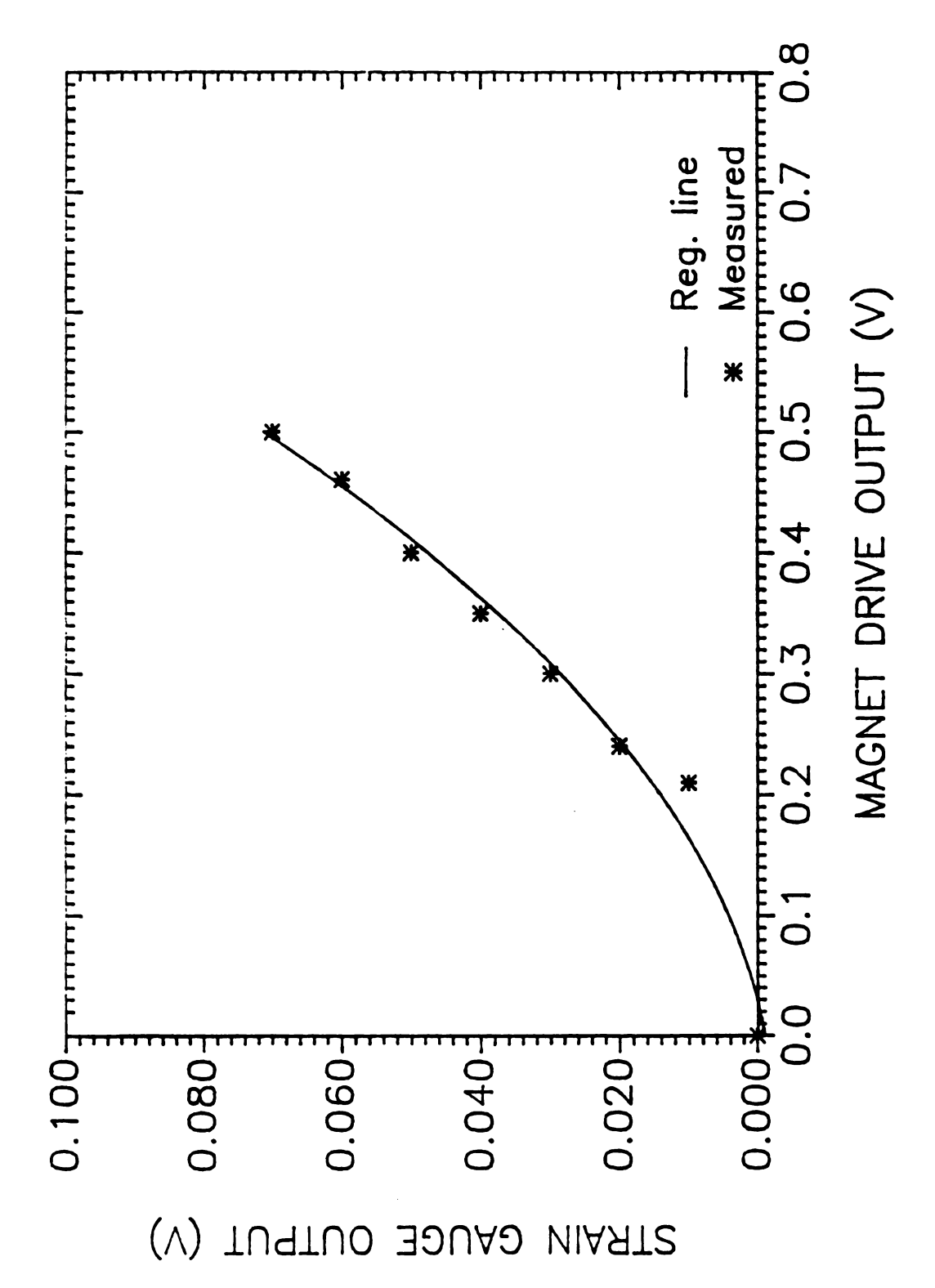


Figure A6 Strain gauge calibration results for the exciting force

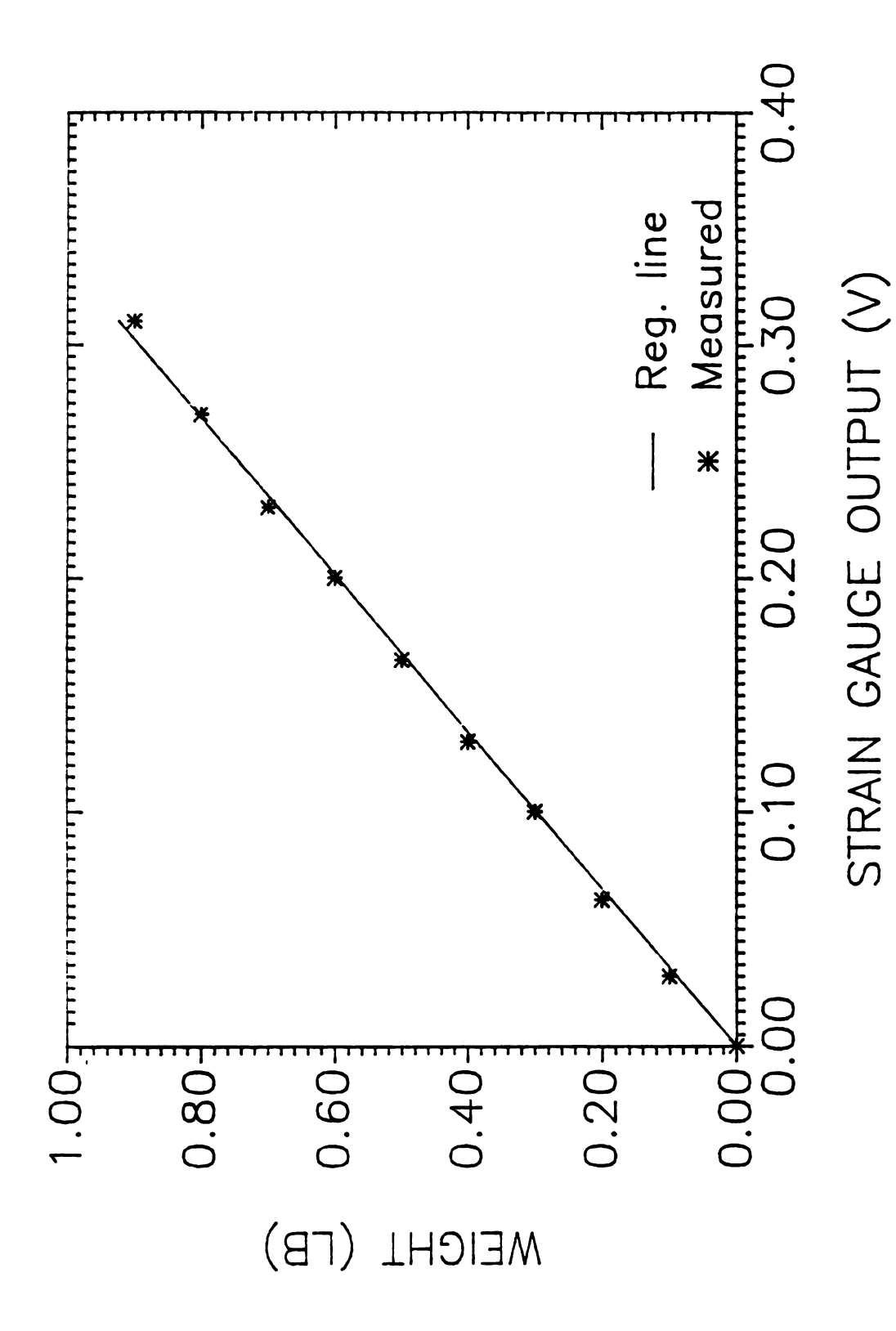


Figure A7 Magnet drive signal calibration results.for

$$y_w = 2.97975y_s$$
 LB (A.6)

substituting from (A.5) into (A.6) yields

$$y_w = 2.97975(0.02988x_e + 0.22966x_e^2)$$
 LB
= $0.397x_e + 3.044x_e^2$ N (A.7)

By knowing the exciting magnet drive output signal; x_e the corresponding exciting force can be calculated using equation (A.7).

APPENDIX B

Real Time Record For The Steady-State Second-Mode Test Results For $\alpha = 35.46$ N

In chapter 4, the prototype control system was presented to demonestrate and verify the approach and to evaluate its performance. The basic measured quantities were the transverse vibration y(x,t), the control force and the exciting force. The measured quantities were fed into DEC LSI $/23^+$ for the data acquisition. A subset of the measured quantities for the steady-state second-mode test results for control gain = 35.46 N are given in table B.1 as an example.

Table B.1 A subset of the measured displacement, exciting force and control force histories for the steady state second mode test result for $\alpha=35.46~\text{N}$

Time	Exciting Force	Displacement	Control Force
50G	•	v	y
	2	•	_
0.0000 0.1250E-02,	0.606 0.459	-2.395	0.049
0.2500E-02,	0.274	-2.121 -1.667	0.044 0.044
0.3750E-02,		-1.051	0.039
0.5000E-02, 0.6250E-02,		-0.323	0.034
0.7500E-02		0.445	-0.572 -1.369
0.8750E-02	-0.665	1.168 1.769	-1.359
0.1000E-01,		2.204	-1.359
0.1125E-01, 0.1250E-01,		2.429	-1.364
0.1375E-01,		2.434 2.219	-0.073 0.049
0.1500E-01,	-0.386	1.789	0.044
0.1625E-01,		1.173	0.039
0.1750E-01, 0.1875E-01,		0.435	-0.420
0.2000E-01,		-0.415 -1.095	-1.364 -1.354
0.2125E-01,		-1.745	-1.344
0.2250E-01, 0.2375E-01,		-2.234	-1.344
0.2500E-01		-2.546 -3.6 7 8	-1.359 0.054
0.2625E-01	0.616	-2.659 -2.581	0.049
0.2750E-01,		-2.312	0.044
0.2875E-01, 0.3000E-01,		-1.857	0.044
0.3125E-01		-1.251 -0.533	0.039 0.039
0.3250E-01,	-0.352	-0.523 0.254	-0.132
0.3375E-01,		0.987	-1.373
0.3500E-01, 0.3625E-01,		1.618	-1.364
0.3750E-01		2.082	-1.364 -1.251
0.3875E-01,	-0.684	2.33 6 2.366	-0.010
0.4000E-01,		2.185	0.044
0.4125E-01, 0.4250E-01,		1.774	0.039
0.4375E-01		1.183	0.039 -0.239
0.4500E-01,	. 0:244	0.469 -0.288	-1.369
0.4625E-01,		-1.022	-1.354
0.4750E-01, 0.4875E-01,		-1.657	-1.349
0.5000E-01		-2.136 -2.434	-1.349 -1.359
0.5125E-01,	0.709	-2.546	0.054
0.5250E-01,		-2.463	0.044
0.5375E-01, 0.5500E-01,		-2.185	0.044
0.5625E-01		-1.725 -1.105	0.039 0.039
0.5750E-01,		-0.367	0.039
0.5875E-01,		0.425	0.029
0.6000E-01, 0.6125E-01,		1.178	-0.978 -1.373
0.6250E-01		1.823 2.297	-1.373 -1.369
0.6375E-01,		2.556	-0.533
0.6500E-01,		2.605	0.044
0.6625E-01, 0.6750E-01,		2.439	0.039 0.034
0.6875E-01		2.058 1.422	0.034
0.7000E-01,	0.015	0.777	0.029
0.7125E-01,		0.020	-1.163
0.7250E-01, 0.7375E-01,		-0.718	-1.369 -1.359
0.7500E-01		-1.369 -1.872	-1.359 -1.364
0.7625E-01		-2.195	-1.202
0.7750E-01		-2.326	0.044
0.7875E-01		-2.263	0.039
0.8000E-01,	0.757	-2.004	0.039

Table B.1 (continued)

Time	Exciting Force	Displacement	Control Force
50G	•	•	v
0.8250E-01 0.8375E-01 0.8500E-01 0.8625E-01 0.8750E-01 0.8875E-01 0.9000E-01 0.9125E-01	-0.112 , -0.323 , -0.508 , -0.645 , -0.728 , -0.743 , -0.699	-0.958 -0.230 0.547 1.285 1.921 2.380 2.634 2.683	0.034 0.034 0.029 -0.679 -1.378 -1.378 -0.665
0.9375E-01 0.9500E-01 0.9625E-01 0.9750E-01 0.9875E-01 0.1000 0.1012 0.1025 0.1037	-0.425 -0.225 -0.010 0.215 0.411 0.572 0.679 0.728 0.714	2.512 2.141 1.564 0.850 0.083 -0.679 -1.359 -1.887 -2.239	0.034 0.029 0.029 0.024 -1.153 -1.373 -1.364 -1.364 -1.364
0.1050 0.1062 0.1075 0.1087 0.1100 0.1112 0.1125 0.1137 0.1150 0.1162	, 0.635 , 0.503 , 0.327 , 0.122 , -0.098 , -0.313 , -0.494 , -0.635 , -0.723 , -0.748	-2.370 -2.087 -1.725 -1.139 -0.445 0.318 1.051 1.051 2.155 2.424	0.039 0.034 0.034 0.034 0.029 0.024 -0.371 -1.256 -1.207
0.1175 0.1187 0.1200 0.1212 0.1225 0.1237 0.1250 0.1262 0.1275	-0.704 -0.396 -0.448 -0.244 -0.024 0.200 0.396 0.557 0.674	2.483 2.312 1.965 1.398 0.694 -0.068 -0.826 -1.500	-0.415 0.034 0.029 0.029 0.024 0.024 -0.459 -1.383 -1.373
0.1287 0.1300 0.1312 0.1325 0.1337 0.1350 0.1362 0.1375 0.1387	, 0.728 , 0.718 , 0.645 , 0.518 , 0.342 , 0.137 , -0.078 , -0.293 , -0.484	-2.390 -2.556 -2.527 -2.307 -1.901 -1.329 -0.630 0.132 0.880	-1.369 -1.129 0.039 0.034 0.029 0.029 0.029 0.024 0.024
0.1400 0.1412 0.1425 0.1437 0.1450 0.1462 0.1475 0.1487	, -0.630 , -0.718 , -0.748 , -0.709 , -0.606 , -0.455 , -0.259 , -0.039	1.544 2.053 2.366 2.463 2.346 2.019 1.486 0.811	-1.158 -1.158 -0.420 0.029 0.024 0.024 0.024 0.020 -0.318
0.1512 0.1525 0.1537 0.1550 0.1562 0.1575 0.1587 0.1600 0.1612	, 0.381 , 0.547 , 0.665 , 0.728 , 0.718 , 0.650 , 0.528 , 0.357 , 0.152	-0.674 -1.344 -1.877 -2.239 -2.414 -2.395 -2.180 -1.784 -1.212	-1.388 -1.378 -1.373 -1.373 0.034 0.029 0.029 0.029

Table B.1 (continued)

Time	Enciting Force	Displacement	Control Force
	▼	▼	▼
0.1662	, -0.621	2.229	-1.378
0.1675	, -0.714	2.571	-0.308
0.1687 0.1700	, -0.748 , -0.714	2.674	0.034
0.1712	, -0.616	2.581 2.278	0.02 9 0.029
0.1725	-0.464	1.774	0.024
0.1737 0.1750	, -0.274	1.114 0.367	-1.056
0.1762	, -0.054 , 0.171	-0.386	-1.373 -1.364
0.1775	0.371	-1.085	-1.359
0.1787	, 0.538	-1.647	-1.364
0.1800 0.1812	, 0.660 , 0.723	-2.043 -2.248	-0.665
0.1825	, 0.723	-2.263	0.039 0.034
0.1837	, 0.660	-2.0 B 2	0.034
0.1850	, 0.538	-1.716	0.034
0.1862 0.1875	, 0.367 , 0.166	-1.178 -0.494	0.02 9 0.024
0.1887	, -0.049	0.259	-0.929
0.1900	, -0.264	1.007	-1.378
0.1912	, -0.459	1.672	-1.373
0.1925 0.1937	, -0.611 0.709	2.190 2.512	-1.373 -0.348
0.1950	, -0.748	2.630	-0.249 0.039
0.1962	, -0.718	2.532	0.034
0.1975	, -0.626	2.224	0.029
0.1987 0.2000	, -0.474 , -0.298	1.711	0.029
0.2012	, -0.073	0.274	-1.134 -1.373
0.2025	0.156	-0.499	-1.359
0.2037	, 0.357	-1.212	-1.354
0.2050	, 0.528	-1 ,799	-1.364
0.20 <i>6</i> 2 0.207 5	, 0.650 , 0.723	-2.219 -2.454	-0.508 0.044
0.2087	, 0.723	-2.498	0.039
0.2100	, 0.665	-2.346	0.039
0.2112	, D.547	-2.004	0.034
0.2125 0.2137	, 0.381 . 0.181	-1.500 -0.841	0.03 4 0.02 9
0.2150	, -0.034	-0.103	-0.327
0.2162	, -0.249	0.635	-1.378
0.2175	, -0.445	1.344	-1.373
0.2187 0.2200	, -0.601 , -0.704	1.848 2.195	-1.227 -0.143
0.2212	, -0.748	2.331	-0.142 0.039
0.2225	, -0.723	2.258	0.034
0.2237	, -0.630	1.965	0.029
0.2250 0.2262	, -0.489 0.303	1.457 0.806	0.029
0.2275	, -0.088	0.064	-0.474 -1.378
0.2287	, 0.137	-0.689	-1.364
0.2300	, 0.342	-1.393	-1.359
0.2312 0.232 5	, 0.518 . 0.645	-1.970 -2.380	-1.364 -0.597
0.2323	, 0.718	-2.605	-0.587 0.044
0.2350	, 0.728	-2.644	0.039
0.2362	, 0.670	-2.488	0.034
0.2375	, 0.557	-2.146 -1.633	0.034
0.2387 0.2400	, 0.396 . 0.196	-1.632 -0.968	0.029
0.2412	, -0.015	-0.215	0.02 9 -0.391
0.2425	, -0.235	0.547	-1.378
0.2437	, -0.435	1.251	-1.373
0.2450	, -0.591	1.823	-1.373

Table B.1 (continued)

Time	Resiting Forces	Displacement	Coatrol Force
205	▼	▼	▼
0.2475	, -0.748	2.214	-1.373 -0.259
0.2487 0.2500	-0.728 -0.640	2.395	0.039
0.2512	, -0.503	2.356 2.107	0.034
0.2525	, -0.318	1.647	0.034
0.2537	, -0.103	1.026	0.029
0.2550 0.2562	, 0.122 , 0.327	0.308	-0.112 -1.378
0.2575	, 0.508	-0.430 -1.124	-1.369
0.2587	, 0.640	-1.701	-1.364
0.2600	, 0.718	-2.116	-1.369
0.2612	, 0.728	-2.351	-0.132
0.2625 0.2637	, 0.679 , 0.567	-2.390	0.03 9 0.034
0.2650	, 0.367	-2.239 -1.896	0.034
0.2662	, 0.210	-1.383	0.G34
0.2675	, 0.000	-0.718	0.029
0.2687	, -0.220	0.088	0.029
0.2700 0.2712	, -0.420 0.582	0.811 1.520	0.024 -0.899
0.2725	, -0.694	2.102	-1.383
0.2737	, -0.748	2.488	-1.041
0.2750	, -0.728	2.674	-0.020
0.2762	, -0.650	2.649	0.029 0.02 9
0.2775 0.2787	, -0.513 , -0.327	2.414 1.97 5	0.029
0.2800	, -0.117	1.354	0.024
0.2812	0.108	0.630	0.020
0.2825	, 0.318	-0.127	-1.388
0.2837	, 0.494	-0.846	-1.373 -1.364
0.2850 0.2862	, 0.630 , 0.714	-1.457 -1.911	-1.369
0.2875	, 0.728	-2.180	-0.621
0.2887	0.684	-2.263	0.039
0.2900	, 0.577	-2.146	0.034
0.2912	, 0.420	-1.838	0.029
0.2925 0.2937	, 0.230 . 0.015	-1.359	0.029 0.029
0.2950	, -0.205	-0.718 0.010	0.029
0.2962	, -0.406	0.758	0.024
0.2975	, -0.572	1.457	-1.193
0.2987	, -0.689 0.743	2.023	-1.378 -1.378
0.3000 0.3012	-0.733	2.405	-0.425
0.3025	-0.635	2.586 2.556	0.034
0.3037	, -0.523	2.322	0.029
0.3050	, -0.342	1.877	0.029
0.3062	, -0.132 . 0.093	1.246	0.024 -0.088
0.3075 0.3087	0 202	0.513 -0.259	-1.383
0.3100	0.484	-1.002	-1.369
0.3112	, 0.621	-1.632	-1.359
0.3125	, 0.709	-2.111	-1.364
0.3137	, 0.733 . 0.689	-2.405	-1.129 n n39
0.3150 0.3162	n 597	-2.512 -2.424	0.039 0.034
0.3175	0.430	-2.146	0.034
0.3187	, 0.239	-1.657	0.029

APPENDIX C

TIME DOMAIN TEST RESULTS FOR TWO-MODE EXCITATION

As mentioned in test case 2 chapter 4, that the most severe working conditions for a mechanical structure is when it works under the effect of an exciting force having more than one frequencies that are equal to the eigenvalues of the structure. The two mode excitation case was considered to demonstrate the efficiency of the control law to limit resonant amplitudes resulting from two-mode excitation. The exciting force was due to two sinsoidal waves having frequencies of the first and second modes and were added together then fed to the magnet drive power amplifier. The time domain data for control gains $\alpha = 0$, 41.71 and 50 N are shown in Figures Cl, C2 and C3. Figures Cla, C2a and C3a show the exciting force versus time for various control gains. Figures Clb, C2b and C3b show the response under the action of the exciting force for various control gains. The required control forces are shown in Figures C2c and C3c. As discussed in case 2b chapter 4 and by the help of FFT of the responses for various control gains, (Figure 4.14), the amplitude of the first-mode was reduced from .95 mm to .55 mm and that of the second-mode was reduced from .8 mm to .65 mm for $\alpha = 50$ N which demonstrates the effectiveness of the control action in limiting the resonant amplitudes resulting from the two-mode excitation.

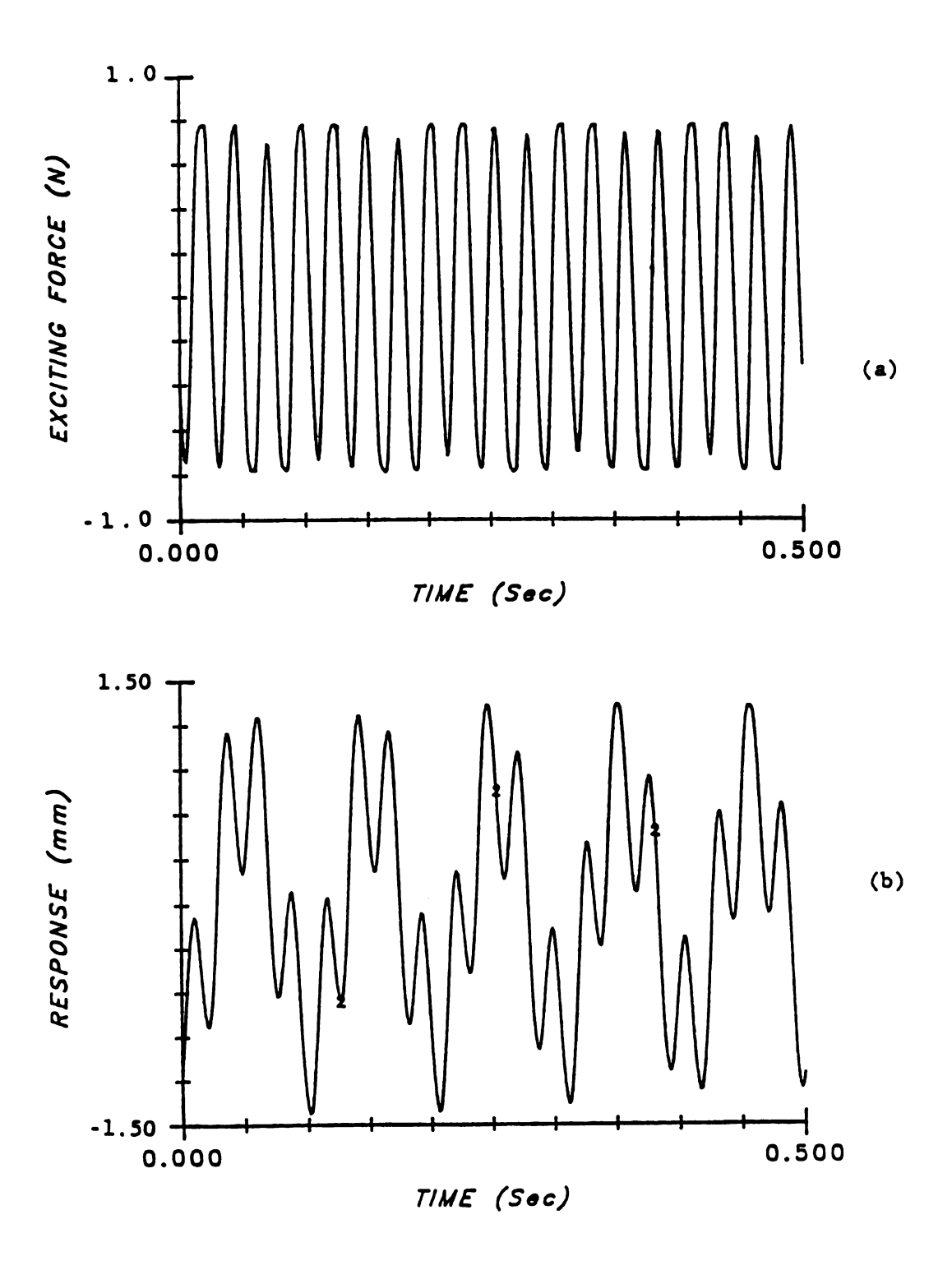


Figure Cl Steady state two-mode test results for the uncontrolled beam.

- a) the exciting force.
- b) the response at x = 367.2 mm

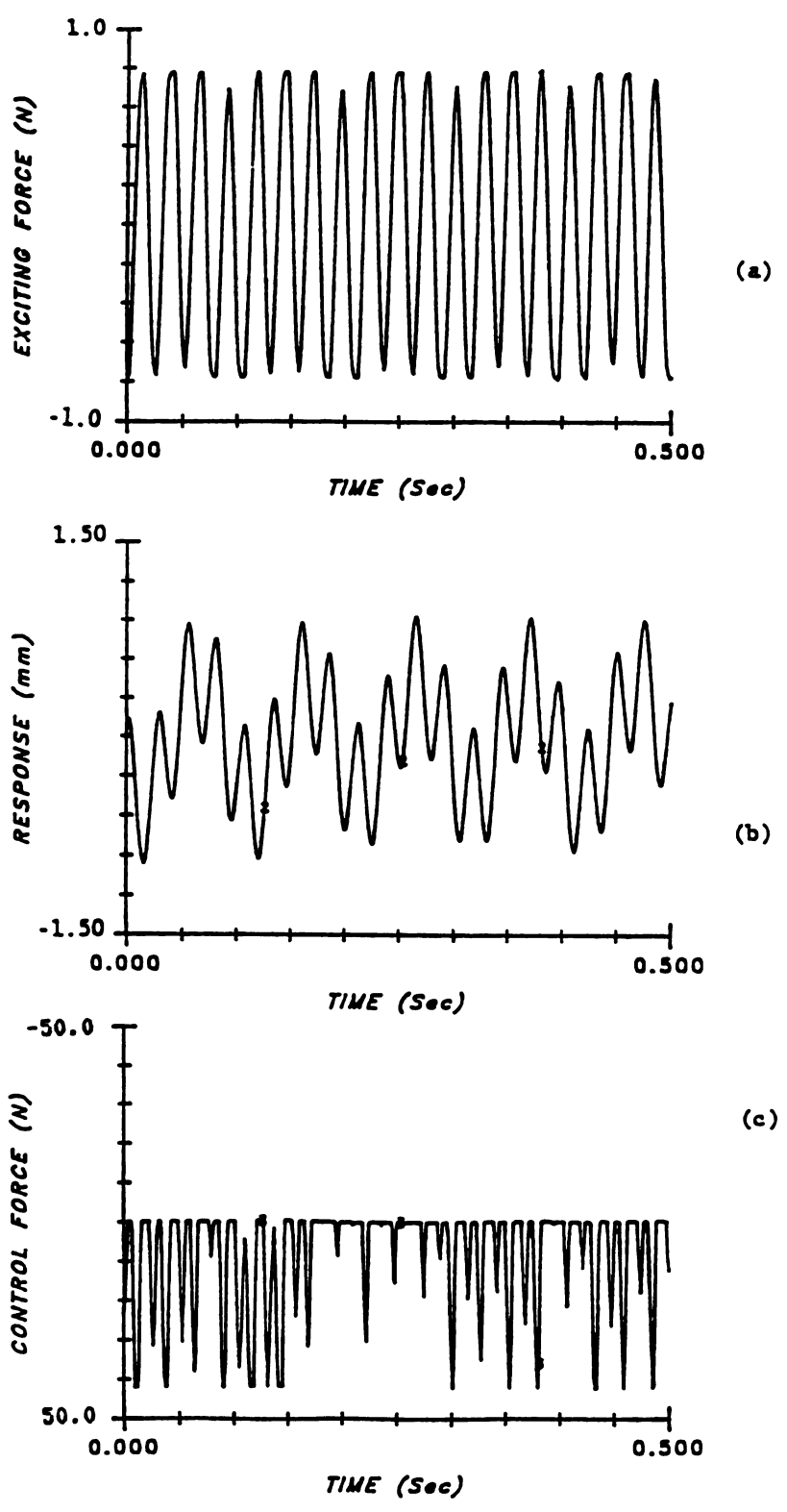


Figure C2 Steady state two-mode test results for control gain α = 41.7 N.

- a) the exciting force.
- b) the response at x = 367.2 mm
- c) the control force

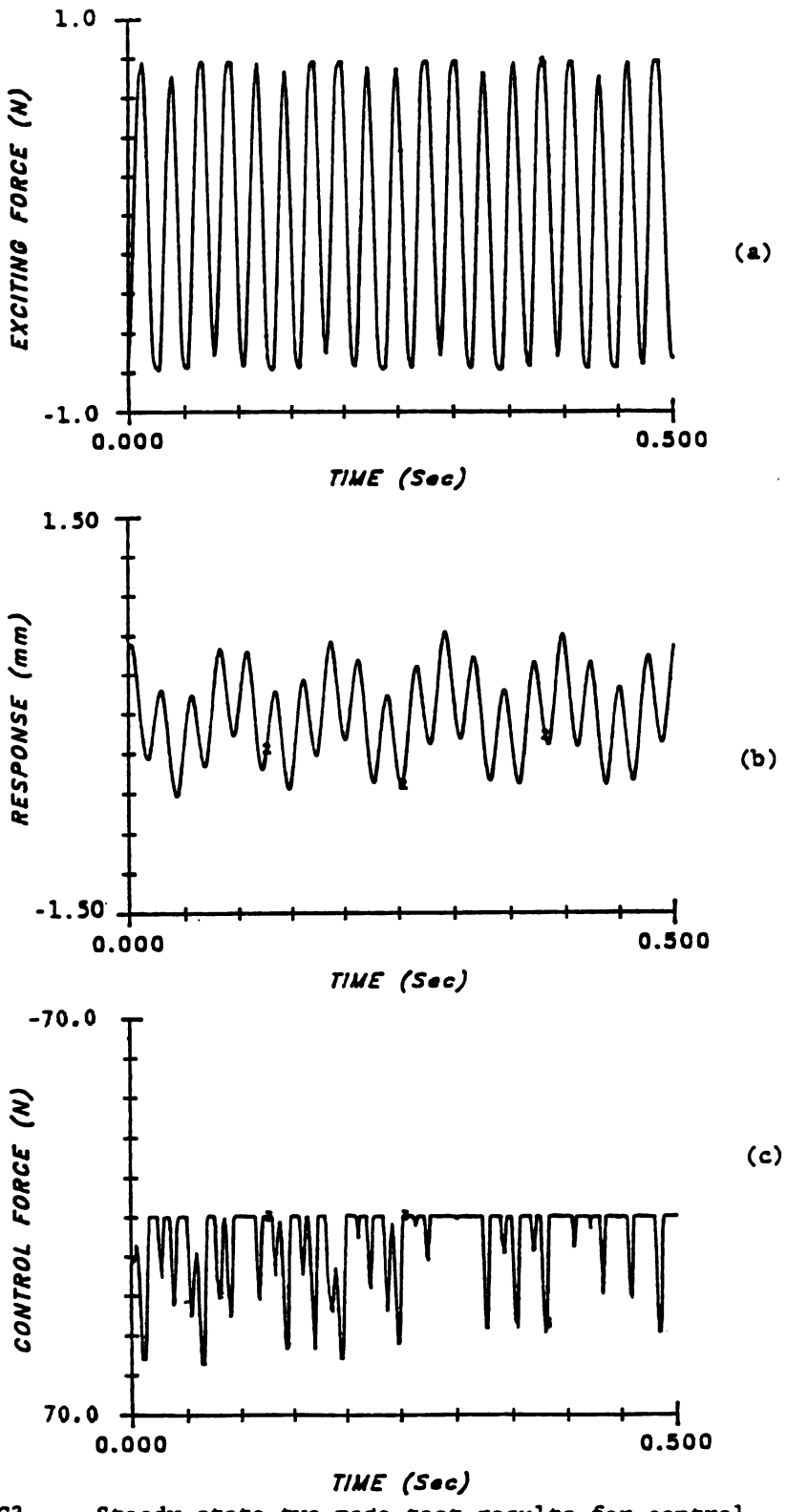


Figure C3 Steady state two-mode test results for control gain $\alpha = 50 \text{ N}$

- a) the exciting force.
- b) the response at x = 367.2 mm
- c) the control force

LIST OF REFERENCES

152

REFERENCES

- 1. Schaechter, B. E., Optimal Local Control of Flexible Structures, AIAA J. Guidance and Control, Vol. 4, No. 1, 1979, pp. 22-26.
- 2. Schaechter, B. E., Hardware Demonstration of Flexible Beam Control, AIAA Paper 80-1794, Aug. 1980.
- 3. Schafer B.E. and Holzach H., Experimental Research on Flexible Beam Modal Control, AIAA, J. Guidance, Vol.8, No. 5, Sept. Oct. 1985, pp. 597-604.
- 4. Meirovitch, L., Analytical Methods in Vibrations, The Macmillan Co. NY, 1967.
- 5. Balas, M. J., Trends in Large Space Structure Control Theory: Fondest Hopes, Wildest Dreams, IEEE Transactions on Automatic Control, Vol. AC-27, No. 3, June 1982, pp.522-535.
- 6. Balas, M., J., Modal Control of Certain Flexible Dynamic Systems, SIAM J. Control and Optimization, Vol. 16, No. 3, May 1978, pp. 450-462.
- 7. Meirovitch, L., Baruh, H., On the Problem of Observation spillover in Self Adjoint Distributed Parameter Systems, Journal of Optimization Theory and Applications, Vol. 39, No. 2, Feb. 1983, pp.269-291.
- 8. Radcliffe, C. J. and Mote, C. D., Identification and Control of Rotating disc vibration, Journal of Dynamics Systems, Measurement and Control, Vol. 105, March 1983.
- 9. Butkovskiy, A., Distributed Control Systems, American Elsavier, New York, 1969.
- 10. Kohne, M., The Control of Vibrating Elastic Systems, Distributed parameter systems Identification, Estimation, and Control, Marcel Decker; Inc., New York and Basel, 1978, pp.387-457.

- 11. Baily, T. and Hubbard Jr., J.E., Distributed Piezoelectric-Polymer Active Vibration Control of a Cantilever Beam, AIAA J. Guidance, Vol. 8, No. 5, Sept-Oct. 1985.
- 12. Lubkin, S. and Stoker J. J., Stability of Columns and Strings under Periodically Varying Forces, Quart. Appl. Math. Vol. 1, No. 3, 1943, pp.215-236.
- 13. Woodall, S. R., On the Large Amplitude oscillations of a Thin Elastic Beam, Int. J. Nonlinear Mechanics, vol. 1, 1966, pp.217-238.
- 14. Zauderer, E., Partial Differential Equations of Applied Mathematics, Wiley-Interscience pub., Wiley & Sons, New York, NY, 1983, pp.332-340.
- 15. Leipholz, H., Application of Liapunov's Direct Method to the Stability Problem of Rods Subject to Follower Forces, Instability of Continuous Systems, Symposium Herrenlab (Germany) Sept 8-12, 1969.
- 16. Crandall, S. H., Numerical Treatment of Fourth Order Parabolic Partial Differential Equation, Journal Association for Computing Machinary, 1., 1954, pp.111-118.
- 17. Ames, W. F., Numerical Methods for Partial Differential Equations, pp.279-281, 2nd Edition, Academic Press, New York, NY, pp.279-281
- 18. Lin, C. C. and Segel, L. A., Mathematics Applied to Deterministic Problems in the Natural Sciences, Macmillan Co., NY, 1974, pp. 401-403
- 19. Chen, G. and russell, D., A Mathematical Model For Linear Elastic Systems with Structural Damping, Quarterly of Applied Mathematics, Jan. 1982, pp.433-454.
- 20. Ball, J. and Slemrod, M., Feedback Stabilization of Distributed Semilinear Control Systems, Appl. Math. Optim. 5, 1979, pp. 169-179.

- 21. Ball, J., Marsden, J. and Slemrod, M., Controllability for Distributed Bilinear Systems, SIAM J. Control and Optimization, Vol. 20, No. 4, July 1982, pp. 575-597.
- 22. Courant, R. and Hilbert, D., Methods of Mathematical Physics, Vol.1, Interscience, NY, 1453, pp. 164-274.
- 23. Weinstock, R., Calculus of Variations with Applications to Physics and Engineering, Dover, 1974,pp.72-90.
- 24. Timoshinko, S., Young, D and Weaver, W., John Wiley, 1974, chapter 5.
- 25. Meirovitch, L., Analytical Methods in Vibrations, Macmilian, 1967.
- 26. Bolotin, V. V., The Dynamic Stability of Elastic System, Holden-Day, inc., Sanfrancisco, 1964, pp. 111-112.
- 27] RayLigh, J. W., The Theory of Sound, Vol. 1, Second Edition, Dover Publications, NY, pp. 244-246 and pp. 296-297.
- 28. Hoff, N. J, The Dynamics of The Buckling of Elastic Columns, Journal of Applied Mechanics, Vol. 18, Tran. AS'ME, Vol. 73, 1951, pp. 68-74.
- 29. Sevin., E., On The Elastic Bending of Columns Due to Dynamic Axial Forces Including Effects of Axial Inertia, Journal of Applied Mechanics, March, 1960, pp. 125-131.
- 30. Davison, J., Buckling of Structures Under Dynamics Loading, Journal of The Mechanics and Physics of Solids, Vol. 2, 1953, pp. 54-66.
- 31. Reiss, E., and Matkowsky, E., Nonlinear Dynamic Buckling of A Compressed Elastic Column, Quarterly of Applied Mathematics, July, 1971, pp. 245-259.

- 32. Zubov, V. I., Methods of A. M. Liapunov and their Application, Leningard, 1957; English Translation, P. Noordhoff Ltd., Gromingen, Holland, 1964.
- 33. Wang, P. K., Stability Analysis of Elastic and Aeroelastic Systems Via Liapunov's Direct Method, Journal of Franklin Institute, Vol. 281, No. 1, 1966, pp. 51-72.
- 34. Wang, P.K., Stability Analysis of A Sipmlified Flexible Vehicle Via Liapunov's Direct Method, AIAA Journal, Vol. 3, No. 9, 1967, pp. 1764-1766.
- 35. Lapidus, L. and Berger, A., An Introduction to the Stability of Distributed Systems Via A Liapunov Functional, Aiche Journal, July, 1968, pp. 558-568.
- 36. Leipholz, H., Application of Liabunov's Direct Method to the Stability Problem of Rods Subject to Follower Forces, Instability of continuous Systems, Symposium Herrenlab (Germang) Sept. 8-12, 1969, pp. 1-23.
- 37. LEipholz, H., Some Remarks on Liapunov Stability of Elastic Dynamical Systems, Buckling of Structures, IUTAM Symposium, Cambridge, 1974, Springer-Verlag, 1976, pp. 208-217.
- 38. Dym, C. L., Stability Theory and Its Applications to Structural Mechanics, Noordhoff International Publishing, Leyden, the Netherlands, 1974, pp. 52-75.
- 39. Friedman, A., Foundations of Modern Analysis, Dover, 1982, pp. 90-102.
- 40. Richtmyer, R. and Morton, K., Difference Methods For Intial-Value Problems, Second Edition, Wiley, NY, 1967 Chapters 3 and 11.
- 41. Lapidus, L. and Pinder, G.F., Numerical Solution of Partial Differential Equations in Science and Engineering, Wiley, NY, 1982, pp. 186-187.

- 42. Yakubovich, V. A. and Starzhinskii, V. M., Linear Differential Equations With Periodic Coefficients, Wiley, 1975, Chapter 2.
- 43. Radcliffe, C. J., Active Control of Vibration in Rotating Circular Discs, Ph. D. Dissertation, University of California, Berkeley, 1980.

